Aus der Fachrichtung 2.4, Experimentelle und Klinische Pharmakologie und
Toxikologie der Medizinischen Fakultät
der Universität des Saarlandes, Homburg

Novel functions of the calcium

channel β3 subunit

Dissertation zur Erlangung des Grades eines Doktors der Naturwissenschaften

der Medizinischen Fakultät

der UNIVERSITÄT DES SAARLANDES
2014

vorgelegt von: Anouar Belkacemi
geb.am: 07.02.1985 in Souk Naamane - Algerian

The uncaging experiments have been performed together with Dr. Xin Hui in Prof. Dr. P. Lipp´s laboratory in Homburg.

The skin wound healing experiments have been performed under the guidance of Prof. Dr. Matthias Laschke in the department of experimental surgery in Homburg

TABLE OF CONTENT

List of Figures

LIST OF FIGURES

List of Tables

List of Abbreviations

%   Percentage

$X^{-/-}$ Deficient of both alleles of gene "X"

°C   Celsius grad

µJ   Microjoule

µM   Micromolar

µm   Micrometer

aa   Amino acid

AID   Alpha Interacting Domain

AM   Acetoxymethylester

AUC   Area under the curve

BID   Beta Interacting Domain

BSA   Bovine Serum Albumin

Ca^{2+} Calcium

Cavs   Voltage-Gated Calcium Channel

cDNA   Complementary Deoxyribonucleic acid

cm   Centimeter

CO_2 Carbon dioxide

DAG   Diacylglycerol

DAPI   4',6-diamidino-2-phenylindole

DHP   Dihydropyridine

DMEM   Dulbecco's modified Eagle's medium

DMSO   Dimethylsulfoxide

EGTA   Ethylene Glycol Tetraacetic Acid

ER   Endoplasmic Reticulum

FCS   Fetal Calf Serum

GK   Guanylate Kinase

GPCR   G-protein coupled receptor

h   Hour

HVA   High Voltage Activated

IP3   Inositol 1,4,5-trisphosphate

IP3R   Inositol 1,4,5-trisphosphate Receptor

J   Joule

K^+ Potassium ion

kDa   KiloDalton

ko   Knockout

LVA	Low Voltage Activated
M	Molar
MEFs	Mouse Embryonic Fibroblasts
mg	Milligram
min	Minute
mM	Millimolar
mm	Millimeter
Na^+	Sodium ions
NGS	Normal Goat Serum
nm	Nanometer
nM	Nanomolar
PBS	Phosphate-Buffered Saline
PIP2	Phosphatidylinositol 4,5-bisphosphate
PKA	cAMP-dependent protein kinase
PLC	Phospholipase C
P-L-L	Poly-L-lysine
pmol	Picomol
RNA	Ribonucleic acid

ROCE	Receptor-Operated Calcium Entry
ROI	Region of interest
RT	Room temperature
s	Second
SDS	Sodium Dodecyl Sulfate
SDS-PAGE	Sodium Dodecyl Sulfate Polyacrylamide Gel Electrophoresis
SEM	Standard Error of the Mean
SERCA	Sarcoplasmic/Endoplasmic Reticulum Calcium ATPase
SH3	Src Homology domain
SOCE	Store-Operated Calcium Entry
TG	Thapsigargin
TRP	Transient Receptor Potential
TS	Tyrod´s solution
UV	Ultra violet
wt	Wild-type

ACKNOWLEDGMENTS

SUMMARY

The Ca^{2+} channel β subunits (Cavβs) 1, 2, 3 and 4 are essential for trafficking the pore-forming Cavα1 subunit to the plasma membrane and for modulation of Ca^{2+} currents. We identified the Cavβ3 protein in embryonic fibroblasts (MEFs) isolated from wild-type mice but we did not detect any functional depolarization-induced Ca^{2+} influx into these cells. Subcellular fractionation and confocal imaging of MEFs and Cavβ3 cDNA expressing HEK293 and Cos-7 cells reveal a localization of Cavβ3 all over the cytoplasm even when the Cav1.2 cDNA had been co-expressed. Fura-2 measurements during agonist-induced IP3 generation and flash photolysis of caged-IP3 show that IP3-dependent Ca^{2+} release was significantly increased in β3-deficient MEFs compared to wild-type cells. Vice versa, expression of Cavβ3 cDNA in cells which hardly express Cavβ3 gene endogenously like Cos-7 cells and HEK293 cells decreases significantly the IP3-dependent Ca^{2+} release. Using the anti-Cavβ3 antibody, the Cavβ3 protein was precipitated, and among the proteins associated with the retained Cavβ3 were the IP3R and vice versa. Cavβs contain two conserved regions, C1 and C2, essential for Cav channel regulation, which share homology with Src homology (SH) 3 domains (C1) and guanylate kinase (GK, C2). Results obtained with SH3- and GK-deficient and plasma-membrane targeted β3-protein show that i) the SH3-domain and ii) the localization within the cytoplasm are required for Cavβ3-IP3R interaction and for the β3-dependent decrease of agonist-induced Ca^{2+} release. Using glutathione S-transferase-pull-down experiment two novel binding sites for Cavβ3 protein were mapped to amino acid residues 346-917 and 1387-2249 of the IP3R type 3. MEFs obtained from Cavβ3-deficient mice revealed significant differences in migration compared to wild-type cells. By transferring this behavior into an *in vivo*

integrative pathophysiological response we studied skin wound healing which occurred significantly faster in β3-deficient mice than in wild-type mice. In summary, we discovered a novel Cav-independent function of the Cavβ3 protein, which desensitizes cells to low IP3 concentrations apparently by interacting with the internal coupling domain of IP3R *via* its SH3 domain. This novel Cavβ3 function has a significant impact on fibroblasts migration *in vitro* and skin wound closure *in vivo*.

ZUSAMMENFASSUNG

Die β Untereinheiten Spannungs-aktivierter Kalzium (Ca^{2+}) Kanäle, Cavβ 1, 2, 3 und 4, sind verantwortlich für den Transport der Poren-bildenden Cavα1 Untereinheit zur Plasmamembran und sie beeinflussen die Kinetik der Ca^{2+}-Ströme. In primären embryonalen Fibroblasten der Maus (MEFs) konnten wir Cavβ3 identifizieren, aber nach Depolarisation war kein Ca^{2+}-Einstrom in diesen Zellen zu detektieren. Subzelluläre Fraktionierung und konfokale Fluoreszenzaufnahmen der Fibroblasten und von Cavβ3 cDNA exprimierenden HEK293 und Cos-7 Zellen zeigen eine Lokalisation von Cavβ3 in Zytoplasma auch nach Koexpression der Cavα1.2 cDNA. Fura-2 Messungen während einer Agonisten-induzierten IP3 Bildung und Flash-Photolyse von „caged" IP3 ergaben, dass β3-defiziente Fibroblasten im Vergleich zu Wildtyp Zellen eine signifikant erhöhte IP3-abhängige Ca^{2+}-Freisetzung aufweisen. Andererseits führt die Expression von Cavβ3 cDNA in Cos-7 und HEK293 Zellen, Zellen, die das Cavβ3 gen normalerweise nicht (Cos-7) oder nur sehr schwach exprimieren (HEK293), zu einer Reduktion der IP3-abhängigen Ca^{2+}-Freisetzung. Mithilfe von anti-Cavβ3 Antikörpern wurde das Cavβ3 Protein präzipitiert und unter den Proteinen, die mit dem präzipitierte Cavβ3 assoziiert sind, befand sich der IP3 Rezeptor. Die Koimmunpräzipitation funktioniert auch umgekehrt. Cavβ Proteine besitzen zwei konservierte Regionen, C1 und C2, die essentiell zur Regulation der Cav Kanäle sind und Homologien zur Src-Homologiedomäne 3 (SH3, C1) sowie Guanylatkinase (GK, C2) aufweisen. Experimente mit SH3- und GK-defizienten sowie mit Plasmamembran-assoziierten β3 Proteinen, die jeweils nach Mutation der cDNA erhalten wurden, zeigen, dass die SH3 Domäne und die zytosolische Lokalisation von β3 notwendig für die Interaktion von Cavβ3 und IP3 Rezeptoren sowie die β3-

abhängige Reduktion der Agonisten-induzierten Ca^{2+}-Freisetzung sind. Mithilfe von Glutathion S-Transferase "Pull Down" Experimenten wurden zwei neue Bindestellen für Cavβ3 im Bereich der Aminosäurereste 346-917 und 1387-2249 des IP3R3 lokalisiert. Die Migration der Fibroblasten, die aus Cavβ3-defizienten Tieren präpariert werden, war signifikant verändert gegenüber Fibroblasten von Wildtyp-Tieren. Diese *in vitro* Experimente haben wir versucht in ein *in vivo* Experiment zu übertragen und haben die Wundheilung von Wildtyp Mäusen und β3-defizienten Mäusen vergleichend untersucht. Die Wundheilung der Haut verlief signifikant schneller bei β3-defizienten Mäusen im Vergleich zu Wildtyp Mäusen. Zusammenfassend haben wir eine bisher unbekannte Cav-unabhängige Funktion des Cavβ3 Proteins entdeckt: In Gegenwart Cavβ3 sind Zellen weniger sensitiv gegenüber niedrigen IP3 Konzentrationen, wahrscheinlich indem Cavβ3 über seine SH3-Domaine mit der internen Bindedomäne des IP3-Rezeptors interagiert. Dies hat eine signifikanten Einfluss auf die Migration von Fibroblasten *in vitro* und die Wundheilung der Haut *in vivo*.

1 Introduction

Calcium as a metal ion "Ca^{2+}" is one of the life's most important elements and plays a crucial role in most if not all cellular processes. But at higher concentrations Ca^{2+} becomes toxic to cells. Under resting conditions, intracellular calcium concentration is kept as low as ~100 nM and upon stimulation it increases to tens or hundreds of μM. This response to stimulation provides calcium for many cellular processes including neurotransmitter and hormone release, muscle excitation-contraction coupling, cell division, cell death and migration. In excitable cells and endocrine cells, voltage-gated calcium channels (also known as Cavs) are the principle Ca^{2+} entry pathway. These channels are important pharmacological targets in the treatment of many diseases including epilepsy, hypertension and pain. The distinctive properties of different subtypes of the pore forming subunit and their modulation by accessory subunits allow the role of voltage-gated calcium channels to be adapted to different roles and situations in various organs, tissues, cell types and subcellular localizations.

1.1 Subtypes, pharmacology and structure of voltage-gated calcium channels

Voltage-gated calcium channels molecular characterization started by purification of the channel from the transverse tubule membranes of skeletal muscle (Curtis and Catterall, 1984). This channel showed an extensive binding of ^{3}H-DHPs (^{3}H-Dihydropyridines; L-type calcium channel blockers) and this property was used to identify the channel during purification processes (Flockerzi et al., 1986). The purified channel complex contains five subunits termed α1 (~175-240 kDa), α2 (~150 kDa), β

(~54 kDa), δ (~17-25 kDa) and γ (~32 kDa), where α2 and δ subunits are linked by disulfide bonds into a single subunit called α2δ (Table 1-1 and Figure 1-1) (Takahashi et al., 1987). Voltage-gated calcium channels can be divided into 2 major types: High voltage-activated (HVA) channels that open in response to large membrane depolarization and low voltage-activated (LVA) channels which open by lower membrane depolarization (Simms and Zamponi, 2014).

Table 1-1 Subunits of the voltage-gated calcium channel complex

Channel type	Channel protein	gene	Pharmacology
High Voltage Activated			
L-type	α1S (Cav1.1)	*cacna1s*	Phenylalkylamines, DHPs, Diltiazem, Cd^{2+}
	α1C (Cav1.2)	*cacna1c*	
	α1D (Cav1.3)	*cacna1d*	
	α1F (Cav1.4)	*cacna1f*	
P/Q-type	α1A (Cav2.1)	*cacna1a*	ω-agatoxine IVA, Cd^{2+}
N-type	α1B (Cav2.2)	*cacna1b*	ω-conotoxins GVIA, Cd^{2+}
R-type	α1E (Cav2.3)	*cacna1e*	SNX-482, Cd^{2+}
Auxiliary subunits	β1 (Cavβ1)	*cacnb1*	
	β2 (Cavβ2)	*cacnb2*	
	β3 (Cavβ3)	*cacnb3*	
	β4 (Cavβ4)	*cacnb4*	
	α2δ-1 (Cavα2δ-1)	*cacna2d1*	
	α2δ-2 (Cavα2δ-2)	*cacna2d2*	
	α2δ-3 (Cavα2δ-3)	*cacna2d3*	
	α2δ-4 (Cavα2δ-4)	*cacna2d4*	
	γ1 (Cavγ1)	*cacng1*	Only associated with α1S
Transmembrane AMPA receptor regulatory protein	γ2 (TARP2)	*Cacng2*	Calcium channel subunit?
	γ3 (TARP3)	*Cacng3*	
	γ4 (TARP4)	*Cacng4*	Apparently not calcium channel subunit
	γ5 (TARP5)	*Cacng5*	
	γ6 (TARP6)	*Cacng6*	
	γ7 (TARP7)	*Cacng7*	
	γ8 (TARP8)	*Cacng8*	
Low Voltage Activated			
T-type	α1G (Cav3.1)	*cacna1g*	Mibefradil, phenytoin, Ni^{2+}
	α1H (Cav3.2)	*cacna1h*	
	α1I (Cav3.3)	*cacna1i*	

1.1.1 The α1 subunit

Cavα1 is the key determinant and principle component of voltage-gated calcium channels. It has 24 transmembrane α-helices divided into four homologous repeats (I-IV) connected with cytoplasmic loops (Figure 1-1). Ten mammalian α1 subunit cDNAs were cloned and can be divided into 3 major families structurally related (termed Cav1, Cav2 and Cav3), each of which have several members (Table 1-1) (Hofmann et al., 2014).

The Cav1 channel family encodes four members termed Cav1.1, Cav1.2, Cav1.3, and Cav1.4, all of which are sensitive to DHP agonists and antagonists. The Cav1 and Cav2 channels response to large membrane depolarization. Because of the long lasting current, the Cav1 channels are also called L-type channels. L-type calcium channels are also sensitive to other organic drugs in addition to dihydropyridines including Phenylalkylamines and Diltiazem (Catterall et al., 2005).

Cav1.1 channel is the skeletal muscle isoform of the L-type calcium channel (Tanabe et al., 1987). An autosomal recessive lethal mutation in the Cav1.1 α1 gene of mice served as the first Cav1.1 α1 deficient mouse model. The mutation causes muscular dysgenesis (mdg) and the homozygous mdg/mdg (Cav1.1-deficient) mice die at birth from asphyxia because of the failure of their skeletal muscle to contract; they are not able to breath sufficiently (Chaudhari, 1992). The second member of this family is the Cav1.2 channel which predominates in cardiac muscle; Deletion of this channel by gene targeting leads to death in utero at embryonic day 14.5 (Seisenberger et al., 2000; Weissgerber et al., 2006). Mice deficient in the third member of the Cav1 family Cav1.3 are deaf due to the important role of this channel in the auditory hair cells (Platzer et al., 2000). Cav1.4 plays a crucial role in photoreceptors, where it is responsible for calcium entry that triggers exocytosis of neurotransmitters. Mutations in the Cav1.4

gene cause x linked congenital stationary night blindness type 2 in humans (Bech-Hansen et al., 1998) and a similar phenotype in mice (no b-wave in the electroretinogramm "nob2-mice") (Chang et al., 2006).

The Cav2 channel, also open in response to large depolarization and comprises 3 members termed Cav2.1, Cav2.2 and Cav2.3. They are present in neurons and are insensitive to Dihydropyridines. The Cav2.1 conducts the P/Q-type calcium current and is blocked by ω-agatoxine IVA, a peptide isolated from the American funnel web spider venom. Deletion of the Cav2.1 gene in mice leads to severe ataxia and the mice develop absence seizures before dying approximately 4 weeks after birth (Simms and Zamponi, 2014). The Cav2.2 gene encodes the neuronal N-type calcium channel which is blocked by ω-conotoxins GVIA and MVIIA, toxins isolated from the venom of cone snail and fish-hunting marine mollusks. Cav2.2 gene deficient mice show hyposensitivity to inflammatory and neuropathic pain (Simms and Zamponi, 2014). The last member of the Cav2 family is the Cav2.3 channel responsible for the residual or R-type calcium current, which can be recorded when N-, P/Q-, and L-type channels are blocked. The Cav2.3 current can be abolished by SNX-482, a peptide toxin derived from the venom of tarantula hysterocrates gigas. Deletion of the Cav2.3 gene in mice reveal hyposensitivity to pain, resistance to chemically induced seizures (Simms and Zamponi, 2014) and significant reduction in glucose-evoked insulin secretion (Jing et al., 2005).

The Cav3 genes Cav3.1, Cav3.2 and Cav3.3 encode the ion conducting pores of the T-type channels. This family of low voltage activated (LVA) Cavs is insensitive to calcium channel blockers like DHPs, Phenylalkylamine, Diltiazem and to the spider and cone snail toxins. The organic calcium channel blocker mibefradil is somewhat selective to T-type versus L-type current (3- to 5-folds) (Catterall et al., 2005). Cav3

channels are blocked by Ni^{2+} but are resistant to Cd^{2+} ions which block the HVA channels in the low micro-molar range. Cav3.1 null mice show bradycardia due to slowing of sinoatrial node peacemaking and reduced atrioventricular conduction. Cav3.2-deficient mice show compromised coronary function due to a permanent constriction of coronary arterioles. Finally Cav3.3-deficient mice exhibit compromised sleep spindles in thalamic reticular neurons (Astori et al., 2011).

1.1.2 The α2δ subunit

The Cav1 and Cav2 subfamilies but not the Cav3 subfamily contain auxiliary subunits especially α2δ and β. Four mammalian α2δ genes have been cloned; they encode α2δ-1, α2δ-2, α2δ-3 and α2δ-4 proteins. Each α2δ protein is encoded by a single mRNA and is post-translationally cleaved; the α2 and δ fragments are then linked by disulfide bonds (Figure 1-1) (Dolphin, 2013). The α2δ subunits have been shown to increase the maximum current density of Cav1 and Cav2 channels and they also modify biophysical properties of the calcium current. Recently, it has been suggested that the α2δ subunit can fulfil non-calcium channel roles (Dolphin, 2012). In support to this suggestion, the α2δ-1 and α2δ-2 proteins have been identified as receptors for gabapentin and pregabalin (Gee et al., 1996), drugs used to treat neuropathic pain and certain types of epilepsy.

1.1.3 The γ subunit

To date there are eight γ subunit genes, encoding proteins with four transmembrane domains and the N- and C-termini are located in the cytosol. Only the γ1 subunit is a *bona fide* Ca^{2+} channel subunit. It is associated with Cav1.1 and deletion of the Cavγ1 gene increases Cav1.1 currents and alters channels inactivation properties (Freise et al., 2000). Some of the remaining γ subunits have been shown to regulate trafficking,

localization and biophysical properties of α-amino-3-hydroxy-5-methyl-4-isoxazole propionic acid (AMPA) receptors and are referred to as Transmembrane AMPA receptor regulatory protein (TARPs) (Nicoll et al., 2006).

1.1.4 The β subunit

The purified Cav1 and Cav2 channels protein complexes contain tightly bound cytosolic Cavβ proteins which have predicted α helices but no transmembrane segments (Ruth et al., 1989). There are β1, β2, β3 and β4 subunits encoded by four distinct genes. Cavβ subunits are cytoplasmic proteins, responsible for the trafficking of Cav1 and Cav2 channels to the plasma membrane and the regulation of calcium current through the pore forming subunit.

1.2 Cavα1-Cavβ interaction

Cavβ subunits have been shown to bind with high affinity to the Cavα1 subunit of Cav1s and Cav2s channels. A region of 14 amino acid located in the I–II loop of all the Cav proteins is sufficient to bind β1a, β2a, β3 and β4 subunits (Pragnell et al., 1994; Marquart and Flockerzi, 1997). The sequence analysis of this region, called "α-Interacting Domain" (AID) has identified the amino acid sequence QQxExxLxGYxxWIxxxE (Figure 1-1). Single mutations of the conserved residues in the AID region markedly altered Cavβ-binding and Cavβ-induced stimulation and regulation of Cav currents which were reduced or abolished (Pragnell et al., 1994). This AID region binds all Cavβs and the interaction has an affinity ranging from 2 to 54 nM (Walker and De Waard, 1998).

Few months after the identification of the AID region (Pragnell et al., 1994), the same group identified a 31 amino acid segment of Cavβ subunit referred to as "Beta

Interacting Domain" or BID as the main binding site for AID. This 31 amino acid appeared to be sufficient to stimulate and shift the voltage dependence of activation of the Cav currents. Nevertheless, this shift was not with the same extent as the full–length Cavβ subunit protein (De Waard et al., 1994).

For 10 years, it had been widely accepted that Cavβ interacts with Cavα1 through the BID domain. However, in the year 2004, three groups (Chen et al., 2004; Opatowsky et al., 2004; Van Petegem et al., 2004) revealed the crystal structure of the conserved core region of Cavβ2 and Cavβ3 alone and in complex with AID. The structure showed that the β subunit core region contains two highly conserved regions homologous to the Src homology 3 (SH3) and guanylate kinase (GK) domains. It was also shown that the AID does not bind to BID, but to a hydrophobic groove buried in the GK-domain, named α-binding pocket or ABP. By binding to the AID via the ABP, the Cavβ promotes an α-helical conformation on the AID which propagates to the IS6 of the ion conducting Cav protein and thereby influences channel gating (Almagor et al., 2012). Apparently the BID plays a crucial role for the structural integrity and bridging of the SH3 and GK domains (Figure 1-1, Figure 1-2), but the question arises at this stage how could BID enhance Cav currents as shown by De Waard et al., in 1994? It seems that the current enhancement by BID was a nonspecific effect since the coexpression of an artificial peptide not related to Cavβ (fake β3 core) together with Cav2.1 in Xenopus Oocytes greatly enhanced the whole oocyte current; however, the mechanism is not clear, by which an artificial peptide enhances the Cav currents (Chen et al., 2004).
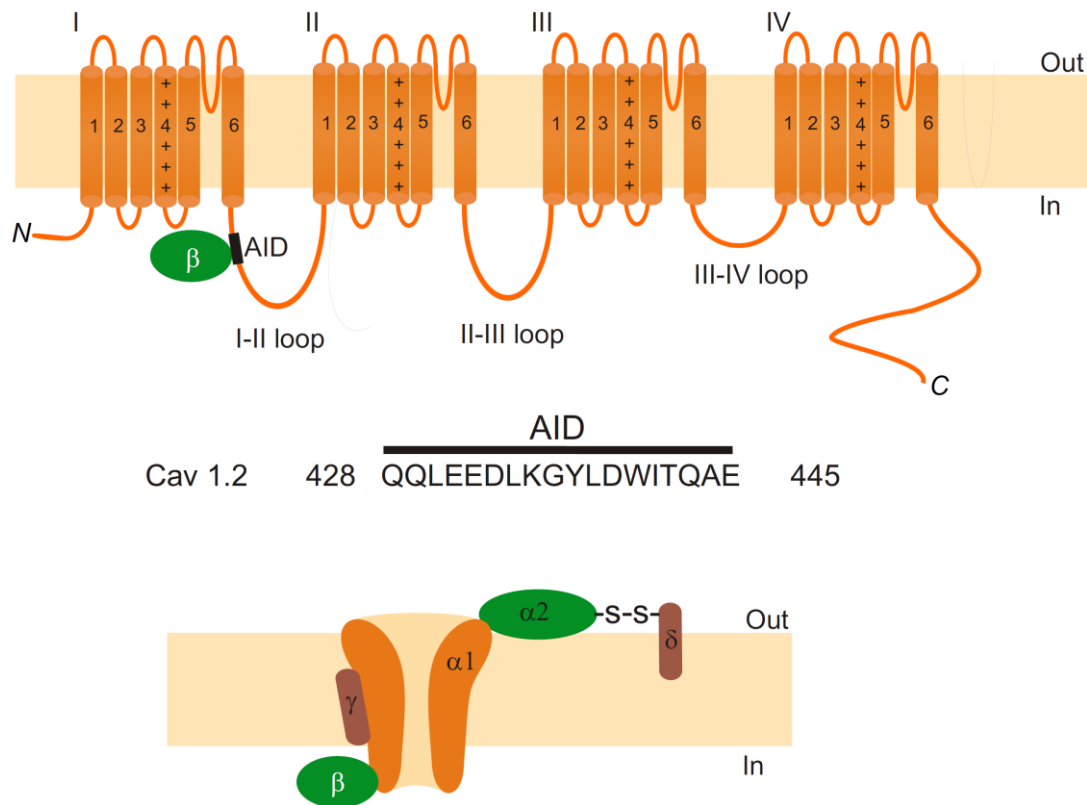
Figure 1-1. Voltage-gated calcium channel topology

Voltage-gated calcium channels subunits. **(Upper panel)** The α1 subunit is a protein of about 2000-2400 amino acid residues in length and comprises 24 transmembrane α-helices. These 24 segments are organized into four homologous repeats (I-IV). The segment S4 in each repeat (+) has 4 to 6 positively charged amino acids. The pore forming region is located between S5 and S6 of each repeat. The AID (alpha interacting domain) region (black segment) located within the I-II linker binds the β subunit (green circle). Below, the amino acid sequence of the Cav1.2-AID region. **(Lower panel)** Subunit composition of high-voltage activated (HVA) calcium channels showing the pore forming α1 subunit (orange) together with the auxiliary subunits; β (green), α2δ (green-brown) and γ (brown) subunits.

1.3 Modulation of voltage-gated calcium channels gating properties by Cavβ subunits

One of the major major functions of Cavβ subunit is to shift the voltage dependence of activation of Cavs to more negative potentials in overexpression system (Canti et al., 2000; Hullin et al., 2003). *In vivo,* using cells from Cavβ-deficient animals the voltage dependence of activation was shifted to more positive potentials (Murakami et al., 2002; Weissgerber et al., 2006). Regarding voltage dependent inactivation (VDI) properties, it was shown that Cavβ subunits shifted the voltage dependence of inactivation to more negative potentials [reviewed, e.g., in (Buraei and Yang, 2010)].

1.4 Cavβ:Cavα1 stoichiometry

The crystal structures of Cavβs showed that one Cavβ binds a single AID region (Chen et al., 2004; Opatowsky et al., 2004; Van Petegem et al., 2004). Jones and colleagues showed that the coexpression of Cavα1 together with Cavβ2a and Cavβ3 showed two different calcium channels with two distinct biophysical properties rather than one channel with mixed properties (Jones et al., 1998). Subsequently, Colecraft group showed, by expressing a covalently bonded Cavβ2b to the C-terminus of Cavα1c (Cav 1.2) in HEK 293 cells, that this recombinant L-type calcium channel (Cav1.2) has the same channel properties as coexpressing Cavα1c subunit with Cavβ2b. Coexpression of Cavβ2a, which yields different gating properties than Cavβ2b does, had only little effect on the channel function (Dalton et al., 2005).

1.5 Cavβ subunits and voltage-gated calcium channles function

Expressed without auxiliary subunits like Cavβ or Cavα2δ, the Cavα1c subunit was not sufficient to produce functional Cav channels, or the currents were very very small (Perez-Reyes et al., 1989). Coexpression of the Cavβ cDNA increased the current drastically reflecting an enhancement of surface expression and open probability of the Cav channels (Singer et al., 1991). This effect was observed with all the four subfamilies of β subunit and in different expression systems (Mori et al., 1991; Josephson and Varadi, 1996). Tareilus et al., showed that Xenopus oocytes express 2 closely related β subunit mRNAs and expression of the Cav1.2 and Cav2.3 cDNAs alone was sufficient to form functional channels in this system presumably by interacting with the endogenous Cavβs (Tareilus et al., 1997).

1.6 The Cavβ subunit structure

Based on amino acid sequence alignment, biochemical, functional and recently, the crystal structure, Cavβ proteins consists of a conserved core region flanked by non-conserved N- and C-termini (Figure 1-2).

The amino acid sequences of the N- and C-termini of Cavβs are highly variable in length and bear no or only little sequence identity. No structural data are available for these regions. The Cavβ core region consists of a split Src homology 3 (SH3) domain, a HOOK region and a guanylate kinase (GK) domain. The amino acid sequence of the core regions of β1, β2, β3 and β4 are very similar but not identical. The guanylate kinase (GK) domain of Cavβ resembles the structure of guanylate kinases, which catalyze the formation of GDP from ATP and GMP, but the Cavβ-guanylate kinase domain has no enzymatic activity. As mentioned in 1.2, it contains the α-binding pocket

(ABP) and thereby binds tightly to Cavα1 protein. It is well known that SH3 domains are protein binding modules comprising a highly conserved hydrophobic surface which binds Proline rich-regions (PxxP) present in target proteins. The SH3 domain of the Cavβs consists of five β-strands where the fifth β-strand is separated from the fourth by the HOOK region (Figure 1-2). The HOOK region is variable in length and amino acid sequence. Whether it plays a role in the regulation of calcium current inactivation has still to be shown.

β1   β2   β3   β4

MYDDSYVPGFEDSEAGSADSYTSRPSLDSDVSLEEDRESARREVESQAQQQLERAKHKPVAFAVRTNVSYCGVLDEECPVQGSGVNFEAKDFLHIKEKYSNDWWIGRLVKEGGDIAFIPS 120

β5

PQRLESIRLKQEQKARRSGNPSSLGDIGNRRSPPPSLAKQKQKQAEHVPPYDVVPSMRPVVLVGPSLKGYEVTDMMQKALFDFLKHRFDGRISITRVTADLSLAKRSVLNNPGKRTIIER 240

SSARSSIAEVQSEIERIFELAKSLQLVVLDADTINHPAQLAKTSLAPIIVFVKVSSPKVLQRLIRSRGKSQMKHLTVQMMAYDKLVQCPPESFDVILDENQLEDACEHLAEYLEVYWRAT 360

HHPAPGPGLLGPPSAIPGLQNQQLLGERVEEHSPLERDSLMPSDEASESSRQAWTGSSQRSSRHLEEDYADAYQDLYQPHRQHTSGLPSANGHDPQDRLLAQDSEHDHNDRNWQRNRPWP 480

KDSY 484

Cavβ3	N	SH3	HOOK		Guanylate kinase (GK)	C
	1	60	121	176	361	484

Figure 1-2. Cavβ3 subunit structure

(Upper panel) Amino acid sequence of Cavβ3 protein which is identical in rat and mouse. Domain structure is shown in the top line with N- and C-termini in gray. SH3 domain shown in orange with black arrows indicating the five β-strands, HOOK domain in light blue and GK domain in pink. **(Lower panel)** Cavβ3 crystal structure in complex with the AID region [Figure adapted from (Chen et al., 2004)].

1.7 Tissue distribution of Cavβ proteins

Mammalian Cavβs are encoded by four distinct genes *Cacnb1, Cacnb2, Cacnb3 and Cacnb4,* which are widely expressed in excitable tissues but also in non-excitable tissues and cells. Table 1-2 summarizes the Cavβs gene expression pattern.

Table 1-2. Tissue distribution of Cavβs

Tissue	β1	β2	β3	β4	References
Heart	-	+	+	-	(Weissgerber et al., 2006; Link et al., 2009; Meissner et al., 2011)
Cardiomyocytes	-	+	-	-	(Link et al., 2009; Meissner et al., 2011)
Cardiac fibroblasts	-	+	+	-	(Link et al., 2009; Meissner et al., 2011)
Brain	+	+	+	+	(Ludwig et al., 1997; Link et al., 2009; Meissner et al., 2011)
Lung		+	+	-	(Freise et al., 1999)
β-islets (pancreas)	-	+	+	+	(Berggren et al., 2004)
Liver	-	-	-	-	(Powers et al., 1992; Freise et al., 1999; Buraei and Yang, 2010)
Bone	+	+	+	-	(Shao et al., 2009)
Skin		+	+		Our lab – not published yet
T Lymphocytes	+	+	+	+	(Badou et al., 2006; Jha et al., 2009)
Skeletal muscle	+				(Ruth et al., 1989; Hullin et al., 1992)
Kidney	-		+		(Powers et al., 1992; Bernardo et al., 2009)
Ileum smooth muscle	-	+	+	-	(Held et al., 2007)
Dorsal root ganglions	+	+	+	+	(Murakami et al., 2002)
Retina	+	+	+	+	(Ball et al., 2011; Katiyar et al., 2015)
Placenta			+	+	(Singh et al., 2007)
Corti organ (inner ear)	+	+	+	+	(Kuhn et al., 2009)

1.8 Cavβ subcellular localization

Most Cavβs are expected to have a localization within the cytoplasm when their cDNA is expressed without the cDNA of the Cavα1 pore forming subunit. Only the β1a (Bogdanov et al., 2000), the palmitoylated β2-N3 splice variant (Qin et al., 1998) and the β2-N5 splice variant (Miranda-Laferte et al., 2014) are tethered to the plasma membrane. The β2-N3 corresponds to the β2a and the β2-N5 to the β2e referring to the old nomenclature. After replacing amino acid residues responsible for the palmitoylation by site directed mutagenesis, the palmitoylation-deficient β2-N3 was still able to traffic the Cav1.2 channel to the plasma membrane (Qin et al., 1998). Cavβ1a was also shown to target to the plasma membrane when expressed alone in Cos-7 cells as well as in the polarized Medin Darby Canine Kidney (MDCK) epithelial cell line. In contrast Cavβ3 and Cavβ4 subunits showed a diffuse localization within the cytoplasm when expressed in Cos-7 cells. Even though the different subcellular localization of Cavβs, they were all able to produce a membrane trafficking of Cavα1 subunit in Cos-7 cells (Bogdanov et al., 2000).

Several studies demonstrated targeting of β4 into the nucleus and suggested a direct function in activity-dependent gene regulation (Colecraft et al., 2002; Hibino et al., 2003; Subramanyam et al., 2009; Xu et al., 2011; Tadmouri et al., 2012; Etemad et al., 2014). However, many aspects of the regulation and function of this new signaling pathway are still controversial.

1.9 Cavβ interacting proteins

In Addition to bind to the ion conducting Cavα1 pores of high voltage activated calcium channels, β subunits have been demonstrated to bind to other proteins.

Ahnak is a 700 kDa protein (Shtivelman et al., 1992) and has been shown to interact with Cavβ subunits by coimmunoprecipitation and immunohistochemistry in cardiomyocytes (Haase et al., 1999; Alvarez et al., 2004; Haase, 2007), CD4$^+$ T-lymphocytes (Matza et al., 2008) and osteoblasts (Shao et al., 2009). Ahnak might scavenge Cavβ2 which then becomes no longer available for Cav1.2 and as a result Cav1.2 channel activity decreases. Phosphorylation of Cavβ2 and Ahnak might reduce their interaction and more Cavβ2 might be available for Cav1.2 binding (Haase, 2007).

Large conductance Ca^{2+}-activated K$^+$ channels (BK$_{Ca}$ or K$_{Ca}$1.1) are expressed in many tissues and are activated by voltage and internal Ca^{2+}. BK channels have been co-purified under high stringency conditions with Cav2 channel complexes and are presumably components of the Cav2 channel nanoenvironment (Muller et al., 2010).

Human Bestrophin (Best1) is a calcium-activated chloride channel from the retinal pigment epithelium where mutations are associated with macular degeneration or Best disease (Yu et al., 2008). It has been shown that Best1 can modulate L-type Cav1.3 channel function through the interaction with the Cavβ4 subunit and the effect of Best1 on Cav1.3 was no longer detectable in the absence of Cavβ4 (Yu et al., 2008).

Dynamin is a GTPase responsible for endocytosis and several SH3-containing proteins participate in the regulation of this process by associating with dynamin, which excises endocytic vesicles from the plasma membrane (Weng et al., 2014). Gonzalez-Gutierrez et al., showed that β2N3-SH3 induces a removal of the Cav1.2 channel from the plasma membrane in a dynamin dependent manner and that *in vitro*, β2N3-SH3 binds to dynamin (Gonzalez-Gutierrez et al., 2007).

By yeast two-hybrid screens, Cavβs were shown to interact with synaptic proteins like Synaptotagmin I (Syt1) and microtubule-associated protein 1A (MAP1A)

(Subramanyam et al., 2009). RIM1, which is part of a protein scaffold at the presynaptic membrane, was also shown to directly interact with the Cavβ4 (Kiyonaka et al., 2007).

By yeast two-hybrid screen an interaction of Cavβ4c (a new splice variant in chicken cochlear) with a nuclear protein (chromo shadow domain of chromobox protein 2/heterochromatin protein 1γ (CHCB2/HP1γ), a nuclear protein involved in gene silencing and transcriptional regulation HP1) was revealed and both proteins were found to localize in the nucleus. Co-expression of Cavβ4c with HP1 attenuates the gene silencing activity of HP1 protein (Hibino et al., 2003).

Pax6(S) (transcription factor which plays an important role in the eye, brain and pancreas development) has been shown to interact with Cavβ3 protein. Pax6(S) expressed in xenopus oocytes overexpressing the pore forming Cavα1 and the auxiliary Cavβ3 cDNAs did not change any of the Cav currents properties. Nevertheless, Cavβ3 protein suppresses the transcriptional activity of Pax6(S) and when both proteins are expressed together, the Cavβ3 proteins translocate into the nucleus instead of its predominant cytoplasmic localization (Zhang et al., 2010).

Unbound or bound to the ion-conducting Cavα1, the β-subunits can interact with additional proteins. Following skeletal muscle excitation the Cav1.1-bound β1a interacts with a cytosolic domain of the ryanodine receptor type 1 (RyR1) (Cheng et al., 2005) and thereby triggers Ca^{2+} release from the sarcoplasmic reticulum. This so-called conformational coupling is the underlying mechanism for excitation coupling in skeletal muscle. Yeast two-hybrid screens revealed that in the brain β-proteins interact with small Rem, Rem2 and Gem/Kir-GTPases (Fan et al., 2012) and a novel β-anchoring and β-regulatory protein (Beguin et al., 2014) whereas β4 binds Ppp2r5d/PP2A, (synonym B56δ). Ppp2r5d is a regulatory subunit of protein

phosphatase 2A (PP2A), known to target this phosphatase to the nucleus. Electrical activity induces nuclear translocation of β4/Ppp2r5d/PP2A, which associates with tyrosine hydroxylase (TH) gene promoter and represses the TH gene (Tadmouri et al., 2012).

1.10 Phenotypes of Cavβ gene-deficient animals

To control Cavβ-specific functions various β-gene deficient animals have been generated by gene targeting; however inactivation of Cavβ4 occurred by a spontaneous mutation (Table 1-3).

Table 1-3 Cavβ gene-deficient animals

gene	β-subunit	gene targeting		lethal	references
		global	**conditional**		
Cacnb1	β1	+		at birth	(Gregg et al., 1996)
Cacnb2	β2	+		yes	(Ball et al., 2002)
		+		<12.5	(Weissgerber et al., 2006)
			cardiomyocytes	<14.5	(Weissgerber et al., 2006)
Cacnb3	β3	+		no	(Namkung et al., 1998)
		+		no	(Murakami et al., 2002; Berggren et al., 2004; Held et al., 2007; Jha et al., 2009)
Cacnb4	β4	spontaneous mutation		no	(Burgess et al., 1997)

1.10.1   Cavβ1–deficient animals

The Cavβ1 type "a" subunits are associated with the Cav1.1α1 protein and are responsible for excitation-contraction (EC) coupling in skeletal muscle. Cavβ1-deficient mice die at birth from asphyxia, like Cav1.1-deficient mdg mice. Cavβ1-deficent

muscles are twitchless upon electrical stimulation, but contraction can still be induced by caffeine. L-type Ca^{2+} currents and the surface expression of Cav1.1 were reduced in the Cavβ1-deficient myotubes (Gregg et al., 1996). The lethal phenotype of Cavβ1-deficient mice was rescued by expressing the Cavβ1 cDNA under the control of the human skeletal actin (HSA) promoter. These HSA-Cavβ1 transgene mice were viable and did not show any obvious phenotype (Ball et al., 2002).

1.10.2   Cavβ2–deficient animals

Cavβ2 subunit is the predominant Cavβ protein expressed in adult cardiomyocytes and thus it is not surprising that Cavβ2 deficient mice are not viable (Ball et al., 2002; Weissgerber et al., 2006). They have a functionally compromised heart and die following embryonic day E10.5 (Weissgerber et al., 2006). Cardiomyocyte specific β2 gene deletion yielded a very similar phenotype (Weissgerber et al., 2006). Treatment of pregnant mothers with the calcium channel DHP-type agonist (-)-Bay K 8644 partially rescued Cav currents and significantly postponed death of Cavβ2$^{-/-}$ embryos (Weissgerber et al., 2006).

Embryonic death in all these β2 gene deficient mice is caused by heart failure leading to a defective remodeling of intra and extra embryonic blood vessels. A rescue of β2-deficient mice has been accomplished by two groups, (Ball et al., 2002) and our laboratory (Katiyar et al., 2015). Ball et al., expressed the rat β2-N3 splice variant as a transgene in cardiomyocytes and crossed these mice back to a Cavβ2 deficient genetic background. The palmitoylated β2-N3 is the "wrong" Cavβ subunit because it is predominantly expressed in brain but not in hearts from mice (Link et al., 2009), rabbits, rats and humans (Hofmann et al., 2014). Our group expressed the cDNA of the two Cavβ2 splice variants predominantly expressed in cardiomyocytes, β2-N1 and β2-N4. Both cDNAs were expressed as transgene under the control of the α-MHC promoter

in cardiomyocytes. The rescue worked because the β2-N1 and β2-N4 mice (on a β2 gene deficient background) are viable. Ongoing work aims at i) the characterization of β2-N1 and β2-N4 containing calcium channels in cardiomyocytes and ii) the study of extra-cardiac functions of β2 using the β2-N mice (which are extracardial β2 knockout) as controls.

1.10.3   Cavβ4–deficient animals

Lethargic mice are naturally occurring β4 knockouts. The underlying mutation is a four nucleotides insertion in the cacnb4 gene causing exon skipping and a premature stop codon (Burgess et al., 1997). *Lethargic* mice exhibit ataxia, absence seizures, epilepsy and paroxysmal dyskinesia as well as reduced body size and defects in the immune system (Badou et al., 2006). The abnormal phenotype starts to appear 15 days after birth while wild-type animals at this time show an increased β4 expression in the brain. Interestingly, Cav currents are not changed in neurons lacking β4 most probably because of the compensation by other Cavβ subunits (Burgess et al., 1999).

1.10.4   Cavβ3–deficient animals

Cavβ3 gene deficient mice have been generated by two groups, in the laboratory of Hee-Sup Shin (Namkung et al., 1998) and Veit Flockerzi (Murakami et al., 2000). They are viable, fertile and they grow normally under physiological conditions. However, under stress conditions, β3-deficient mice show several abnormalities indicating the importance of Cavβ3 protein (Namkung et al., 1998; Murakami et al., 2000).

Deletion of β3 gene in mice has been shown to affect pain perception. Pain induced by chemical inflammation was damped in β3-deficient animals and this was explained by a decreased expression of N-type calcium channel (Cav2.2) (Murakami et al., 2002).

In β3-deficient mouse adrenal gland, Cav2.2 and Cav1.2 protein levels were decreased compared to wild-type animals (Ohta et al., 2010). These data correlate with the electrophysiological studies where N-type and L-type calcium currents were reduced in β3-deficient cells (Ohta et al., 2010).

The Cav current density in aortic smooth muscle cells from β3-deficient mice were reduced by ~30% as was the amount of Cav1.2 protein in the plasma membrane. The blood pressure was not altered but under high salt diet, blood pressure was enhanced in β3 gene deficient mice compared to controls whereas after 2 weeks of Angiotensin II (Ang II) treatment, β3-deficient mice had a lower blood pressure (149±4 mm Hg) compared to wild-type mice (180±5 mm Hg). Mesenteric arteries from wild-type mice showed an enhanced amount of Cav1.2 protein after Ang II treatment, whereas in β3-deficient arteries the Cav1.2 protein levels were not changed (Kharade et al., 2013).

Behaviorally, β3 knockout mice showed lower anxiety, enhanced aggression and increased night time activity (Murakami et al., 2007). Cavβ3 protein has been shown to be highly expressed in the hippocampus. Using Cavβ3-deficient mice, electrophysiological experiments did not show any alteration in the biophysical properties of the Cav channels in the hippocampus. In contrast N-methyl-D-aspartate receptor (NMDAR)-mediated synaptic currents were increased in the Cavβ3-deficient animals. The protein levels of the NMDAR-2B were slightly increased and long term memory was also improved in the Cavβ3-deficient mice (Jeon et al., 2008).

In CD4^{+} T-lymphocytes, non-excitable cells, nuclear translocation of NFAT and cytokine production were attenuated in β3-deficient mice (Badou et al., 2006). Deficiency in β3 gene led to a remarkable survival defect of CD8^{+} T-Lymphocytes as well as a decrease in the expression of Cav1.4 pore forming subunit. (Jha et al., 2009).

In the year 2004, our group (Berggren et al., 2004) showed that deletion of Cavβ3 by gene targeting in mice did not affect Cav currents but lead to more efficient glucose clearance which was explained by two observations: i) increased Ca^{2+} oscillations frequency apparently caused by IP3-releasable Ca^{2+} and ii) enhanced insulin secretion in pancreatic β-islets. According to these results, the β3-protein has been suggested to constitute an interesting target for small molecules used to treat diabetes, because deletion of the cacnb3 gene does not affect resting blood glucose levels but increases glucose clearance at elevated blood glucose levels. However, the molecular mechanism underlying the increased Ca^{2+} oscillations in β3-deficient pancreatic β-islets remains unclear. Clarifying a Cav-independent function of Cavβ3 would lead to a great progress in our understanding of β3-protein signal transduction in pancreatic β-islets and also in other cells.

1.11 Objectives

The starting point of this study was the previous observation of our group showing enhanced cytosolic Ca^{2+} oscillations in β3-deficient pancreatic β-islets (Berggren et al., 2004) which pointed to Cav-independent functions of Cavβ3. An important question was to elucidate whether the β3 protein does have a Ca-independent functions. Therefore the aims of this study were mainly focusing on the following three points:

First, to identify novel Cavβ3-functions which are independent of its role as a subunit of Cav channels. To achieve this goal, we looked for primary cells which do express the Cavβ3 gene but are devoid of depolarization induced Ca^{2+}-entry. We identified mouse fibroblasts as appropriate cells and established their isolation and culture. Second, to identify and to characterize Cavβ3 functions in these fibroblasts using as controls for these studies fibroblasts isolated from Cavβ3-deficient mice. Third, to study the impact of the β3 subunit on fibroblasts functions *in vitro* and *in vivo*. The results obtained are discussed also in regard to the enhanced cytosolic Ca^{2+} oscillations observed in β-islets isolated from β3-deficient mice (Berggren et al., 2004).

2 Materials and Methods

2.1 Reagents

Table 2-1. Reagents and compounds

Compound	Supplier	Code
Thapsigargin	Invitrogen	T-7459
Fura-2/AM	Invitrogen	F1221
Bradykinin	Sigma-Aldrich	B3259
L-α-Lysophosphatidic acid, Oleoyl, Sodium (LPA)	Sigma-Aldrich	L7260
Carbamoylcholine chloride	Sigma-Aldrich	C4382
Bay K (-) 8644	Sigma-Aldrich	B133
Nimodipine	Sigma-Aldrich	N149
Geneticin	Gibco	G-418, 10131-019
Vectashield Hard+set mounting medium	Vector Lanoratories	H-1400
Trypsin-EDTA (10X)	Sigma-Aldrich	SLBG 7827
DMEM	Life Technologies	41966-029
FCS	Life Technologies	10270106
Penicillin/Streptomycin	Sigma-Aldrich	SLBH 50008V
Glutamax	Life Technologies	35050-038
DMSO	Sigma-Aldrich	D2650
Cryovials	Thermo Scientific	375418
Mr. Frosty	VWR	479-3200
Liberase TM	Roche applied science	05401 127 001
DNase I	Roche applied science	11 284 932 001
100 µm filters	PARTEC	04-004-2328
150 µm filters	PARTEC	04-004-2329
M199	Life Technologies	31153-26

HBSS	Life Technologies	14025-050
MEM	Life Technologies	31095-029
FuGENE HD	Promega	E2312
Poly-L-lysine	Sigma-Aldrich	P1274
Opti-MEM	Life Technologies	51985-026
Western lightning Plus-ECL	PerkinElmer	NEL 105001EA
BSA	Applichem	A1391,0100
Dynabeads protein A	Life Technologies	10001D
Dynabeads protein G	Life Technologies	10003D
Digitonin	Applichem	A1905,9030
Paraformaldehyde	Sigma-Aldrich	441244
Triton X-100	Amersham	17-1315-01
Normal goat serum	Vector laboratories	S-1000
DAPI (Bisbenzimide)	Sigma-Aldrich	33258
Viacount	Millipore	4000-0040
Transwell 8 µm	Fisher scientific	353097
24 well plates for migration	Fisher scientific	353504
^{35}S-Methionine, L-[^{35}S]	PerkinElmer	NEG709A

2.2 Antibodies

Table 2-2. List of antibodies

Antibody	Supplier	Code	Dilution	Source
Cavβ1	In-house	234b	1:2000	Rabbit polyclonal
Cavβ2	In-house	425	1:333	Rabbit polyclonal
Cavβ3	In-house	828 / MM2	1:500	Rabbit polyclonal
Cavβ3	Alomone	Acc 008	1:200	Rabbit polyclonal
Cavβ4	In-house	A.L	1:200	Rabbit polyclonal
GAPDH	Santa Cruz	sc-25778	1:200	Rabbit polyclonal
IP3R1	Neuromab	75-035	1:1000	Mouse monoclonal
IP3R2	Santa Cruz	sc-7278	1:200	Goat polyclonal
IP3R3	BD	BD - 610313	1:1000	Mouse monoclonal
MLC2	Cell Signaling	3672	1:1000	Rabbit polyclonal
Phospho-MLC2	Cell Signaling	3675	1:1000	Mouse polyclonal
Myosin IIA	Abcam	ab24762	1:1000	Rabbit polyclonal
Na^+/K^+ ATPase	Abcam	Ab 7671	1:2000	Mouse polyclonal
Calnexin	Stressgen	SPA-865	1:2000	Rabbit polyclonal
G-Actin	Cytoskeleton	AAN01	1:1000	Rabbit polyclonal
PLCγ1	Cell Signaling	2822	1:1000	Rabbit polyclonal
Phospho-PLCγ1	Cell Signaling	2821	1:1000	Rabbit polyclonal
PLCβ3	Santa Cruz	sc -13958	1:200	Rabbit polyclonal
p-PLC β3 (Ser 537)	Santa Cruz	sc-34392	1:200	Rabbit polyclonal
Rabbit IgG	GE Healthcare	NA 934	1:40000	Donkey
Dylight 488 anti- rabbit	Jackson immunoresearch laboratories	111-485-003	1:200	Goat

2.3 Buffers

Table 2-3. Phosphate Buffered Saline (PBS)

Substance	M.W (g/mol)	Final conc. (mM)
NaCl	58.44	136
KCl	74.55	2.5
KH_2PO_4	136.09	1.5
Na_2HPO_4	177.99	8

pH 7.4 adjusted with HCl

Table 2-4. Tyrode's solutions used for cardiomyocytes isolation

Substance	M.W (g/mol)	Final conc. (mM)
NaCl	58.44	134
KCl	74.55	4
$MgCl_2$	203.3	1.2
Na_2HPO_4	177.99	1.2
HEPES	238.31	10
Glucose	180.16	11

pH 7.35 adjusted with NaOH

Table 2-5. Tyrode's solutions used for Fura-2 measurements

Tyrode's solution	Substance	M.W (g/mol)	Final conc. (mM)
2 mM Ca^{2+}	NaCl	58.44	140
	KCl	74.55	4
	MgCl$_2$	203.3	1
	HEPES	238.31	10
	Glucose	180.16	10
	CaCl$_2$	147.02	2
10 mM Ca^{2+}	NaCl	58.44	140
	KCl	74.55	4
	MgCl$_2$	203.3	1
	HEPES	238.31	10
	Glucose	180.16	10
	CaCl$_2$	147.02	10
Ca^{2+}-free	NaCl	58.44	140
	KCl	74.55	4
	MgCl$_2$	203.3	1
	HEPES	238.31	10
	Glucose	180.16	10
High K$^+$	KCl	74.55	144
	MgCl$_2$	203.3	1
	HEPES	238.31	10
	Glucose	180.16	10
	CaCl$_2$	147.02	2

pH 7.35 adjusted with NaOH

Table 2-6. SDS denaturing buffer (2 times concentrated)

Substance	Concentration
SDS	8 % (w/v)
Tris	120 mM
Bromophenol blue	0.01 % (w/v)
Glycerol	20 % (v/v)
β-mercaptoethanol	10 % (v/v)

pH 6.8 adjusted with HCl

Table 2-7. Cell lysis buffer (Immunoprecipitation)

Substance	Concentration
HEPES	50 mM
NaCl	150 mM
$CaCl_2$	1 mM
Digitonin	1 % (v/v)

pH 7.5 adjusted with NaOH

2.4 Isolation of primary cells

2.4.1 Isolation of primary Mouse Embryonic Fibroblasts (MEFs)

All animal procedures were performed in accordance with the animal care guidelines issued by the Federal Republic of Germany. Primary mouse embryonic fibroblasts (MEFs) were prepared from C57BL6/N wild-type (wt) and Cavβ3-deficient (β3ko) mice which have an identical strain background, to reduce the risk of possible genetic background–dependent variations. On embryonic day E14.5 of gestation, female mice from both genotypes were sacrificed by performing a cervical dislocation. Uterine horns were exposed and removed into a sterile disposable petri dish containing 10 ml PBS (Table 2-3). Embryos were released by opening the embryonic sacs and the head and visceral tissues were separated from embryos. Further, tissues were minced and

transferred into a 50 ml conical tube. Then, tissues were incubated with 1 ml trypsin (0.5 g/ml) per embryo at 37°C for 10 min. After pipetting vigorously up and down, the cell suspension was distributed into cell culture 175 cm^2 flasks (BD Biosciences) containing Dulbecco's modified Eagle's medium (DMEM) supplemented with 10 % fetal calf serum (FCS), 100 U/ml Penicillin, 100 µg Streptomycin and 1 % GlutaMAX (Invitrogen). After 24 hours, fibroblast cultures were observed and media replaced. When they reached 90 % confluency, they were harvested and used for subsequent experiments up to passage five or were permanently preserved in liquid nitrogen.

2.4.1.1 Cryopreservation and thawing of cells

Cryogenic preservation (storage below -100°C in liquid nitrogen) of cells is widely used to maintain backups of cells for prolonged period of time. To freeze MEFs, cells at 90 % confluency were trypsinized, pelleted and then resuspended in fresh media containing 10 % DMSO (Sigma Aladrich) and then transferred immediately into 1.5 ml cryovials. Cryovials were placed into Mr. Frosty container (VWR 479-3200) to achieve a cooling rate very close to -1°C/minute. The freezing container was immediately placed into the -80°C freezer and the following day, vials were transferred into liquid nitrogen.

For thawing, cryovials were warmed up to 37°C for 10 min and then suspended in fresh culture medium. The cell suspension was centrifuged at 188 xg for 5 min to remove DMSO and the cell pellet was resuspended in fresh cell culture medium. Cells were plated into 175 cm^2 flasks and incubated at 37°C and 5 % CO_2. The medium was changed after 18 hours and cells were kept in culture until confluency.

2.4.2 Isolation of primary mouse cardiomyocytes

2.4.2.1 Principle

Isolated cardiomyocytes have been employed as an important research tool in molecular and cellular cardiology. The adult cells are strongly connected by intercalated discs and extracellular matrix, and therefore difficult to isolate (Mitcheson et al., 1998). For isolation, the most common and successful method is the Langendorff method (Figure 2-1). The important steps in this method are as follows: (1) Washing the heart to get rid of blood, (2) perfuse the heart with a calcium-free solution in order to weaken intercellular connections, (3) enzymatic digestion, (4) mechanical agitation to free the cells from the tissue and (5) centrifugation at low speed to separate viable from non-viable cells (Bouron et al., 1990).

2.4.2.2 Method

Cardiomyocytes were isolated as described previously (Meissner et al., 2011). Eight to ten weeks old mice were anesthetized by intraperitoneal injection of Avertin (0.5 mg/g of body weight) including heparin (20 units/g of body weight) to avoid blood clots; the heart was quickly removed *via* thoracotomy and transferred to an ice-cold modified Tyrode's solution (Table 2-4). Afterwords, the heart was cannulated *via* the aorta, attached to a Langendorff apparatus (Figure 2-1) and perfused retrogradely with carbogen (5 % CO_2, 95 % O_2)-saturated Tyrode's solution (Table 2-4) containing 200 µM EGTA for 7 min. The perfusion solution was then changed to constantly gassed (carbogen) Tyrode's solution containing Liberase TM at a final concentration of 166 µg/ml for 7 to 12 minutes at 37°C (Liberase TM contains highly purified Collagenase I and Collagenase II in a precise ratio and with a medium concentration of Thermolysin, a non-clostridial neutral protease). The ventricles were isolated, dissected, and transferred into Tyrode's solution (Table 2-4) supplemented with DNase I.at a final

concentration of 1.37 ng/ml. The ventricles were cut into small pieces followed by homogenization of the tissue by gently pipetting. For Fura-2 measurements, Ca^{2+} concentration in the cell suspension was enhanced gradually until 1 mM; then cells were transferred onto glass coverslips pre-coated with extracellular matrix gel (ECM gel) and were allowed to attach for at least 2 hours.

For biochemical analysis, the cell suspension was filtered (150 µm pore size) and incubated in Tyrode's solution (Table 2-4) containing DNase I for 10 min at 37°C. By this procedure cardiomyocytes were concentrated in the pellet, while the fibroblasts remained in the supernatant. The supernatant containing the fibroblasts were transferred into a new tube and centrifuged. The cardiomyocytes within the pellet were resuspended in Tyrode's solution (Table 2-4) containing DNase I and plated for 2 hours at 37°C and 5 % CO_2 to remove adherent cells. The non-adherent cells were collected by centrifugation at 40 xg for 2 min and then washed 2 times with PBS to remove cell debris as well as blood cells. The cell pellet was then frozen at -80°C until use for biochemical analysis.
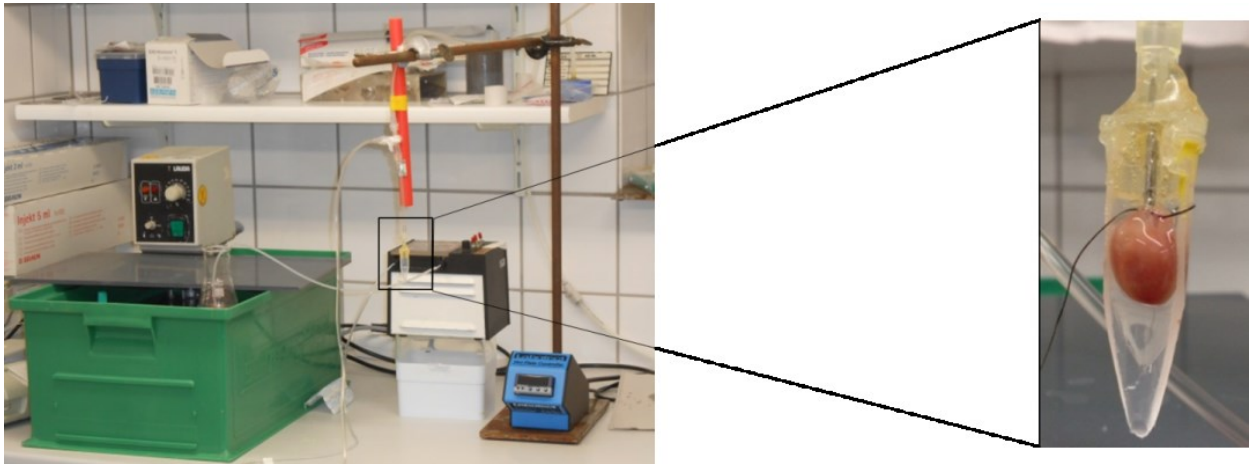
Figure 2-1. Langendorff apparatus.

The home-made Langendorff apparatus was used to isolate cardiomyocytes through cannulation of the aorta and perfusion of the heart with a liberase TM containing solution. The water bath (left in green) was used to maintain the temperature of the perfused solution at 37°C. For a constant flow perfusion, the peristaltic pump (black box) was used; it allowed regulating the speed of perfusion.

2.5 Cell lines

Cos-7 cells were maintained in Dulbecco's Modified Eagle's Medium (DMEM) supplemented with 10 % fetal calf serum, 100 U/ml Penicillin, 100 μg Streptomycin) and 1 % GlutaMax and maintained under standard cell culture conditions (37°C, 5 % CO_2). Cells were split at 1:10 and allowed to grow till confluency.

HEK293 cells and HEK293 cells stably expressing the Cavα1c (Cav1.2) cDNA of the pore forming subunit of the voltage-gated calcium channel (generated previously in our laboratory) were cultured in Minimum Essential Medium (MEM) containing 10 % FCS at 37°C and 5 % CO_2. The Cavα1c-HEK293 stable cell line was permanently cultured

in the presence of G418 (Geneticin, final concentration of 0.5 mg/ml). Cells were cultured until confluency and then split at a ratio of 1:10 and allowed to grow again until they reach confluency.

2.6 Cell transfection

2.6.1 Principle

The process of introducing nucleic acids into eukaryotic cells by a non-viral method is defined as transfection. Fugene HD transfection reagent is a proprietary blend of lipids and other components supplied in 80 % ethanol. Fugene HD lipids interact with DNA molecules to form a positively charged complex and delivers DNA into the cell when getting in contact with it (Felgner et al., 1987).

2.6.2 Method

Cos-7 cells, HEK 293 cells or HEK 293 cells stably expressing the cDNA of Cavα1c pore forming subunit of Cav1.2 channel were plated on poly-L-Lysine pre-coated coverslips. Cells at a confluency of 70-80 % were treated with a mixture of plasmid DNA and Fugene HD. 2 µg DNA encoding plasmids were diluted in 100 µl Opti-MEM and 5 µl Fugene HD was added. The mixture was vortexed for 5 seconds, incubated for 15 min at 21°C and then applied directly to cells. Twenty four to forty eight hours after transfection, cells were ready for Fura-2 measurements, confocal imaging and biochemical analysis.

2.7 Western blot analysis

2.7.1 Principle

Western blotting (immunobloting), firstly introduced by Towbin et al., 1979 (Kurien and Scofield, 2006), is a qualitative and semi-quantitative technique. It's a widely used technique for immunodetection of proteins.

The first step of Western blot analysis is to separate proteins according to their size by gel electrophoresis. The separated proteins are transferred from the Sodium dodecyl sulfate (SDS) polyacrylamide gel (PAGE) to an adsorbent membrane, generally a nitrocellulose membrane. Later on, unoccupied binding sites on the membrane are blocked with non-fat milk and subsequently the membrane is incubated in the presence of the primary antibody. After washing, the bound primary antibody is detected by a secondary antibody, usually conjugated to horseradish peroxidase.

2.7.2 Sample preparation

SDS denaturing buffer (Table 2-6) was used for sample preparation. It contains bromophenol blue (BPB), glycerol, β-mercaptoethanol, Sodium Dodecyl Sulphate (SDS) and Tris-HCl. The bromophenol blue runs within the front and glycerol increase the density of the samples. The β-mercaptoethanol reduces the inter- and intra-molecular disulfide bonds. The ionic detergent SDS denatures proteins and gives them a uniform negative charge enabling proteins to be separated solely on basis of their sizes.

SDS-denaturing buffer (Table 2-6) was added either directly onto the cells cultured in dishes (Ø 3.5 cm dish) or cells collected by trypsin (75-150 µl SDS-denaturing buffer per Ø 3.5 cm dish). Samples were pipetted up and down several times and sheared

by a 26-gauge needle. SDS-denaturing buffer was also added to protein samples at a volume ratio of 1:1. Then samples were heated for 20 min at 60°C on a heating block, cooled down and either loaded onto SDS-PAGE or stored at -20°C until use.

2.7.3 Method

Cell lysates were solubilized, denatured, and subjected to SDS-PAGE separation. Proteins were transferred onto a nitrocellulose membrane (Hybond-C Extra, GE Healthcare) and probed with different primary antibodies as indicated. Bound primary antibodies were detected by secondary antibodies conjugated to horseradish peroxidase after the addition of Western Lightning chemiluminescence reagent (From PerkinElmer). Original scans after 15 s, 1 min, 5 min and 60 min exposure were saved as TIFF images from LAS 3000 (Fujifilm).

2.8 BCA protein assay

Bicinchoninic acid (BCA) has been firstly introduced by Paul K. Smith, et al. in 1985 (Smith et al., 1985). Since then it has been the most popular method for colorimetric detection and quantification of total proteins.

The BCA assay is based on 2 reactions:

1. Reduction of Cu^{2+} to Cu^{1+} by proteins in alkaline buffer (called biuret reaction).

2. The cuprous cation (Cu^{1+}) forms a purple complex with bicinchoninic acid (Figure 2-2), which is water soluble and exhibit a strong linear absorbance at 562 nm with increasing protein concentration. Bovine serum albumin (BSA) was prepared with defined concentrations and was used as standards. Protein concentration estimation

was performed as described in the manufacturer´s protocol (Pierce BCA protein assay).
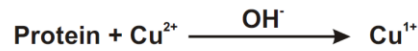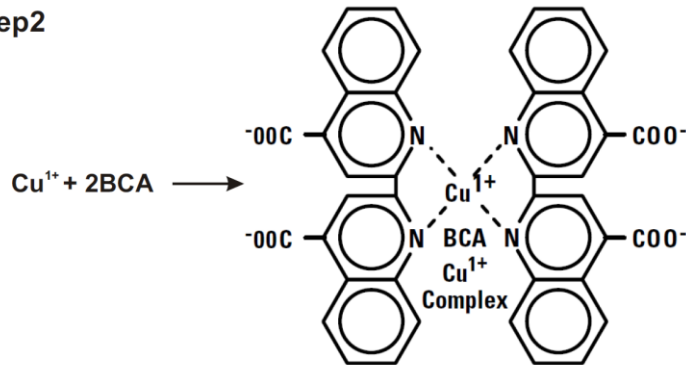
Figure 2-2. Schematic reaction for the bicinchoninic acid BCA-containing protein assay (Smith et al., 1985)

2.9 Protein interactions and coimmunoprecipitation

Antibody based affinity purification is a widely used method to study protein complexes. In a first step, 30 µl of magnetic beads (Dynabeads) labelled with protein A for the binding of rabbit immunoglobulins or protein G for the binding of mouse immunoglobulins were incubated in the presence of 5 µg antibody diluted in 200 µl PBS supplemented with 0.02 % Tween 20 under end-over-end rotation at 21°C for at least 1 hour. Then the supernatant was removed and beads containing the bound primary antibodies were washed with lysis buffer (Table 2-7). Thereafter, these beads were used to immunoprecipitate the target protein complex.

For coimmunoprecipitation Cos-7 cells were transfected with Cavβ3 cDNA (full length or mutants) with one of the IP3Rs type 1, 2 and 3 cDNAs. 48 hours after transfection, cells from 5 dishes (Ø 3.5 cm) were trypsinized and collected by centrifugation at 188 xg for 5 min. Each pellet (collected from 5 dishes) was resuspended in 2 ml ice-cold lysis buffer (Table 2-7) supplemented with protease inhibitors (0.3 µM aprotinin, 10 µM leupeptin, 1 µM pepstatin, 1 µM phenylmethanesulfonyl fluoride "PMSF", 90 mM iodoacetamid and 1 µM benzamidine). The cell suspension was passed 10 times through a 22-gauge needle than another 10 times through a 27-gauge needle and thereafter incubated for 1 hour at 4°C under rotation. After centrifugation at 100,000 xg for 45 min at 4°C, the supernatant was incubated with the magnetic beads which bind the corresponding antibody for 2 hours at 4°C under end-over-end rotation. 30 µl of cell lysate from each sample was kept on ice to be used as input control.

After 2 hours incubation of cell lysate with primary antibodies bound to the beads, the supernatant was removed by placing eppendorf tubes on the magnetic rack and extensively washed (5 times) with modified washing buffer (Table 2-7) containing 0.1% digitonin. Subsequently proteins bound to beads were eluted by adding SDS-denaturing buffer (Table 2-6) to beads and incubated for 20 min at 60°C. Thereafter, denatured proteins were separated by SDS-PAGE and transferred to nitrocellulose membrane. To look for the interaction between Cavβ3 and IP3R, the β3 protein complex was immunoprecipitated by the anti-Cavβ3 antibody thereafter we looked by Western blotting whether IP3R is among the proteins retained by the β3 protein and vice versa.

2.10 *In vitro* translation and ^{35}S-Methionine labeling

The TNT T7 coupled reticulocyte lysate system (Promega) was used for a one step transcription/translation of the mouse IP3R3 fragments F1 to F11 subcloned into the pcDNA3 vector by Stefanie Buchholz in our laboratory. Proteins incorporated by this procedure ^{35}S-Methionine (Easy Tag[TM] Methionine, L-[^{35}S]-NEG709A, PerkinElmer) according to the manufacturer's protocol. Briefly, the TNT lysate reaction containing 25 µl of TNT reticulocyte lysate quick master mix, 1 µl of 9.3 nM ^{35}S-Methionine (1175 Ci/mmol), 1.5 µg plasmid DNA and nuclease-free water in a total volume of 30 µl was incubated at 30°C for 90 min. ^{35}S-methionine labeled IP3R3 fragments were purified by gel filtration using a sephadex G-50 column (ilustra[TM] Nick[TM]Columns Sephadex[TM] G-50 DNA Grade–GE Healthcare Life Sciences) in buffer containing 20 mM Tris-HCl pH7.5, 100 mM NaCl, and 0.1 % Triton-X 100. Samples were stored at -20°C until use for GST pull down assay.

To check the integrity of the *in vitro* translated IP3R protein fragments, samples corresponding to 50,000 counts per minute (cpm) from each fragment (~1-5 µl) were incubated with the same volume of SDS-denaturing buffer at 60°C for 20 min. Thereafter, proteins were separated by either 10% or 12 % SDS-PAGE depending on the expected molecular size of the respective IP3R fragment. The gel was dried and ^{35}S-labeled proteins were analyzed by phosphor-imaging (see section 2.11).

2.11 Analysis of radioactively labeled proteins

[35]S-labeled *in vitro* translated proteins were run on a SDS-PAGE under denaturing conditions. Gels were dried under vacuum and placed on a whatman blotting paper covered with a plastic film. Dried gels were exposed to a phosphor-imager screen

(BAS-MS 2040, Fujifilm) for a time ranging between 3 hours to 2 days. The phosphor-imager screen was read by the phosphor-imager reader BAS-2500 (Fujifilm) and the software BAS-reader 3.14 version. Images were exported as BMP files and transferred to AIDA and then coral DRAW X4 software for labeling and clarity.

2.12 GST pull-down assay

To map the domain of IP3R3 responsible for binding the Cavβ3 we used GST pull-down assays as previously described in (Boulay et al., 1999). The β3-GST fusion protein was immobilized on glutathione agarose beads. The mIP3R3 protein fragments F1 to F11 obtained by *in vitro* translation (Figure 3-14 B) were incubated with either Cavβ3-GST fusion protein or as a negative control GST protein alone at 21°C for 30 min under shaking in 500 μl binding buffer (20 mM Tris-HCl pH7.5, 100 mM NaCl, and 0.1 % Triton-X 100). Thereafter, the beads were extensively washed with binding buffer, mixed with 25 μl SDS-denaturing buffer and incubated for 20 min at 60°C. Denatured proteins were separated on 8% or 12% SDS-PAGE and stained with coomassie brilliant blue to visualize the Cavβ3-GST fusion protein (~80 kDa) or GST alone (~25 kDa). Thereafter, gels were dried and exposed to a phosphor-imager screen for 3 hours to 2 days and screens were analyzed as described above in2.11).

2.13 Subcellular protein fractionation

For subcellular fractionation we used the Thermo Scientific Pierce subcellular protein fractionation kit (Thermo 78840) and followed the manufacturer´s instructions. Briefly, MEFs from wild-type and β3-deficient mice or HEK293 cells transfected with the β3 cDNA (confluent 175 cm^2 flask) were collected and pelleted *via* centrifugation at 188

xg for 5 min. After discarding the supernatant, the pellet was incubated in ice-cold cytoplasmic extraction buffer (CEB) for 10 min at 4°C and then centrifuged at 500 xg for 5 min. The supernatant was collected as cytoplasmic extract and the pellet was resuspended in ice-cold membrane extraction buffer (MEB), vortexed for 5 s and incubated for 10 min at 4°C. Thereafter, the suspension was centrifuged at 3000 xg for 5 min and the supernatant was collected as a membrane extract. Ice-cold nuclear extraction buffer (NEB) was added to the remaining pellet, vortexed for 15 s and incubated at 4°C for 30 min with gentle shaking. Following centrifugation at 5000 xg for 5 min, the supernatant was collected as soluble nuclear extract. Protein concentrations were determined (see section 2.8) and proteins of the cytoplasmic, membrane and soluble nuclear fractions were separated by SDS-PAGE (50 μg per lane) and analyzed for the presence of Cavβ3 by Western blot.

2.14 Confocal microscopy and live cell imaging

Confocal images presented in the present study were captured by using a LSM 780 confocal laser scanning microscope and a Plan-Apochromat 63x/1.4 oil DIC M27 objective (Carl Zeiss). For acquisition, Zen software was used and the excitation laser was set at 488 nm for GFP, 514 nm for YFP and 561 nm for RFP using a multiple band beam splitter for 488/561/633 nm.

For live cell imaging, Cos-7 or HEK293 cells were initially plated on glass coverslips pre-coated with PLL (see section 2.16). After 24 hours cells were transfected with cDNAs encoding GFP-, YFP- or RFP-tagged proteins (see section 2.6). 24 to 48 hours after transfection, cells were washed with Tyrode's solution containing 2 mM Ca^{2+} (Table 2-5) and coverslips were placed into a circular open-bottom chamber and supplemented with 300 μl Tyrode's solution containing 2 mM Ca^{2+} (Table 2-5). Images

were processed by adding scale bars and then imported into corelDRAW X4 Version 14.0 for labeling.

2.15 Immunofluorescence

2.15.1   Principle

Albert H. Coons and colleagues (Coons et al., 1941) were the first to develop immunofluorescent techniques in the early 1940s [Reviewed in (Moon et al., 2010)]. Nowadays, immunofluorescence is the most commonly used method to detect and study the expression of a specific protein at high resolution. However as long as the protein is not tagged by a fluorescent reporter, detection highly depends on the specificity of the antibodies for the target proteins. In the latter case, a fluorophore is conjugated to a primary antibody which is used for detection of antigens or a secondary antibody which is used to detect the primary antibody.

2.15.2   Method

MEFs from wild-type and β3-deficient mice were cultured on glass coverslips for 24 hours. Cells were then washed once with PBS and fixed with 4% paraformaldehyde in phosphate-buffered saline PBS (Table 2-3) for 15 min at 21°C. The cells were then permeabilized with 0.5 % Triton X-100 for 15 min and then washed three times with PBS. To block nonspecific binding, cells were incubated with a solution of phosphate-buffered saline (PBS) containing 3 % bovine serum albumin (BSA), 1 % normal goat serum (NGS) and 0.1 % Triton X-100 for 60 min. After three washes with PBS, cells were incubated for 16 hours at 4°C with the primary antibody diluted at appropriate concentrations in PBS containing 1 % BSA and 0.05 % Triton X-100. After incubation with the primary antibody, cells were washed three times with phosphate-buffered

saline and incubated with Dylight 488-conugated affiniPure Goat anti-rabbit IgG secondary antibody. For detecting actin filaments Alexa Fluor 594-conjugated phalloidin was used. The cell nuclei were stained with DAPI 1 µg/ml and the coverslips were then mounted with Vectashield Hard+set mounting medium and imaged using a fluorescence microscope (BZ-8000, Keyence, Osaka, Japan).

2.16 Measurements of cytosoloic Ca^{2+}

2.16.1   Principle

Many physiological and pathological processes are tightly regulated by the intracellular Ca^{2+} concentration ([Ca^{2+}]$_{ic}$). An adequate evaluation of the role of [Ca^{2+}]$_{ic}$ requires quantitative measurements. The most convenient method is the use of fluorescent Ca^{2+} indicator dyes which are commercially available in three forms, as salts, dextran conjugates or acetoxymethyl (AM) esters (Paredes et al., 2008). We used the fluorescent calcium indicator Fura-2 which has been synthesized by Tsien and colleagues in 1985 (Poenie and Tsien, 1986). The equilibrium dissociation constant of Fura-2 for Ca^{2+} is 224 nM and thereby compatible to the resting Ca^{2+} concentration in the cytosol (~100 nM). In our experiments we used Fura-2 AM the ester form of Fura-2. Fura-2 AM is nonpolar and, in contrast to Fura-2, membrane permeable. It diffuses along its concentration gradient into the cytosol where intracellular esterases cleave the ester bound. The remaining polar Fura-2 is trapped within the cell where it binds Ca^{2+} (Figure 2-3).
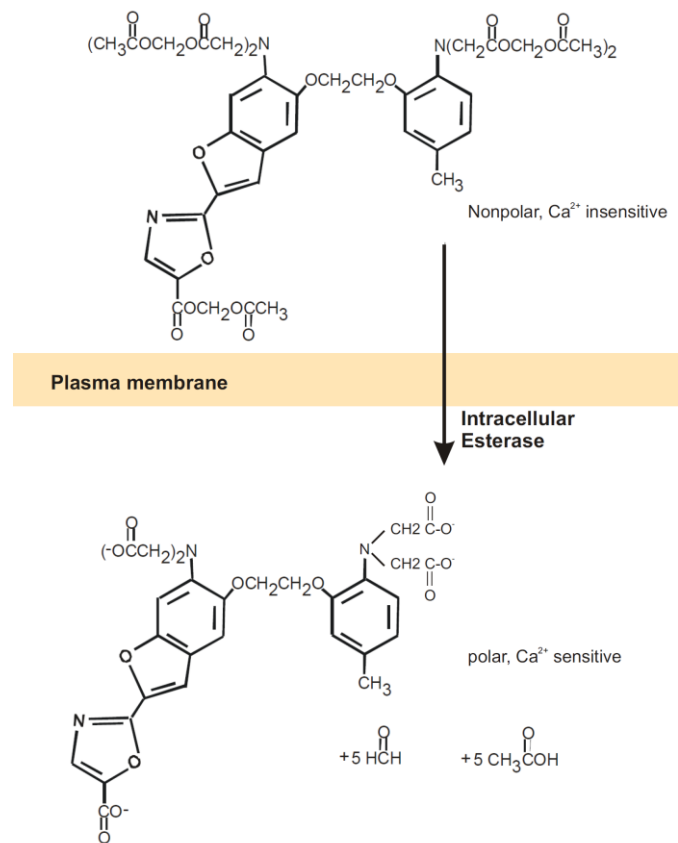
Figure 2-3. Schematic representation of the Fura-2 AM loading

Fura-2 AM is hydrophobic and membrane permeable. After passing the plasma membrane, intracellular esterases hydrolyze the ester bound. The molecule is now negatively charged, trapped within the cytosol and the carboxylated groups chelate Ca^{2+} (Modified from www.biotek.com).

Importantly, the peak excitation wavelength of Fura-2 shifts from 340 nm in the Ca^{2+}-bound state to about 380 nm in the Ca^{2+}-free state but its emission maximum stays at 510 nm (Figure 2-4). The fluorescence emission at 340 nm excitation wavelength increases, while it decreases at 380 nm excitation wavelength with a rising calcium concentration. Reciprocally, 340 nm excitation decreases, while it increases at 380 nm excitation with decreasing calcium concentrations (Figure 2-4). These properties in excitation and emission wavelengths enable Fura-2 to be used as dual excitation (340

and 380 nm) ratiometric Ca^{2+} dye. Measurements of fluorescence at two excitation wavelength are used to estimate the intracellular calcium concentration independent of dye concentration and excitation light intensity. Intracellular Ca^{2+} changes will be given as ratio F340/F380.
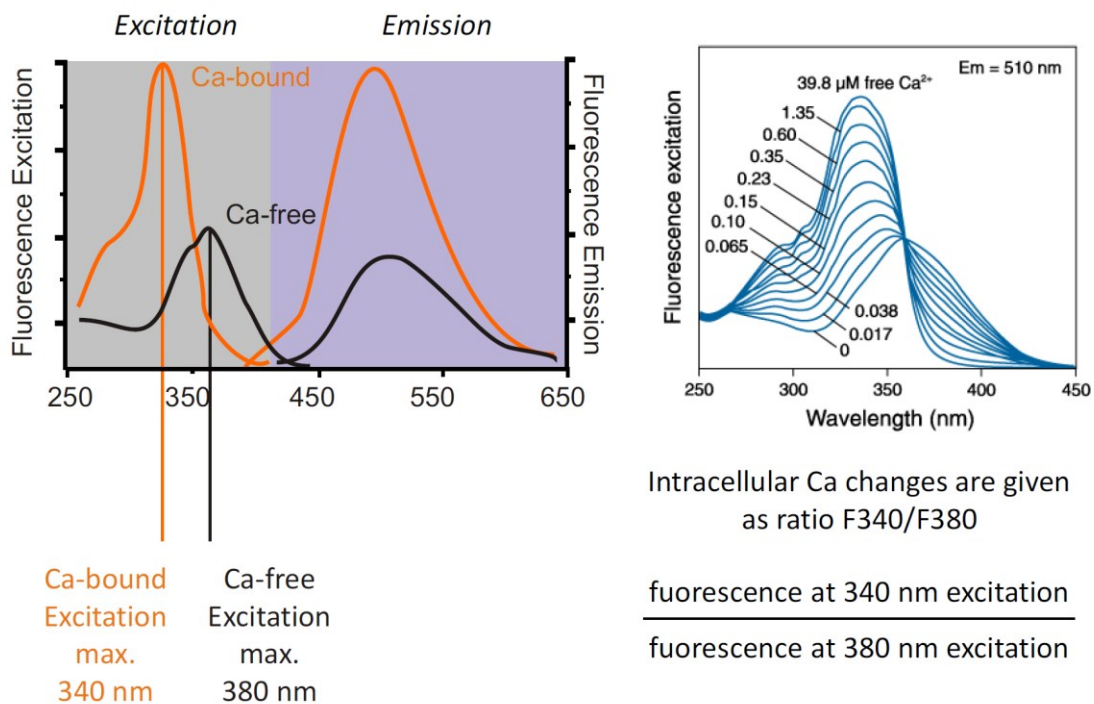
Figure 2-4. Excitation spectra of Fura-2

(Left panel) The wavelength at which Fura-2 absorbs light is dependent on whether Ca^{2+} is bound or not. In the absence of Ca^{2+}, Fura-2 excitation max is at about 380 nm light; when saturated with Ca^{2+} ions, it is at 340 nm and it emits maximum light at ~510 nm in both forms (Modified from http:/invitrogen.com). **(Right panel)** The excitation maxima shift from 380 nm toward 340 nm as Ca^{2+} concentrations increases. At 360 nm is the isosbestic point: the absorbance of Ca^{2+}-bound or Ca^{2+}-free Fura-2 is identical (Modified from www.sinnesphysiologie.de).

2.16.2 Assay for monitoring changes of cytosolic Ca²⁺

For Fura-2-based Ca^{2+} imaging, Cos-7, HEK293 or MEFs from wild-type and β3-deficient mice were cultured on glass coverslip previously coated with 1 mg/ml Poly-L-lysine for 30 min. Twenty four to forty eight hours after plating or after transfection, cells were washed with medium and loaded with 5 µM Fura-2 AM for 45 min in dark at 37°C. Briefly, 50 µg (special packaging) of Fura-2 AM were dissolved in 50 µl dimethylsulfoxid (DMSO) to prepare a stock solution at a final concentration of 1 mM. 5 µl of the stock solution was diluted in 1 ml cell culture media to achieve a final concentration of 5 µM Fura-2 AM. Following 45 min incubation, cells were washed with the Tyrode´s solution (Table 2-5) and the coverslips were placed into a circular open-bottom chamber supplemented with 300 µl Tyrode´s solution and mounted onto the stage of the Zeiss Axiovert S100 inverted microscope. Agonists were dissolved at higher concentrations as a stock solution which was added in appropriate volumes to the cell chamber to obtain the agonist's desired final concentrations.

Coverslips were analyzed on a monochromator equipped (Polychrome V, TILL-Photonics, Germany) inverted microscope (Axivert S100, Carl Zeisss, Germany) at 21°C. Every 2 s (0.5 Hz), Fura-2 fluorescence was alternately excited at 340 nm and 380 for 20 ms each and the emitted fluorescence were recorded with a cooled charge-coupled device (CCD) camera (Imago, TILL-photonics, Germany). After background correction, two images were calculated from 340 and 380 nm pictures. Cells were marked as regions of interest (ROI) and ratio changes of single ROIs were plotted versus time. Monochromator, camera acquisition, and analysis were controlled by Till-Vision software (Till-Photonics). Results in the present study are shown as ratio F340/F380.

2.17 Intracellular IP3 flash photolysis assay

Cos-7 cells transfected with the Cavβ3 cDNA and non-transfected as well as MEFs from wild-type and β3-deficient mice were plated on the same glass coverslip, respectively, to reduce differences in Fluo-4 and caged-IP3 loading. The transfected Cos-7 cells could be distinguished from non-transfected cells by their red fluorescence. The MEFs from wild-type mice were stained with a fluorescent dye (CellVue Claret Far Red Fluorescent Cell Linker kits, at final concentration of 4 µM for 2×10^7 cells according to the manufacturer protocol) prior to mixing them with non-stained MEFs from β3-deficient mice. Cells were loaded in the presence of 1 µM Fluo-4/AM (dissolved at 1 mM in DMSO containing 20 % (w/v) Pluronic) and 3 µM membrane permeable caged IP3 "ci-IP3/PM" (stock solution of 1 mM in DMSO) for 40 min (Figure 2-5). Then, glass coverslips were placed into a circular open-bottom chamber and supplemented with 200 µl Tyrode´s solution. The VT infinity confocal microscope was used for Ca^{2+} imaging *via* a 40X, NA 1.3, S-Fluor, oil immersion objective (Nikon, Düsseldorf, Germany). Fluo-4 was excited with the 491 nm laser and emission was collected through a 515 nm long-pass filter. Images (120x128 pixels) were recorded at 2 frames per second (fps) in a 4:4 binning model. Uncaging of IP3 was obtained by UV flash delivered by a 400 nm long-pass dichroic mirror. The trigger of UV flash and the image acquisition were automatically controlled by the software (This experiment was performed in collaboration with Dr. Xin Hui in the laboratory of Prof. Peter Lipp).
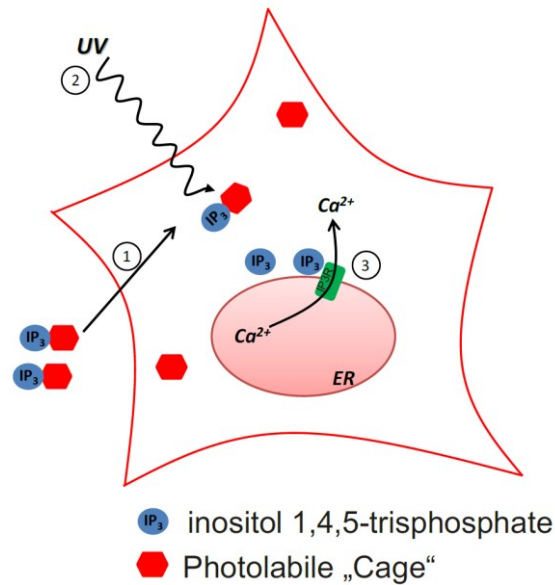
Figure 2-5. UV flash photolysis of caged IP3

UV flash photolysis of caged IP3 was performed in three steps: (1) loading of the cells with caged-IP3, (2) flash photolysis of the "cage" delivering IP3 and (3) binding of IP3 to the IP3-receptor inducing calcium release from the ER; the increase in cytosolic $[Ca^{2+}]$ is monitored by the calcium sensitive dye Fluo-4.

2.18 Cell migration assays

Two types of cell migration assays were employed. First the scratch assay, where MEFs from wild-type and β3-deficient mice were plated on glass slides at a cell density of 6×10^5 cells per slide in complete media and cultured for twenty four hours. Next day, at time point 0, a 200 µL pipette tip was used to perform scratches over the confluent monolayer. The remaining cells were washed with PBS and the media was replaced with media containing either 10 % FCS or 1 % FCS and cells were incubated at 37°C and 5 % CO_2. Different FCS concentrations were used to differentiate the contribution of cell proliferation to the migration behavior. At 10 % FCS we can see both cell

proliferation and migration, whereas at 1 % FCS we would minimize the cell proliferation and we can see mostly the cell motility. Cell migration was observed by phase contrast microscopy (BZ-8000, Keyence, Osaka, Japan) and the rate of cell migration after 6 hours were calculated relative to the initial scratched area. The scratch areas were recorded by BZ Analyzer Software on 16 measurements for each genotype and the experiments were repeated three times with three independent cell preparations, each from wild-type and Cavβ3-deficient mice.

2.19 Boyden chamber cell migration assay

The second migration assay, the Boyden chamber assay, also called filter membrane migration assay, trans-well migration assay or chemotaxis assay, was originally introduced by Boyden for leukocyte chemotaxis (Boyden, 1962). In this assay, two compartments separated by a porous membrane are filled with medium. Cells are plated on the membrane facing the upper compartment and are allowed to migrate through the pores to reach the membrane facing the lower compartment containing the attracting molecule. After a suitable incubation time, the porous membrane was cut, fixed and then stained. The number of migrating cells on the surface facing the lower compartment is determined.

Briefly, MEF cells (2×10^5 cells) from wild-type and β3-deficient mice were suspended in FCS-free medium and then added to the upper chamber of a chemotaxis polyvinylpyrrolidone-coated polycarbonate filters with 8 μm pore-size and the chambers were placed in a 24-well plate containing culture medium supplemented with 1% FCS where cells must migrate toward the FCS. Cells were incubated for 5 h at 37°C in a humidified atmosphere with 5 % CO_2. After incubation, non-migrated cells on the upper side of the insert were removed with a cotton swab and migrated cells,

which were adherent to the lower surface, were fixed with methanol and stained with Dade Diff-Quick (Dade Diagnostika GmbH, Munich, Germany). The number of these migrated cells was counted in 20 randomly chosen microscopic regions of interest (ROIs) at 20X magnification. Numbers are given as cells per ROI each from wild-type and Cavβ3-deficient mice. The experiment was repeated with three independent MEFs preparations.

2.20 Cell proliferation assay

2.20.1   Principle

The fluorescent-activated cell sorting (FACS) is a rapid and reliable method for determining cell count and cell viability and we used the Guava ViaCount assay. The ViaCount reagent differentially stains viable and non-viable cells based on their permeability to the DNA-binding dyes in the reagent, allowing the quantitative assessment of viable and non-viable nucleated cells present in a suspension. The system counts the stained nucleated events, then uses the forward scatter (FSC) properties to distinguish free nuclei and cellular debris from cells, to determine an accurate cell count (Figure 2-6 top panel). The ViaCount reagent contains two DNA-binding dyes. The first fluorochrome, LDS751, penetrates all cells and binds to DNA. LDS751 has an excitation wavelength of 543 nm and fluoresces at a maximum of 712 nm. The second, propidium iodide (PI), penetrates only dead cells where the plasma membrane is compromised and binds to the DNA. It has a 488 nm excitation wavelength and fluorescence is detected between 562-588 nm (Figure 2-6 lower panel).

2.20.2   Method

MEFs from wild-type and β3-deficient mice were plated at a density of 5×10^4 cells per Ø 3.5 cm sterile cell culture dishes with 2 ml media. On daily basis, cells were collected by trypsinization and MEFs suspension was diluted (1:10) with the Guava ViaCount reagent (Guava Technologies) in a total volume of 500 µl and incubated at room temperature for 5 min. Cell counts and viable and dead cell numbers were determined by using Guava ViaCount Software on the Guava easyCyte 8HT (Guava Technologies).
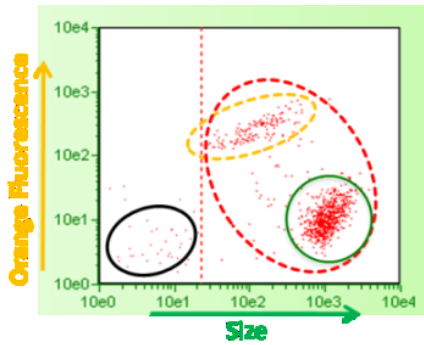
all nucleated cells show red fluorescence

orange fluorescence = dead cells

red cells which are not orange are living cells

LDS751

Propidium Iodide (PI)
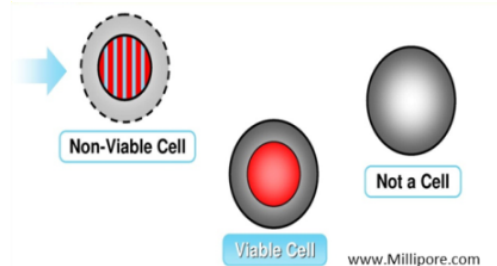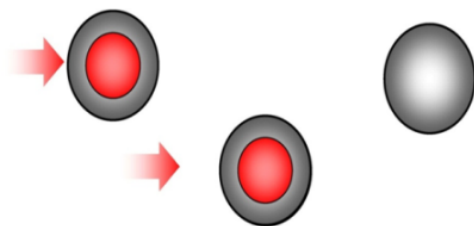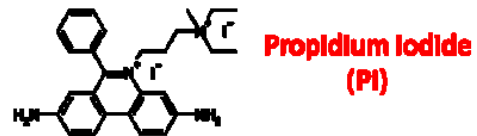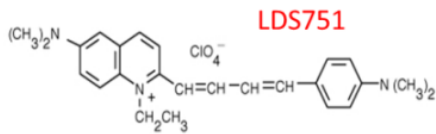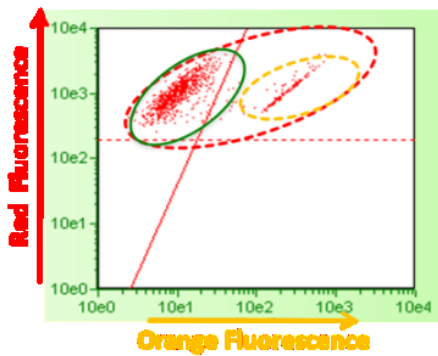
First fluorochrome **LDS751** enters **All Cells**, binds to DNA, excited at 543 nm wavelength and fluoresces at a maximum of 712 nm.

Second fluorochrome **PI** enters **Only Dead Cells**, binds to DNA, excited at 488 nm wavelength and fluorescence is detected between 562-588 nm.

Figure 2-6. Guava ViaCount assay, cell counting and viability

(Upper panel) Living cells show only the red fluorescence from LDS751 whereas the dead cells show the red from LDS 751 and the orange fluorescence from Propidium iodide. **(Lower panel)** ViaCount uses a mixture of two dyes which bind to DNA to provide a sensitive detection of viable and dead cells. LDS751 a permeant dye, which stains all the nucleated cells. Propidium iodide a membrane-impermeant dye stains only damaged cells (those with breaches in the plasma membrane) (Modified from Millipore).

2.21 Implantation of the dorsal skin-fold chamber and monitoring wound healing

Eight wild-type and Cavβ3-deficient C57BL6/N mice (8-12 weeks old) with a body weight of 23 to 27 g were used for the skin wound healing study. Animals were housed in single cages with a 12 hours light/dark cycle and had free access to standard laboratory food and water. The experiment was performed in accordance with the animal care guidelines issued by the Federal Republic of Germany.

Implantation of the dorsal skin-fold chamber and wounding were performed as described previously with the help of Dr. Matthias W. Laschke (Sorg et al., 2007). Mice were anesthetized by intraperitoneal injection of ketamine (90 mg/kg body weight; 10% ketamin) and xylazine (25 mg/kg body weight; 2% Rompun). After removing hair from the back of the mice the chamber was implanted and the dorsal skin fold was sandwiched between two symmetric titanium frames (Figure 2-7 A). The creation of a dermal wound was achieved after marking the area with a standardized biopsy punch (2 mm in diameter, pfm, Köln, Germany). The skin was only wounded at one side of the skin fold by removing the complete skin with epidermis and dermis. The final wound area was 3.5-4.5 mm^2. After the preparation, the wound was covered with a removable

glass coverslip incorporated in one of the titanium frames to prevent desiccation and infections. Animals tolerated the chamber well and showed no signs of discomfort or changes during sleeping and feeding habits.
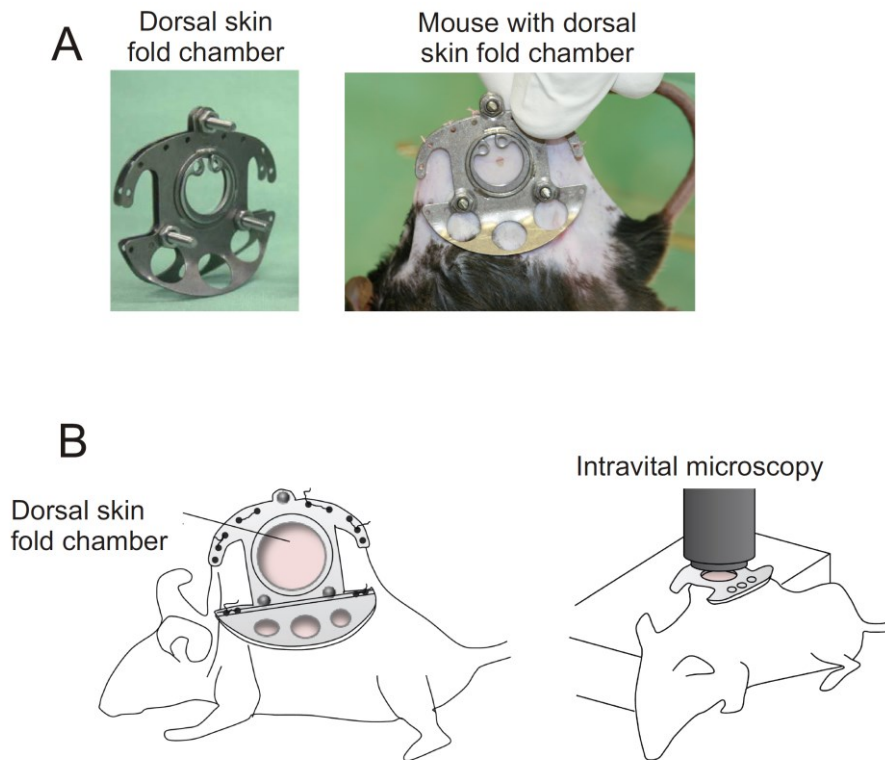
Figure 2-7. Dorsal skin fold chamber

(A, left) Window chamber consisting of two symmetric titanium frames for insertion into the dorsal skin fold of the mouse (chamber weight: ~2 g) (Laschke et al., 2011). **(A, right)** Wild-type mouse after shaving the hair of the back and mounting the dorsal skin fold chamber and applying a 2 mm Ø wound. **(B)** Schematic presentation showing the surgical approach to prepare dorsal skin fold chamber. On the right, the procedure to monitor skin wound closure under the microscope [Adapted from (Wong et al., 2011)].

2.21.1   Microscopic analysis of skin wound repair

Mice were anesthetized with ketamine/xylazine (90/25 mg/kg bw i.p.) and placed on a custom made plexiglas platform which was placed under a stereo microscope (Figure

2-7 B). At the time points indicated, the wound area was determined using a computer-assisted image analysis program (CapImage; Dr. Zeintl Software, Heidelberg, Germany) and plotted as percentage of the wound area immediately after injury.

2.21.2   Histology and immunohistochemistry

Skin samples from the whole wounded area from each mouse were cut after sacrificing the mouse. Skin samples were fixed overnight in 4 % formalin and then embedded in paraffin. Sections of 5 µm were cut and stained with Sirius red or anti-myeloperoxidase antibody.

For collagen fibers staining, deparaffinized sections were rinsed with distilled water and then incubated for 1 hour in Picro-sirius red solution containing (0.1 g Sirius red F3B, 100 ml saturated aqueous solution of picric acid "1.3 % in water"). After two times washing with 3 % acetic acid, sections were rinsed with distilled water. Then, sections were immersed in absolute ethanol 3 times for 3 min each and finally immersed in xylene 3 times for 3 min each.

For neutrophils staining, we used the anti-myeloperoxidase antibody as a marker. Deparaffinized sections were incubated for 17 hours at 60°C in 0.2 M boric acid, then immersed in 3 % H_2O_2 for 10 min. Sections were blocked with 3 % Normal Goat Serum (NGS) for 30 min followed by blocking with avidin (in PBS), then biotin (in PBS) for 15 min each to reduce non-specific background staining. Sections were then incubated with the primary antibody anti-MPO at room temperature for 45 min followed by 45 min incubation with a secondary goat anti-rabbit antibody and then 10 min incubation with horseradish peroxidase-avidin complex. The color reaction was developed by 3,3´-diaminobenzidine substrate (DAB) followed by counter staining with Hemalaun.

Pictures were acquired by using an inverted Zeiss microscope with a digital color camera using AxioVision software.

For Sirius red staining, we quantified collagen fibers stained in red by a macro in the AxioVision software where we had expressed collagen staining as a percentage of the whole image. For MPO staining we counted the number of positive cells on each slide and were expressed as a percentage of the total number of cells on the slide.

2.22 Collagen assay

Collagen in conditioned media was measured by a Sircol Collagen Assay (Biocolor Ltd, UK) following the manufacturer´s instructions. The Sircol dye is an anionic dye that specifically binds to the *(Gly-X-Y)$_n$* helical structure of mammalian collagen under assay conditions.

For our study, 2×10^5 MEFs from wild-type and Cavβ3-deficient mice were plated onto 6 well plates and cultured for 24 hours with medium supplemented with 10 % FCS. After 16 hours, medium was exchanged with medium supplemented with only 1% FCS and incubated for another 48 hours. Subsequently, medium was collected and subjected to the isolation and concentration steps. 1 ml Sircol dye was added to 100 µl samples and tubes were shaken for 30 min. After centrifugation of the sample/dye mixture, the supernatant comprising the unbound dye was removed and the pellet was dissolved in the alkali (0.5 M NaOH) to release Sircol dye from the collagen-dye complex. The absorbance of samples along with known collagen standards was measured by a Tecan infinite M200 plate reader at 540 nm.

2.23 F-actin/G-actin *in vivo* assay

2.23.1   Background

The actin protein contains 375 amino acids and runs at ~43 kDa in SDS-PAGE. It exists in two forms; the globular G-actin and the filamentous F-actin and the ratio of G- to F-actin changes during cell motility and can be determined (Flaherty et al., 1991).

2.23.2   Principle

Cells are lysed in the F-actin stabilization buffer, where G-actin molecules are solubilized but not the F-actin. After centrifugation, F-actin is pelleted and the G-actin stays in the supernatant. Both fractions are run on a SDS-PAGE system and actin is quantified by Western blot (densitometric analysis) using anti-actin antibody.

2.23.3   Method

MEFs $2 \cdot 10^5$ cells from wild-type and Cavβ3-deficient mice were grown on cell culture dishes (Ø 3.5 cm) for 24 hours. Cells were lysed in F-actin stabilization buffer (phalloidin 1x, ATP 1 mM and protease inhibitor cocktail) and homogenized by using a 200 µl pipet tip. After 10 min incubation at 37°C, 100 µl of each sample was centrifuged at 350 xg for 5 min to pellet down unbroken cells and cellular debris. The supernatants were transferred into ultracentrifuge tubes and centrifuged at 100.000 xg for 60 min at 37°C to separate the filamentous F-actin (pellet) from the monomer globular G-actin (supernatant). The supernatants were transferred into fresh tubes labeled as "G-actin fraction" and kept on ice. Pellets were re-suspended in 100 µl F-actin-depolymerization buffer containing 5 M urea, incubated on ice for 1 hour. To improve suspension of the pellet, the slurry was pipetted up and down every 15 min. 25 µl of 5-fold concentrated SDS-denaturing buffer was added to each of the pellet fraction (F-actin) and supernatant fraction (G-actin). Samples were either stored frozen at -20°C or subjected

directly to actin quantitation by SDS-PAGE and Western blot. Equal amounts of proteins were applied per lane. Western blot was performed as described in section 2.7. Actin bands stained by antibodies from each fraction and each genotype were quantified by densitometric analysis using the AIDA Image Analyzer v.4.14 and plotted as G-/F-actin ratio.

2.24 Statistical analysis

Data are presented as mean ± SEM of n independent experiments. Igor Pro 5.01 (Wavemetrics, Oregon, USA) was used for Ca^{2+} imaging data analysis. Corel DRAW X4 Version 14.0 was used for figure labeling. Microsoft excel 2010 was used for statistical analysis and significance was assessed using the Student's t-test or ANOVA followed by Bonferroni test with $P<0.05$ (*), $P<0.005$ (**), $P<0.001$ (***) considered to be significant.

3 Results

3.1 Cavβ3 role in Ca^{2+} homeostasis

3.1.1 The cytoplasmic Cavβ3 modulates agonist- induced Ca^{2+} release

Cavβ subunits are essential for trafficking the ion conducting pore α1 of voltage-gated calcium channels to the plasma membrane. They also modulate kinetics of the Ca^{2+} currents. However, our group in collaboration with Per-Olof Berggren at the Karolinska Institute in Stockholm has shown that deletion of Cavβ3 subunit gene in pancreatic β-cells did not have any effect on voltage-gated Ca^{2+} currents neither on density nor on kinetics. Instead, the frequency of glucose induced Ca^{2+} oscillations were increased (Berggren et al., 2004). From these data it was concluded that 1) other Cavβ subunits are responsible for trafficking the Ca^{2+} channel pore and modulating current kinetics. In fact, other Cavβ proteins present in pancreatic β-cells are Cavβ2 and Cavβ4. 2) It was assumed that Cavβ3 might serve different Ca^{2+} channel independent functions, including contribution to the increased frequency of Ca^{2+}-oscillations. The oscillations of cytosolic Ca^{2+} concentrations depend on the interplay of Ca^{2+} entry to the cytosol both from extracellular space and intracellular stores. With the aim to understand the mechanism behind this observation and to identify new Cav-independent roles of β3 protein, we started looking for subcellular localization of Cavβ3 protein. By expressing Cavβ3 cDNAs tagged with the cDNAs encoding the fluorescent proteins eGFP (green), eRFP (red) and YFP (yellow) in HEK293 and in Cos-7 cells, we started to study the localization by confocal microscopy twenty four to forty eight hours after transfection.

As shown in Figure 3-2 A and C the fluorescence of GFP tagged Cavβ3 was distributed throughout the HEK293 and Cos-7 cells. Even when the Cavβ3 cDNA was co-expressed with the cDNA of the voltage-gated calcium channel pore forming subunit (α1c), the Cavβ3-GFP fluorescence was still distributed all over the cell (Figure 3-2 A and C right images).

To study the effect of the cytoplasmic Cavβ3 subunit on cytosolic [Ca^{2+}], we expressed the Cavβ3-IRES-GFP cDNA (Figure 3-1) in HEK293 and Cos-7 cells. The GFP protein in this experiment was not fused to the β3 protein but was used as a reporter to control the efficiency of Cavβ3 cDNA transfection. As a second control, proteins from transfected HEK293 and Cos-7 cell lysate were separated by SDS-PAGE, transferred into nitrocellulose filters and then incubated with anti-Cavβ3 antibody. As shown in Figure 3-2 B and D, the Cavβ3 protein (55 kDa) was detectable in transfected HEK293 and Cos-7 cells without any sign of protein degradation or cleavage. Non-transfected HEK293 cells might contain a very low amount of endogenous Cavβ3 protein, whereas non-transfected Cos-7 cells did not show any endogenous Cavβ3 protein.

Next we started to study whether Cavβ3 has any effect on changes of cytosolic [Ca^{2+}]. For that purpose we measured agonist-induced changes of cytosolic [Ca^{2+}] in the absence of extracellular Ca^{2+}. Cells were loaded with the Ca^{2+} indicator Fura-2 and changes were monitored in cells revealing green fluorescence (which do express the Cavβ3 cDNA) and as control cells we used HEK293 or Cos-7 cells transfected with the cDNAs encoding the green fluorescent proteins eGFP only. As agonist we used carbachol and ATP which couple to muscarinic receptors endogenously expressed in HEK293 cells and P2Y receptors endogenously expressed in Cos-7 cells. Basal cytosolic [Ca^{2+}] was not different in HEK293 cells (expressing the Cavβ3 cDNA and controls) and in Cos-7 cells (expressing the Cavβ3 cDNA and controls). After addition

of the agonist carbachol (1 mM) or ATP (10 µM) the cytosolic [Ca^{2+}] increased because of IP3-dependent release of Ca^{2+} from intracellular stores. The agonist-induced increase of cytosolic Ca^{2+} was quantified in two ways, by determining 1) the peak amplitude (Peak of [Ca^{2+}]-Basal [Ca^{2+}]) and 2) by calculating the area under the curve (AUC). Importantly, the peak amplitude as well as the area under the curve (Figure 3-2 F and H) were significantly reduced in cells containing the Cavβ3 protein compared to control cells which were not transfected with the β3 cDNA. These results indicate that the Cavβ3 protein interferes with the Ca^{2+} release induced by the G-protein coupled muscarinic and purinergic receptors.
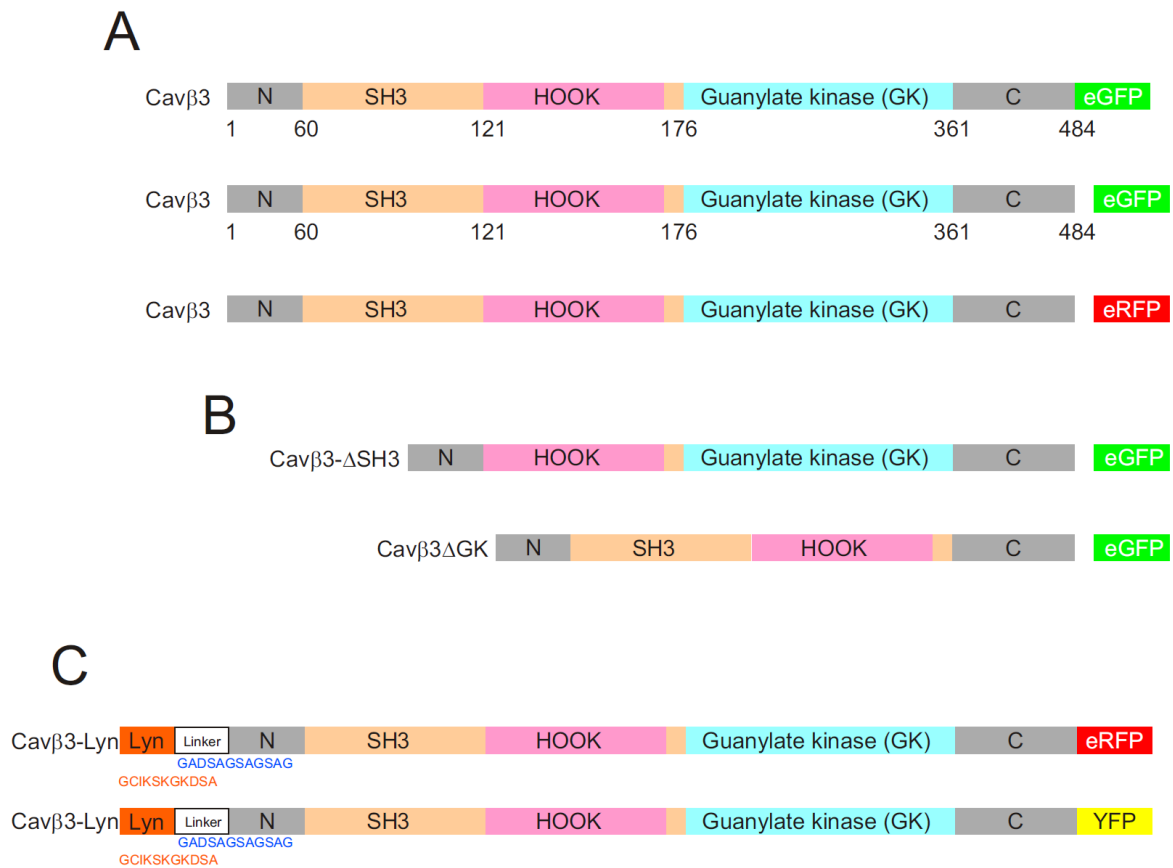
Figure 3-1. Schematic depiction of Cavβ3 constructs

(A) The Full length Cavβ3 cDNA (1455 bp) was expressed as Cavβ3-eGFP-fusion cDNA costruct (top), or as part of a bicistronic cDNA construct Cavβ3-IRES-eGFP (middle) or Cavβ3-IRES-eRFP (bottom). **(B)** The cDNA of Cavβ3 deletion mutants lacking either SH3 domain (Cavβ3-ΔSH3) or GK domain (Cavβ3-ΔGK) were subcloned in the pCAGGS-IRES-eGFP vector. **(C)** The cDNA encoding the amino terminal 12 amino acids of Lyn kinase (H$_2$N-MGCIKSKGKDSA-COOH) followed by 36 nt encoding the linker (white, GADSAGSAGSAG) was subcloned in front of and in frame with the Cavβ3 cDNA. This Lyn-linker cDNA was kindly provided by Byung-Chang Shu (Suh et al., 2012). The cDNA of the Lyn-linker-Cavβ3 cDNA was then ligated to the cDNA of either eRFP or YFP, respectively. For that purpose the STOP codon of the β3 cDNA had to be removed first.
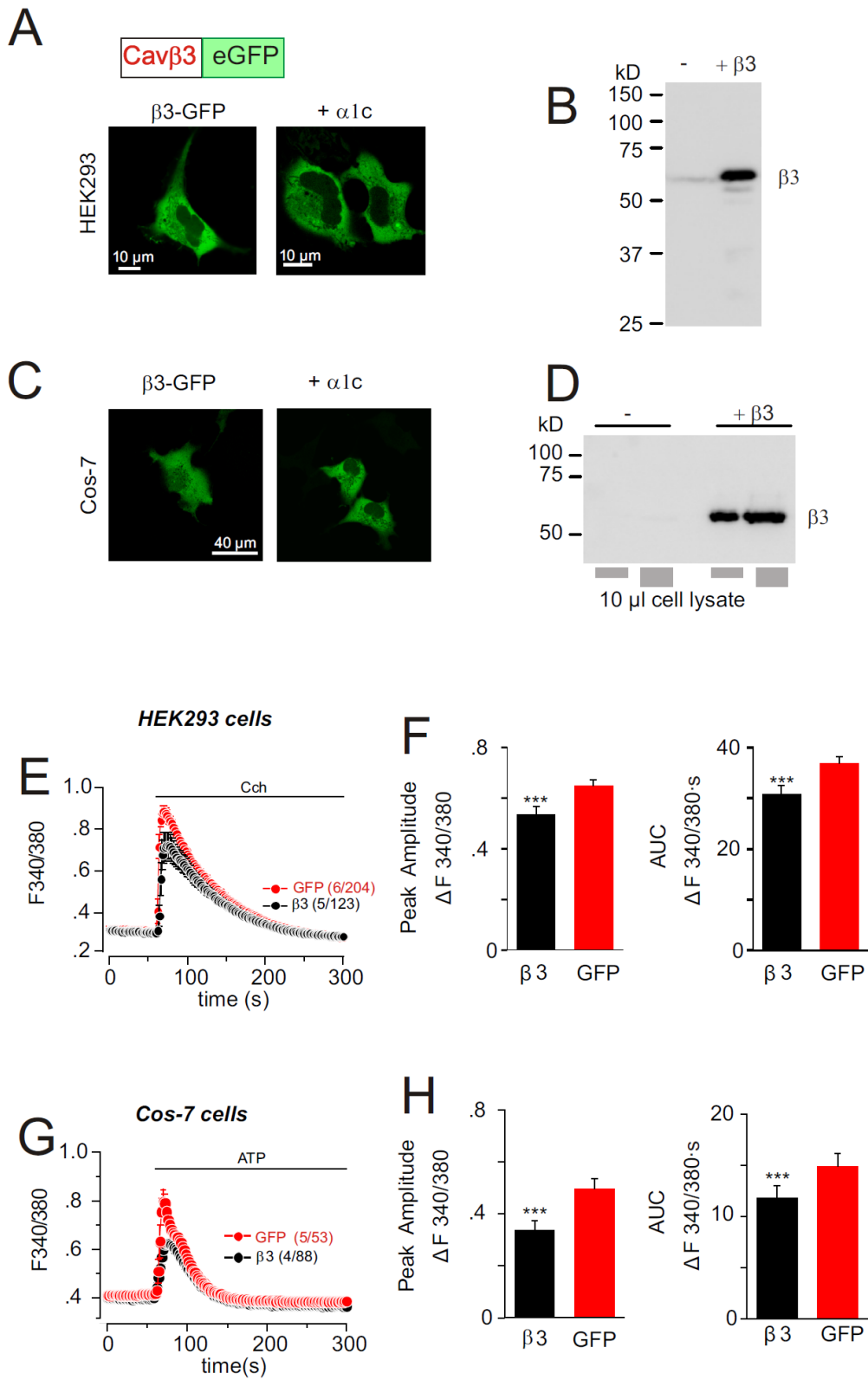
Figure 3-2. Decreased agonist-induced calcium release in Cavβ3-cDNA expressing cells

(A, C) Confocal images of HEK293 cells (A) and Cos-7 cells (C) expressing the GFP tagged Cavβ3 cDNA in the presence (right) or absence (left) of the Cav1.2 (α1) cDNA. Pictures were taken twenty four hours after transfection. **(B, D)** Western blot of Cavβ3 protein in HEK293 cells (B) and Cos-7 cells (D): (-), non-transfected or (+β3), transfected with the Cavβ3 cDNA. **(E, G)** Fura-2 ratio over time before and after addition of agonist (HEK293 cells, Carbachol, Cch, (E); Cos-7 cells, ATP (G)) in the absence of extracellular Ca^{2+}. Red trace: Control; cells were transfected with the GFP cDNA only. Black trace: cells were transfected with the Cavβ3-IRES-GFP cDNA (because of the possible interference of the GFP-fluorescence with Fura-2, GFP cDNA transfected cells were used as controls). Each trace represents the average of all transfected (green fluorescent) cells. **(F, H)** Statistical analysis of the peak amplitude (left bar graph) and area under the curve "AUC" (right bar graph); **(F)** 204 control cells recorded in 6 experiments (red bars) and 123 Cavβ3 transfected cells recorded in 5 experiments (black bars). **(H)** 53 control Cos-7 cells recorded in 5 experiments (red bars) and 88 Cavβ3 transfected cells recorded in 4 experiments (black bars), x̄ ± S.E.M (*** $p < 0.001$).

3.1.2 Cavβ3 subunit desensitizes the IP3R to IP3

To understand whether the Cavβ3 protein interferes with the receptor signal transduction including the receptor, G-protein and phospholipase C or directly modulates IP3R channel function, we designed an experiment to differentiate between these two hypotheses. Cells were loaded with the membrane permeable caged-IP3 and subsequently UV light was applied to uncage IP3 molecules which showed activation of the IP3-receptor. The Ca^{2+} released by the IP3-receptor was monitored by Fluo-4 (Figure 3-3 A). Cos-7 cells were plated on glass coverslips and transfected with Cavβ3-IRES-RFP cDNA (Figure 3-1). Twenty four to forty eight hours after transfection, cells were loaded with the Ca^{2+} indicator Fluo-4 and the membrane

permeable caged-IP3. Transfected cells expressing RFP (as a reporter for transfection) and non-transfected cells (showing no red florescence) plated on the same coverslip were exposed to UV light for photolysis of the cage and release of IP3. Intracellular Ca^{2+} levels were measured simultaneously with UV flashes of 0.625, 2.5, 10 and 40 J which were applied to different cells. The presence of transfected cells (red fluorescence) and non-transfected cells (no red fluorescence) on the same coverslip excluded different loading by Fluo-4 and caged-IP3. For each amount of energy 0.625, 2.5, 10 and 40 J, independent coverslips were employed. The peak amplitude of IP3-dependent Ca^{2+} release monitored by Fluo-4 was quantified and plotted versus the amount (Log μJ) of flash energy generating an energy dose-Ca^{2+} amplitude response curve. As expected, the higher the amount of energy the more IP3 is uncaged, monitored indirectly by the increase of cytosolic Ca^{2+}. Apparently, at very low energy input (0.625 J) no increase in cytosolic Ca^{2+} is detectable (Figure 3-3 B, first pannel). At 2.5 J, only the control cells (not containing the β3 protein) show increased cytosolic Ca^{2+} whereas when applying higher amounts of energy (10 and 40 J) both types of cells (control and β3 containing cells) respond in different amplitudes.

The results (Figure 3-3) show that in the presence of the Cavβ3 protein, the dose-response curve is shifted to the right indicating that the Cavβ3 protein modulates the release of Ca^{2+} by IP3 independently of the upstream signal transduction pathway. The data of Figure 3-3 indicate that Cavβ3 desensitizes cell for low concentrations of IP3.
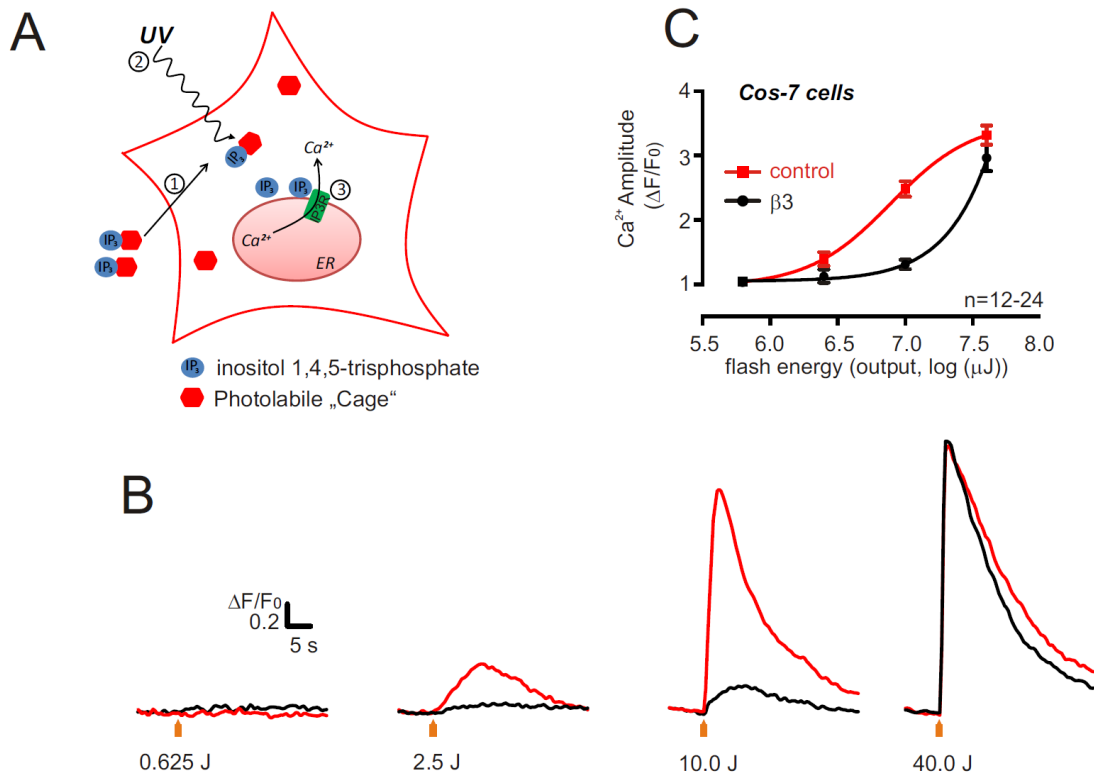
Figure 3-3. Decreased IP3-receptor sensitivity for IP3 in Cavβ3-expressing cells

(A) Scheme of experiment: (1) loading of a cell with caged-IP3, (2) flash photolysis of caged-IP3 and release of IP3 (3) binding of IP3 to the IP3-receptor inducing calcium release which is measured by the calcium sensitive dye Fluo-4. **(B)** Representative Ca^{2+}-release traces ($\Delta F/F_0$) in Cos-7 cells loaded with Fluo-4 (1 μM) and caged-IP3 (3 μM) and transfected with the Cavβ3-IRES-RFP cDNA (black traces) or control non-transfected cells (red traces). Non-transfected and transfected cells were plated in the same coverslip and were distinguished by the presence of red fluorescence (β3 cDNA expressing cells) or its absence (non-transfected cells). UV light flashes of 0.625, 2.5, 10 and 40 J were applied to uncage IP3. **(C)** Energy dose-calcium peak amplitude response curve (fluorescence ratios ($\Delta F/F_0$) plotted as a function of log [flash energy in μJ]) shows a decrease in the sensitivity of the IP3R in the presence of Cavβ3 subunit compared to control cells. Each data point is an average of 12-24 cells ($\bar{x} \pm$ S.E.M).

3.1.3 Cavβ3 in non-excitable mouse embryonic fibroblasts "MEFs"

So far the experiments show that in Cos-7 cells Cavβ3 has an effect on IP3-dependent Ca^{2+}-release. Next we wanted to know whether this effect is also detectable "*in vivo*" in acutely isolated cells. To this end we first set out to identify a cell type which does express the cacnb3 gene but lacks functional voltage gated Ca^{2+} entry. Cells which meet these requirements should be most suitable to study calcium channel independent functions of Cavβ3. We started with fibroblasts, especially mouse embryonic fibroblasts. By Western blot we could identify the Ca^{2+} channel Cavβ2 and Cavβ3 proteins in MEFs cell lysates (Figure 3-4 A). In protein samples obtained from Cavβ3-deficient fibroblasts, the β3 protein is absent (Figure 3-4 A). Next, we depolarized the cells by adding potassium at 74 mM concentration in the presence of extracellular Ca^{2+} (2m M) in order to identify depolarization/voltage-dependent Ca^{2+} entry. However, depolarization does not induce Ca^{2+} entry, neither in wild-type nor in β3-deficient cells. To get prove that the challenge of cells in the presence of high potassium induces depolarization-dependent Ca^{2+} entry we used two independent cell systems, HEK293 cells expressing the cDNAs of Cav1.2 and Cavβ3 (Figure 3-4 C) and acutely isolated cardiomyocytes from mouse (Figure 3-4 D). In both cell types, potassium dependent-depolarization shows a clear Ca^{2+} influx. In addition, this Ca^{2+} influx was decreased in the presence of the L-type Ca^{2+} channel blocker Nimodipin at a concentration of 2 μM. From these data we conclude that MEFs appear to be a suitable model system to characterize calcium channel independent functions of Cavβ3. They do contain Cavβ3 proteins but lack detectable depolarization-induced Ca^{2+} entry function. Therefore we established the isolation and culture of mouse embryonic fibroblasts (MEFs) and started to study the effects of β3 on cytosolic Ca^{2+} in wild-type MEFs and used β3-deficient MEFs as controls.
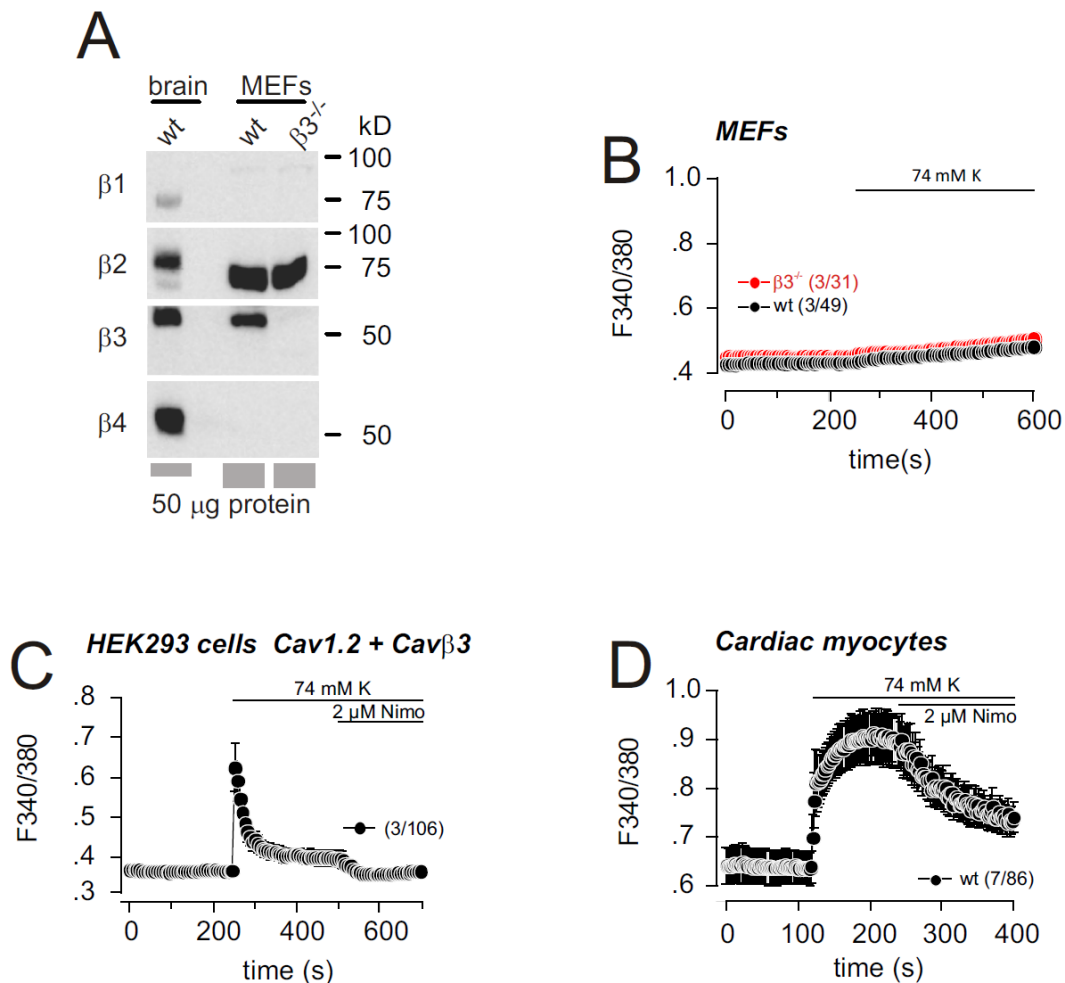
Figure 3-4. Cavβ subunits in primary mouse embryonic fibroblasts (MEFs)

(A) Western blot: Protein extracts from brain (50 µg per lane) and MEFs (100 µg per lane) using Cavβ1, Cavβ2, Cavβ3 and Cavβ4 specific antibodies. The β1, β2, β3 and β4 proteins are present in wild-type brain, the β2 and β3 proteins in wild-type MEFs, and the β3 protein is absent in Cavβ3-deficient (β3$^{-/-}$) MEFs. **(B)** Fura-2 (F340/380) ratiometric traces in the absence and presence of high extracellular potassium (74 mM K$^+$) with 2 mM extracellular Ca^{2+} being present throughout in wild-type MEFs (black traces, n = 49 cell recorded in 3 experiments) and in β3-deficient MEFs (red traces, n = 31 cells recorded in 3 experiments). No depolarization dependent Ca^{2+} influx was detectable. **(C, D)** Fura-2 (F340/380) ratiometric traces in the absence and during the application of 74 mM K$^+$ in HEK293 cells expressing the cDNAs of Cav1.2 α1 and Cavβ3 (C, n = 106 cells recorded in 3 experiments) and cardiomyocytes (D, n = 86 recorded in 7 experiments) showing potassium-depolarization induces Ca^{2+} influx in both cell types which was inhibited in the presence of 2 µM Nimodipin.

3.1.4 Agonist-induced increase of cytosolic Ca^{2+} is modulated by Cavβ3 in mouse embryonic fibroblasts

To investigate the role of the Cavβ3 protein on cytosolic Ca^{2+} we used MEFs from early passages up to the fifth passage at most and we loaded cells with Fura-2. Next we tested whether cytosolic Ca^{2+} increased when several agonists of plasma membrane receptors were applied (Figure 3-5 E). Experiments were performed with wild-type and β3-deficient MEFs in the absence of extracellular Ca^{2+}. Under these conditions, only the agonist-induced release of Ca^{2+} from intracellular stores is measurable. The following agonists were used: vasopressin, ATP, LPA, bradykinin, serotonin, thrombin and histamine. Only bradykinin (10 µM) and Lysophosphatidic acid (LPA) (20 µM) induced consistently Ca^{2+} release from the ER (Figure 3-5 A and C respectively). Bradykinin and LPA are agonists of G-protein coupled BK- and LPA-receptors, respectively (Wettschureck and Offermanns, 2005), which upon stimulation activate PLC-β. Activated PLC-β hydrolysis the phosphatidyl inositol 4,5-bisphosphate (PIP2) into inositol 1,4,5-trisphosphate (IP3) and diacylglycerol (DAG). The IP3 binds to the IP3R, the channel opens resulting in Ca^{2+} release from the endoplasmic reticulum "ER" (Figure 3-5 A). Prior to stimulation with BK or LPA, resting cytosolic Ca^{2+}, calculated from the ratio of Fura-2 signals at 340 nm and 380 nm excitation wavelengths, are not significantly different in wild-type and β3-defficent MEFs (Figure 3-5 A, B, C, D). The reason why other agonists do not result in an increase of cytosolic Ca^{2+} although they also stimulate GPCRs coupled to PLC pathways are not known. Most probably, embryonic fibroblasts at very early passages express only small repertoire of GPCRs including the receptors for bradykinin and LPA. Strikingly, application of 10 µM bradykinin or 20 µM LPA induced a much larger Ca^{2+} release in β3-deficient MEFs compared to control wild-type MEFs (Figure 3-5 A, C). Comparing the peak amplitude

(difference between the peak and the basal Ca^{2+} levels [ΔF 340/380]) and the area under BK- and LPA-induced Ca^{2+} release curve (Figure 3-5 B, D) indicate that both were significantly increased in Cavβ3-deficient MEFs compared to control cells. In summary these data indicate that β3 subunit negatively modulates the IP3-releasable Ca^{2+} in primary mouse fibroblasts. These results are similar to these obtained in Cos-7 cells where expression of the β3 cDNA decreases agonist evoked Ca^{2+} release compared to non-transfected Cos-7 cells, which lack endogenous Cavβ3 (Figure 3-2).

.
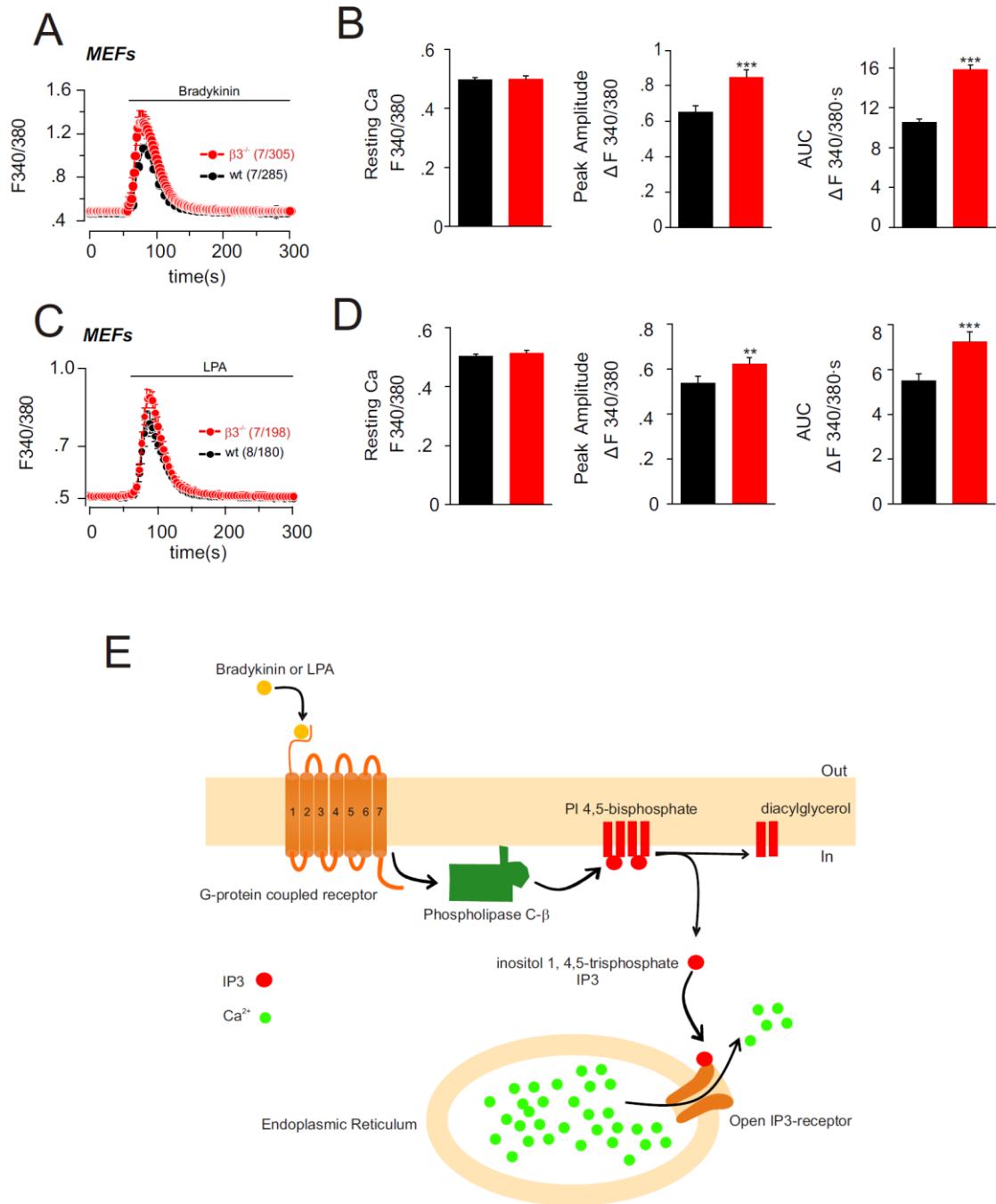
Figure 3-5. Increased agonist-induced calcium release in β3-deficient MEFs

(A and C) Fura-2 (F340/380) ratiometric traces in the absence of extracellular Ca^{2+} before and after addition of bradykinin 10 µM (A) or LPA 20 µM (C) in wild-type MEFs (black traces) and β3-deficient MEFs (red traces). **(B, D)** Statistical analysis of the

resting Ca^{2+} levels (left panel), peak amplitude (middle panel) and the area under the curve AUC (right panel) of 285 wild-type cells recorded in 7 experiments (black bars) and 305 β3-deficient cells recorded in 7 experiments (red bars) stimulated with 10 µM bradykinin (B). 180 wild-type cells recorded in 8 experiments (black bars) and 198 β3-deficient cells recorded in 7 experiments (red bars) stimulated with LPA (D) (x̄ ± S.E.M,** P<0.005, *** P<0.001; student t-test). Bradykinin and LPA mediated calcium release is significantly higher in β3-deficient MEFs. **(E)** Scheme of Gq protein-coupled receptor activation pathway. Bradykinin or LPA receptors stimulation activates PLC-β and thereby cleavage of PIP2 into DAG and IP3. IP3 binds to the IP3R inducing IP3R channel opening and calcium release from the endoplasmic reticulum (ER).

3.1.5 Calcium levels in intracellular stores and store operated calcium entry in wild-type and β3-deficient fibroblasts

So far the results point to agonist-induced Ca^{2+} release mediated by IP3 and β3 acts as a negative regulator of this process. Could other mechanisms be involved?

Previously it has been reported by Tu and colleagues (Tu et al., 2006) that MEFs do not respond to caffeine, excluding the possibility of ryanodine receptors being involved in our observation. It might be that wild-type and β3-deficient MEFs differ in the filling state of the ER Ca^{2+} stores. To address this question, we compared the ER Ca^{2+} levels in cells from both genotypes in the next experiment by adding 1 µM thapsigargin (Figure 3-6 A). Thapsigargin irreversibly inhibits the sarcoplasmic/endoplasmic reticulum calcium ATPase (SERCA) activity. This pump transports Ca^{2+} which leaks out of the ER back into the ER. When this pump is inhibited, cytosolic Ca^{2+} is increased via Ca^{2+} leak channels which so far have not been identified. This leakage is independent of the IP3R activity (Figure 3-6 E). Application of 1 µM thapsigargin leads to cytosolic Ca^{2+} elevation which was not different in wild-type and β3-deficient MEFs

(Figure 3-6 A). We integrated the area under the thapsigargin induced Ca^{2+} increase for cells of both genotypes. Like resting Ca^{2+} levels, the thapsigargin-induced cytosolic Ca^{2+} increase, measured as area under the curve, was not different (Figure 3-6 B). Thus the lack of $Cav\beta3$ protein has no effect on the releasable Ca^{2+} pool arguing against the possibility of $Cav\beta3$ modulation of the ER Ca^{2+} filling state.

In many cell types depletion of intracellular Ca^{2+} stores leads to activation of store operated Ca^{2+} entry. Since the Ca^{2+} release upon receptor activation is more pronounced in $\beta3$-deficient MEFs compared to the wild-type, we suspected that store-operated Ca^{2+} entry might be different in these cells. To distinguish between the increase of the cytosolic Ca^{2+} through Ca^{2+} release from intracellular stores or Ca^{2+}-entry from the extracellular space, we employed a classical Ca^{2+} readdition protocol (Bird et al., 1991). In the first run, the cells are incubated in the absence of extracellular Ca^{2+}, and the stores are emptied by application of an appropriate agonist, LPA in my experiment (Figure 3-5 C). After return of the cytosolic Ca^{2+} to the baseline, extracellular Ca^{2+} (5 mM) is added to cells again. Now a second increase of cytosolic Ca^{2+} occurs, most probably by Ca^{2+}-entry from the extracellular space (Figure 3-6 C). The peak amplitude and the area under the curve of this second increase of cytosolic Ca^{2+} is not different in wild-type compared to $\beta3$-deficeint MEFs (Figure 3-6 C and D).
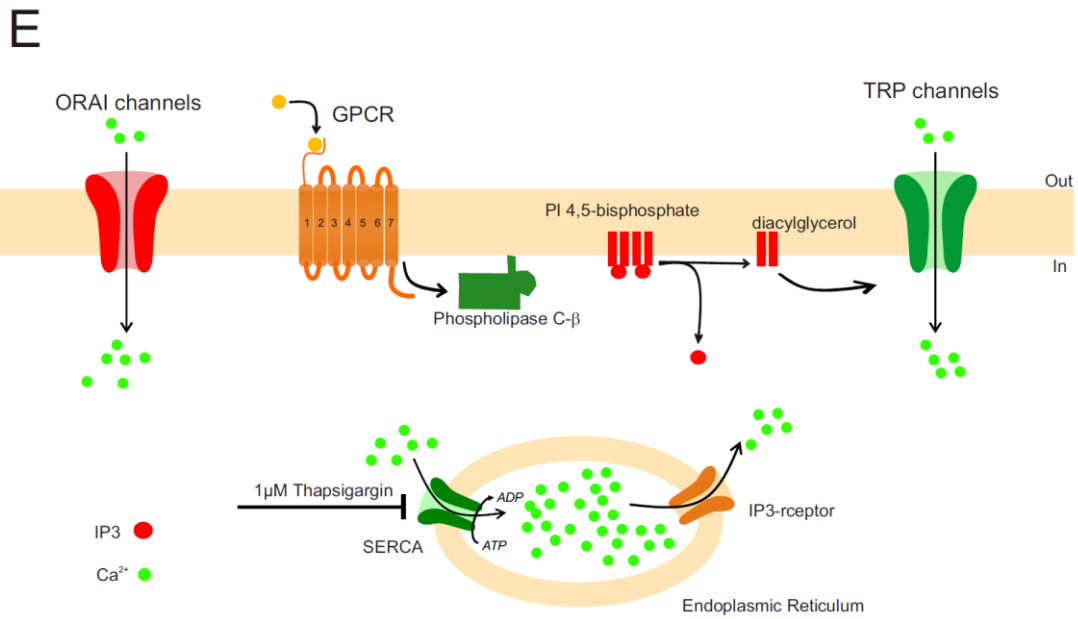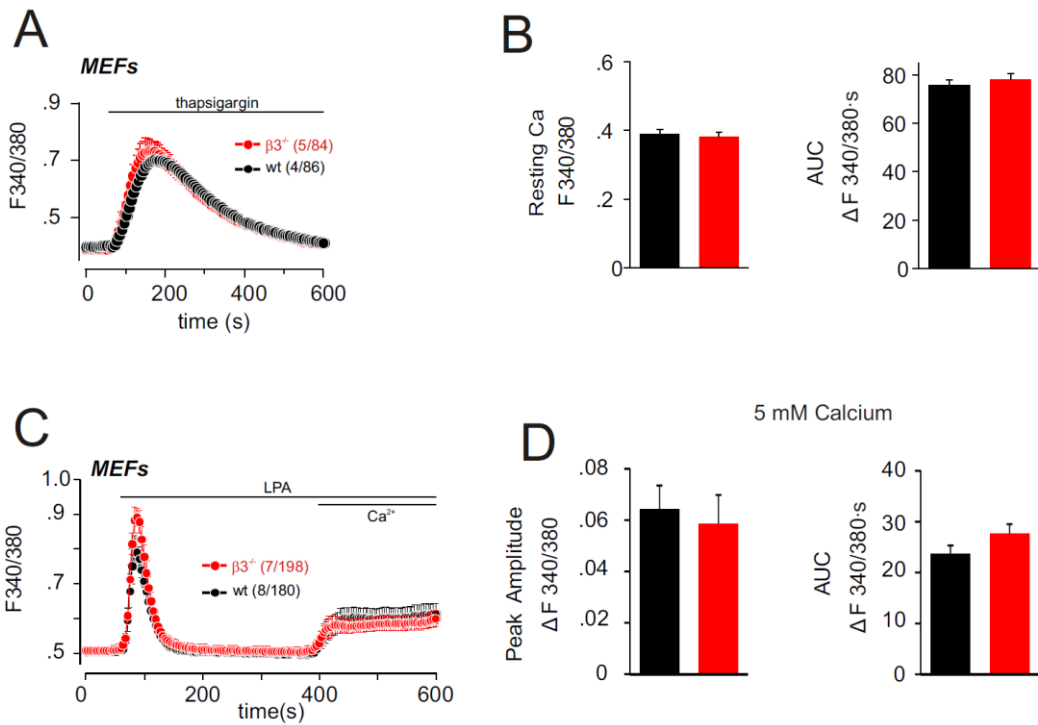
Figure 3-6. Thapsigargin-induced calcium release and store-operated calcium entry in fibroblasts

(A) Fura-2 (F340/380) ratiometric traces in the absence of extracellular Ca^{2+} before and after the addition of thapsigargin (1 µM) in wild-type (black traces) and β3-deficient MEFs (red traces). **(B)** Statistical analysis of the resting calcium levels (left bar graph) and the area under the curve "AUC" (right bar graph) of TG-induced passive calcium release in 86 wild-type cells recorded in 4 experiments (black bars) and 84 β3-deficient cells recorded in 5 experiments (red bars), x̄ ± S.E.M. Passive calcium release in response to the inhibition of SERCA pump by TG was not influence by the deletion of β3 protein **(C)** Fura-2 (F340/380) ratiometric traces in the absence of extracellular Ca^{2+} before and after addition of LPA 20 µM [shown in Figure 3-5] and then the re-addition of 5 mM extracellular Ca^{2+} in wild-type MEFs (black traces) and β3-deficient MEFs (red traces). **(D)** Statistical analysis of the Ca^{2+} peak amplitude (left bar graph) and the area under the curve AUC (right bar graph) of 180 wild-type cells recorded in 8 experiments (black bars) and 198 β3-deficient cells recorded in 7 experiments (red bars) in response to the 5 mM extracellular Ca^{2+} re-addition (x̄ ± S.E.M). **(E)** Scheme explaining the store operated calcium entry pathway. Upon store depletion by inhibiting the SECA pump using thapsigargin, ORAI channels get activated leading to Ca^{2+} entry from the extracellular space. Activation of GPCRs results in IP3 and DAG production. IP3 activates IP3R channels leading to store depletion and thereby activation of ORAI channels. DAG in the plasma membrane might activate TRP channels leading to Ca^{2+} entry from the extracellular space.

3.1.6 Bradykinin- and ATP-induced Ca^{2+} mobilization depends on Phospholipase C activity

The activation of B1 and B2 receptors by bradykinin as well as activation of some P2Y-receptors by ATP leads o activation of PLC followed by IP3 formation and release of Ca^{2+} from the ER (Wettschureck and Offermanns, 2005). To evaluate the contribution of PLC in primary MEFs and Cos-7 cells, we used an inhibitor of PLC (U73122), an aminosteroid derivative. As a control we applied a structural analogue (U73343) which has negligible activity as PLC inhibitor (Figure 3-7 A) (Bleasdale et al., 1989).

Fura-2 loaded MEFs (Figure 3-7 A) or Cos-7 cells (Figure 3-7 B) were pre-incubated for 10 min in the presence of the PLC-inhibitor U73122 (10 µM) or its inactive analogue U73343 (10 µM). In the absence of extracellular Ca^{2+}, Cells pretreated with the U73122 or U73343 show similar basic Ca^{2+} levels. Bradykinin or ATP application induced Ca^{2+} release in U73343 (the inactive analogue) treated MEFs or Cos-7 cells but not in cells pretreated with 10 µM PLC-inhibitor U73122 (Figure 3-7 A and B). The results show that bradykinin and ATP induced Ca^{2+} release requires PLC activity.
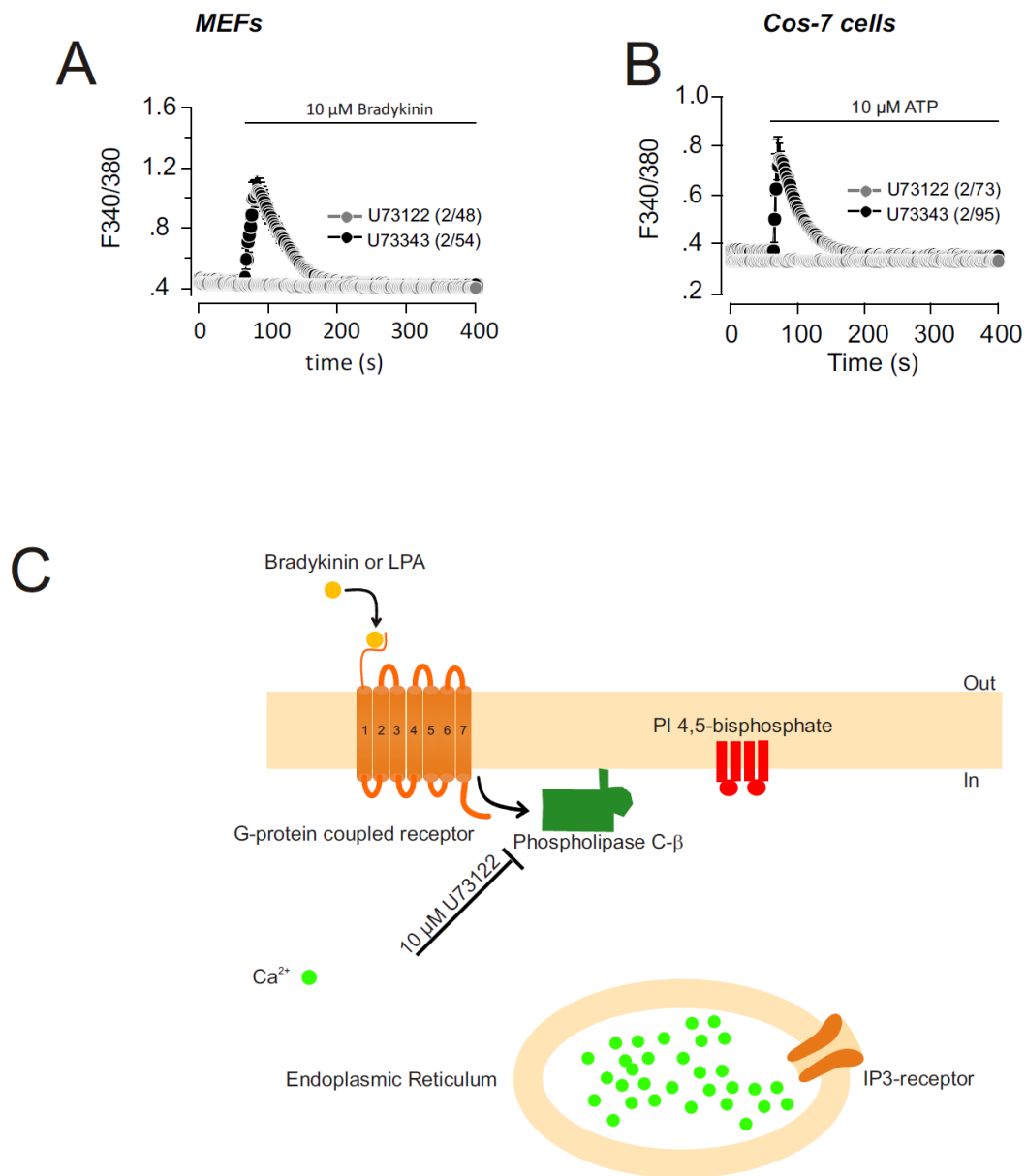
Figure 3-7. Bradykinin and ATP induced calcium release depends on phospholipase C activity

(A) Fura-2 ratiometric traces in the absence of extracellular Ca^{2+} before and after addition of bradykinin 10 µM in MEFs pretreated with the PLC-inhibitor U73122 for 10 min (gray traces, n = 48 cells recorded in 2 experiments) or pretreated with its inactive analogue U73343 (black traces, n = 54 cells recorded in 2 experiments). **(B)** Fura-2 ratiometric traces in the absence of extracellular Ca^{2+} before and after addition of ATP 10 µM in Cos-7 cells pretreated with the PLC-inhibitor U73122 for 10 min (gray traces,

n = 73 cells recorded in 2 experiments) or pretreated with its inactive analogue U73343 (black traces, n = 95 cells recorded in 2 experiments) in response to ATP (10µM). In the presence of the PLC inhibitor U73122, Ca^{2+} release in response to bradykinin and ATP was completely abolished indicating that the Ca^{2+} in response to these agonists is PLC dependent. **(C)** Scheme showing the inhibition of PLC activity by U73122 and thereby inhibition of the agonist-induced calcium release.

3.1.7 Enhanced IP3R sensitivity to IP3 in β3-deficient MEFs

So far the experiments performed in wild-type and β3-deficient MEFs (Figure 3-5) indicate that the Cavβ3 protein negatively modulates agonist induced Ca^{2+} release. Next, we measured IP3-releasable Ca^{2+} in wild-type and β3-deficient MEFs by using flash photolysis of the caged-IP3 as described above (Figure 3-3 A). The β3-deficient MEFs were stained with a fluorescent dye (CellVue Claret Far Red Fluorescent Cell Linker kits, at final concentration of 4 µM for $2×10^7$ cells according to the manufacturer protocol) to differentiate them from wild-type MEFs and cells of both genotypes were plated on the same glass coverslip. The next day, MEFs were loaded with Fluo-4 (1 µM) and caged-IP3 (3 µM) and then subsequently exposed to increased UV flash light energies (0.625, 2.5, 10 and 40 J) (Figure 3-8 A). The Ca^{2+} release peak amplitudes were measured and peak amplitudes were plotted versus the flash energy generating an energy dose-Ca^{2+} amplitude response curve of IP3-induced Ca^{2+} release (Figure 3-8 B, C).

As a control the peak amplitude was also quantified for β3-deficient stained and non-stained MEFs to evaluate the effect of the fluorescent dye on Ca^{2+} amplitudes. Stained and non-stained β3-deficient fibroblasts have shown similar Ca^{2+} peak amplitudes in response to 0.625, 2.5, 10 and 40 J of UV light flash energies (Figure 3-8 C) indicating no influence of the fluorescent dye on the Ca^{2+} signal. The β3-deficient MEFs revealed

a significantly increased sensitivity to IP3 compared to control cells (Figure 3-8 A and B). At 0.625 J, no or only small amounts of IP3 appears to be released because no Ca^{2+} release occurs in wild-type and β3-deficient cells. At 40 J, sufficient IP3 is released to saturate the Ca^{2+} release response (Figure 3-8 A and B). At 2.5 J and 10 J we see Ca^{2+} responses in both genotype but the β3-deficient cells show higher sensitivity to the same amounts of IP3 released. In summary, the data on Cos-7 cells, non-transfected and transfected with the β3 cDNA and embryonic fibroblasts from wild-type and β3-deficient mice are complementary. In the presence of β3 (wild-type fibroblasts or Cos-7 cells transfected with the β3 cDNA) agonist- and IP3-dependent Ca^{2+} release is inhibited compared to cells which lack the β3 protein (β3-deficient fibroblasts and non-transfected Cos-7) (Figure 3-2, Figure 3-3, Figure 3-5 and Figure 3-8).
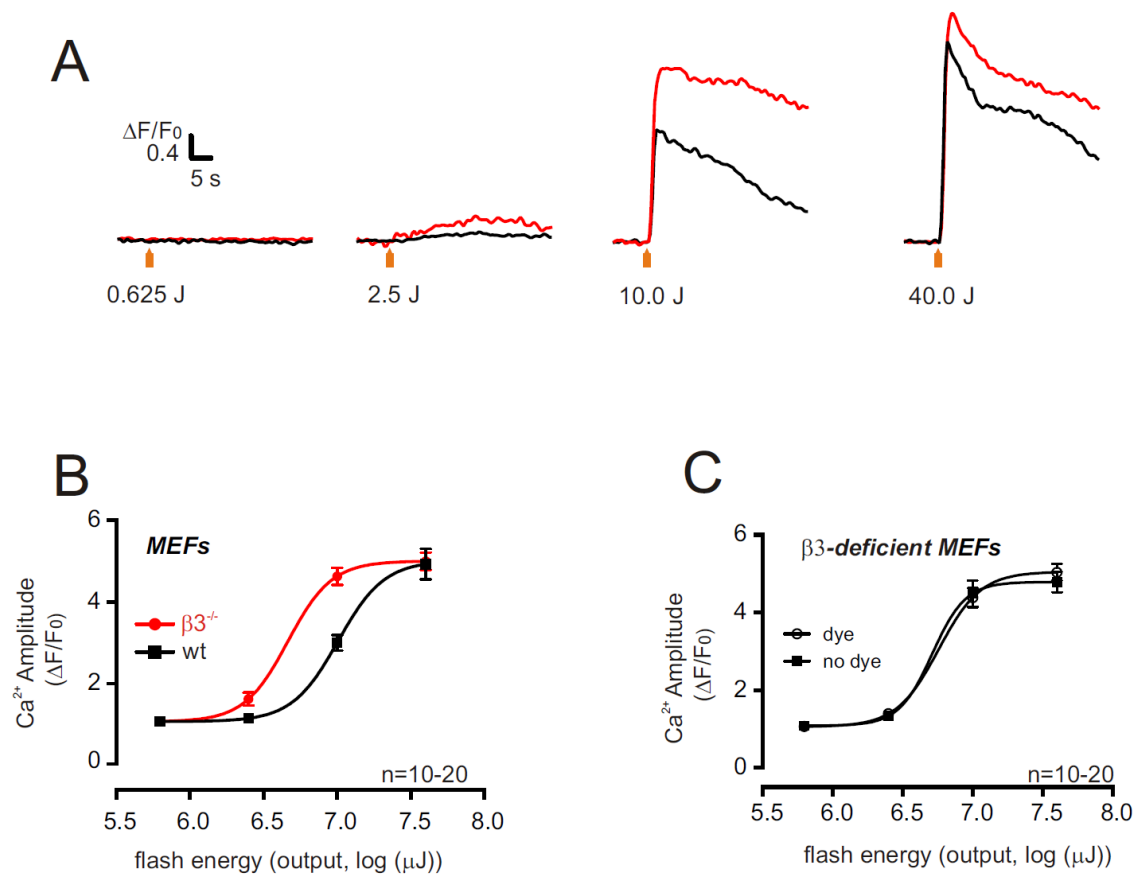
Figure 3-8. Enhanced IP3-receptor sensitivity to IP3 in Cavβ3-deficient mouse embryonic fibroblasts

(A) Representative Ca^{2+} release traces ($\Delta F/F_0$) in wild-type MEFs (black traces, non-stained cells) and β3-deficient MEFs (red traces, stained cells) loaded with Fluo-4 (1 μM) and caged-IP3 (3 μM). Wild-type and β3-deficient MEFs were plated on the same coverslip and were distinguished by the presence of red fluorescence (CellVue) on the β3-deficient MEFs or its absence in wild-type MEFs. UV light flashes of 0.625, 2.5, 10, 40 J were applied to uncage IP3. **(B)** Energy dose-calcium peak amplitude response curve (fluorescence ratio $\Delta F/F_0$ plotted as a function of log [flash energy in μJ]) shows an increased sensitivity of IP3R in β3-deficient MEFs (red) compared to control wild-type MEFs (black). **(C)** Energy dose-calcium peak amplitude response curve (fluorescence ratio $\Delta F/F_0$ plotted as a function of log [flash energy in μJ]) shows that β3-deficient MEFs stained with CellVue and non-stained have similar calcium peak amplitude response in each UV flash energy pulse indicating that the CellVue fluorescent dye has no influence on calcium signals. Each data point is an average of 10 to 20 cells ($\bar{x} \pm$ S.E.M.).

3.1.8 Membrane targeting of the Cavβ3-subunit

The data shown in Figure 3-2 indicate a distribution of the Cavβ3 protein within the cytoplasm even in the presence of the Cav1.2 α1 protein (Figure 3-2 A and C). Similarly, the Cavβ3 is also localized within the cytoplasm even when co-expressed with the Cav2.2 cDNA (Suh et al., 2012). Therefore the localization within the cytoplasm might be prerequisite for the negative effect of the β3 protein on the IP3-dependent Ca^{2+}-release. The question I wanted therefore to investigate was whether after artificial targeting of the β3 subunit to the plasma membrane, the effect on IP3-dependent Ca^{2+} release would still be present? To address this question we introduced an N-terminal 11 amino acid residue sequence of Lyn kinase to the N-terminus of Cavβ3. These 11 amino acid sequence starts with Met-Gly-Cys-Ile-Lys-Ser with the glycine (Gly) becoming myristoylated and the Cysteine (Cys) palmitoylated (Suh et al., 2012). To evaluate the membrane targeting efficiency of Lyn-β3 constructs, we transfected Cos-7 cells with the Lyn-β3-YFP cDNA or the Lyn-β3-RFP cDNA either alone or together with the Cav1.2 channel cDNA. After twenty four hours, transfected cells were imaged by confocal microscopy. The images clearly show that the fusion of the N-terminus of the Lyn kinase to the β3 protein leads to translocation of most of the β3 protein to the plasma membrane either in the absence or presence of the Cav1.2 (α1) protein (Figure 3-9 A).

To test the hypothesis that only cytoplasmic β3 protein might interfere with the IP3-dependent Ca^{2+} release, we transfected Cos-7 cells with Lyn-Cavβ3-YFP cDNA and EYFP cDNA as a control. Twenty-four hours after transfection, Cos-7 cells were loaded with the Ca^{2+} indicator dye Fura-2 followed by stimulation of the P2Y receptors by 10 µM ATP in the absence of extracellular calcium. As expected, we could see agonist-induced Ca^{2+} release from IP3-sensitive stores (Figure 3-9 B). Basic Ca^{2+} levels before

agonist application did not show any difference between Lyn-β3 positive and control cells. However and in contrast to the previous results, agonist induced Ca^{2+} release was not significantly different in Cos-7 cells expressing the Lyn-β3-YFP cDNA and control cells expressing the EYFP cDNA. These data indicate that targeting of the β3 subunit to the plasma membrane abolishes its suppressor effect on the agonist-induced calcium release (Figure 3-9 B). To substantiate this novel finding, we performed similar experiments as described above in Figure 3-3. Cos-7 cells were transfected with the Lyn-β3-RFP cDNA. RFP was chosen (and not YFP) because YFP excitation wavelength could interfere with the Fluo-4 Ca^{2+} signal. Twenty-four to forty-eight hours after transfection, Cos-7 cells expressing Lyn-Cavβ3 cDNA (red fluorescence) and non-transfected (no fluorescence) cells (plated on one dish) were loaded with Fluo-4 and caged-IP3, followed by exposure to UV light flashes of increasing energies (Figure 3-9 C). Again Ca^{2+} peak amplitude was quantified and plotted versus the log of flash energies to generate an energy dose-Ca^{2+}-amplitude response curve. In contrast to the data obtained with the β3 protein localized within the cytoplasm, the Lyn-β3-expressing cells and the control cells reveal no difference in IP3-dependent Ca^{2+} release (Figure 3-9 D). The membrane targeting of the β3 protein (Lyn-β3) to the plasma membrane prevents the suppressor effect of the β3 protein on the IP3-dependent Ca^{2+} release.

A

B

Cos-7 cells

C

D

E

Cos-7 cells
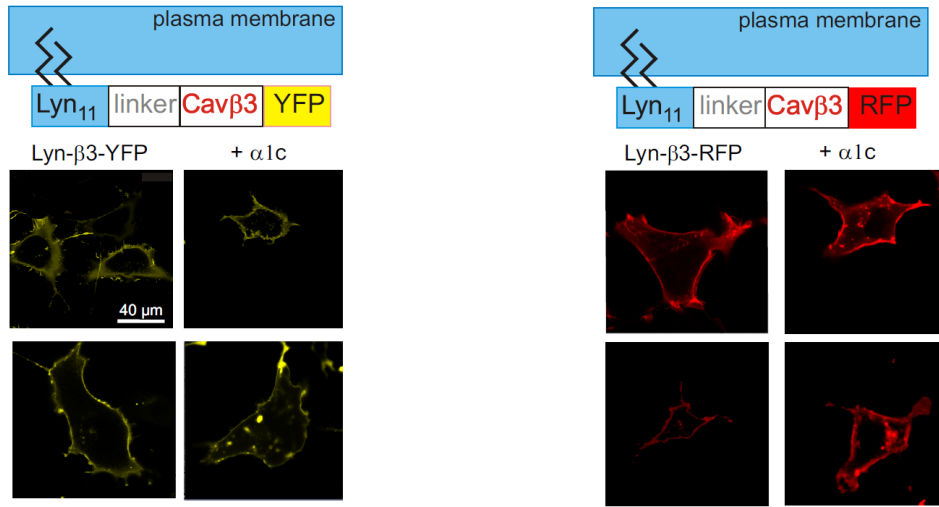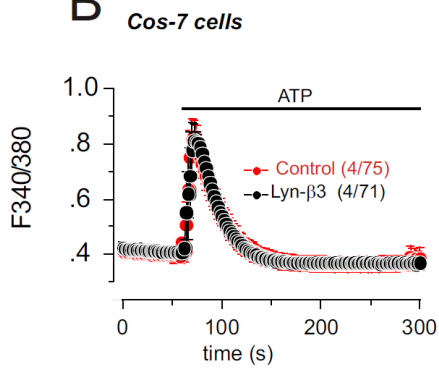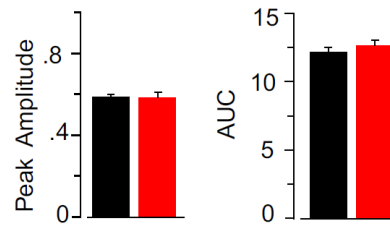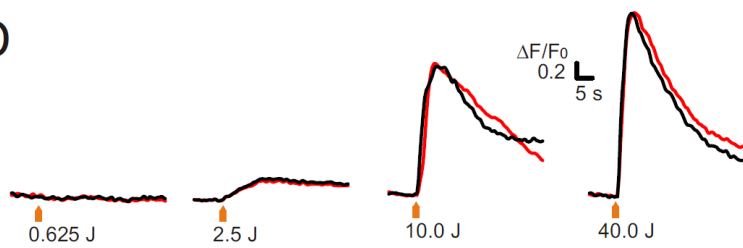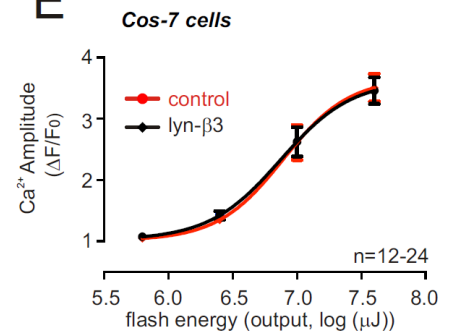
Figure 3-9. Membrane targeting of the Cavβ3 subunit attenuates its Ca²⁺ suppressor effect

(A, upper part) Scheme of the Lyn-Cavβ3 targeted to the plasma membrane. The cDNA encoding the amino terminal 11 amino acids of Lyn kinase (H_2N-MGCIKSKGKDSA-COOH) followed by 36 nucleotides encoding the linker (white, GADSAGSAGSAG) was subcloned in front of and in frame with the Cavβ3 cDNA. The cDNA of the Lyn-linker-Cavβ3 cDNA was then ligated to the cDNA of YFP and RFP, respectively. **(A, lower part)** Confocal images of Cos-7 cells expressing the membrane targeted Lyn-β3-YFP cDNA (left) or Lyn-β3-RFP cDNA (right) either in the absence or presence of Cav1.2 (α1) cDNA. Pictures were taken twenty four hours after transfection and show a clear membrane localization of Cavβ3 protein. **(B)** Fura-2 ratio over time before and after addition of 10 µM ATP in the absence of extracellular Ca^{2+} in Cos-7 cells expressing Lyn-β3-YFP cDNA (black traces) and control transfected cells expressing YFP cDNA (red traces). **(C)** Statistical analysis of the peak amplitude (left bar graph) and the area under the curve AUC (right bar graph) of ATP-induced calcium release in 71 Cos-7 cells expressing Lyn-β3-YFP cDNA recorded in 4 experiments (black bars) and 75 control cells expressing YFP cDNA (red bars) recorded in 4 experiments ($\bar{x} \pm$ S.E.M.). **(D)** Representative Ca^{2+} release traces ($\Delta F/F_0$) in Cos-7 loaded with Fluo-4 (1 µM) and caged-IP3 (3 µM) and transfected with Lyn-β3-RFP cDNA (black traces) or control non-transfected cells (red traces). Non-transfected and transfected cells were plated on the same coverslip and were distinguished by the presence of red fluorescence (Lyn-β3 cDNA expressing cells) or its absence (non-transfected cells). UV light flashes of 0.625, 2.5, 10 and 40 J were applied to uncage IP3. **(E)** Energy dose-Ca^{2+} peak amplitude response curve plotted as a function of log [flash energy in µJ] shows that targeting β3 subunit to the plasma membrane attenuates it effect on the IP3R sensitivity and thereby on the IP3-dependent calcium release. Each data point is an average of 12 to 24 cells ($\bar{x} \pm$ S.E.M.).

3.1.9 The Cavβ3 protein in subcellular fractions

Our data presented above in Figure 3-2 A and C show that expressing the GFP-tagged Cavβ3 cDNA in Cos-7 and in HEK293 cells reveals a diffuse cytoplasmic localization in confocal images. To substantiate this finding further we homogenized HEK293 cells transfected with the Cavβ3 cDNA and embryonic fibroblasts from wild-type and β3-deficient mice. Then, we processed the homogenates to get subcellular fractions containing mainly the cytoplasmic, membrane, and nuclear soluble fractions, respectively. Proteins of the three fractions were separated by SDS-PAGE, transferred into filters and incubated with antibodies for Cavβ3, for Na^+/K^+ ATPase and IP3R3 (for the membrane fraction), Calnexin (for the endoplasmic reticulum) and α-P68 RNA Helicase (for the nuclear fraction). The Cavβ3 protein (Figure 3-10 A and B) is associated with all the three fractions indicating a ubiquitous cellular localization of the β3 protein.
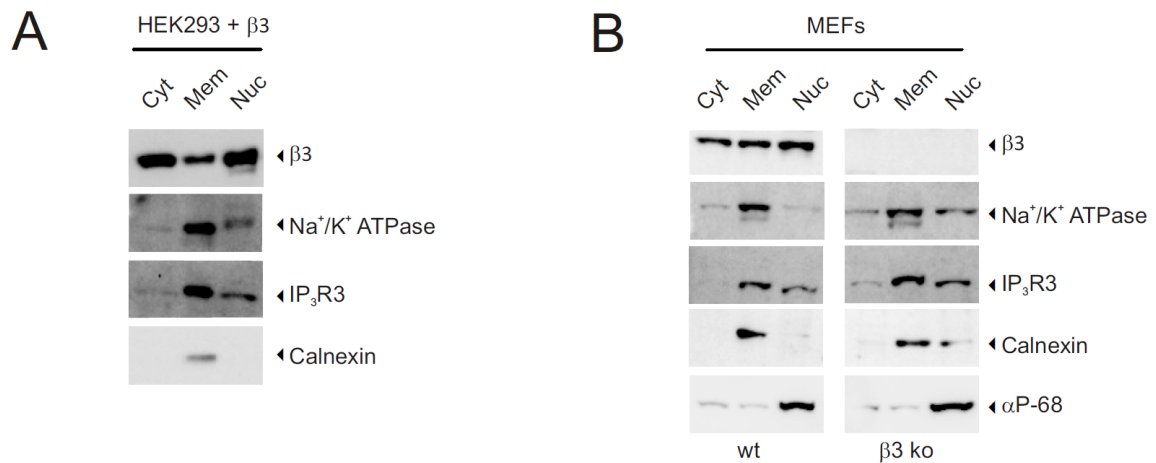
Figure 3-10. Cavβ3 protein subcellular localization

(A, B) Western blot of proteins from membrane (Mem, 50 µg), cytoplasmic (Cyt, 50 µg) and nuclear (Nuc, 50 µg) fractions obtained from Cavβ3 cDNA-expressing HEK293 cells **(A)** and embryonic fibroblasts from wild-type and β3-deficient mice **(B).** Anti-Cavβ3 antibody was used for the detection of the Cavβ3 protein and the purity of different fractions was monitored by antibodies against the Na^+/K^+ ATPase, the IP3R3, Calnexin and α-P68 RNA Helicase. The Na^+/K^+ ATPase, the IP3R3 and Calnexin are mainly associated with the membrane fraction. The α-P68 RNA Helicase is mainly associated with the nuclear fraction. The Cavβ3 is associated with all three fractions.

3.1.10 Estimation of the amount of IP3-receptor type 3 protein in wild-type and β3-deficient fibroblasts

Our data so far show an enhanced agonist induced Ca^{2+} release and an enhanced Ca^{2+} release in response to the uncaging of IP3 in cells lacking β3 protein (Figure 3-2, Figure 3-3, Figure 3-5 and Figure 3-8). We speculate that the expression of β3 subunit might result in a downregulation of the IP3-receptor expression and thereby reducing the Ca^{2+} release in response to IP3 or to agonist stimulation. To further investigate this possibility we estimated the protein levels of IP3-receptor type 3 in wild-type and β3-deficient fibroblasts by Western blot. Whole cell lysate from wild-type and β3-deficient fibroblasts was subjected to protein quantification by BCA technique as described above in section 2.8. Thereafter 50, 100 and 150 µg proteins from each genotype were respectively applied per lane in a polyacrylamide gel and then separated by SDS-PAGE. Proteins were transferred into nitrocellulose filters and then incubated with the anti-IP3R3 antibody. After detection of the IP3R3 protein, and in order to control that equal protein amounts were applied from wild-type and β3-deficient fibroblasts, the filters were washed to remove the primary antibody and incubated with a primary anti-Na^+/K^+ ATPase antibody. Then, the filters were washed again and incubated with anti-β3 antibody to confirm the presence of β3 protein in only wild-type fibroblasts but not in the β3-deficient cells. Our data in Figure 3-11 show the presence of β3 protein only in wild-type cells and show that there are no obvious changes in the IP3R3 protein levels in wild-type and β3-deficient fibroblasts. This argues against our speculation that the expression of β3 subunit might downregulate the IP3R3 expression and thereby might decrease the IP3R3 mediated Ca^{2+} release.
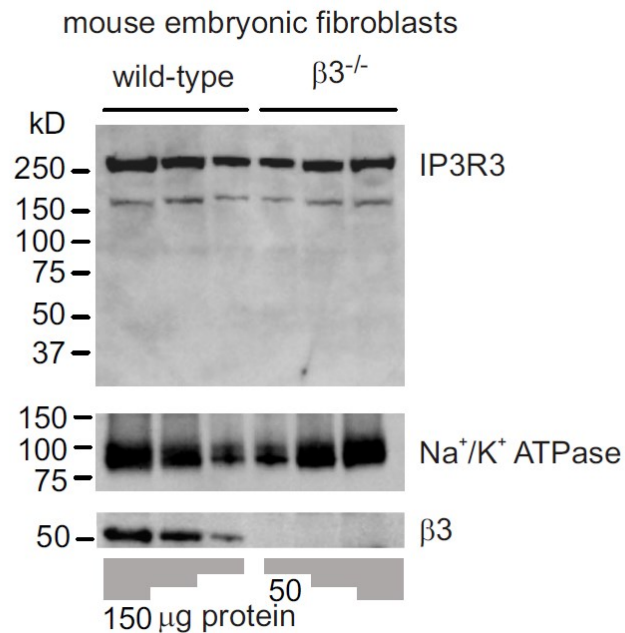
Figure 3-11 Estimation of IP3-receptor 3 protein levels in fibroblasts

Western blot of protein extracts from wild-type and β3-deficient fibroblasts showing an estimation of the IP3R3 protein level in both genotypes. As indicated below in gray boxes 50, 100 and 150 µg of protein extracts from each genotype were applied per lane, respectively. Proteins were separated by SDS-PAGE and analyzed by Western blot using first the anti-IP3R3 antibody. The anti-IP3R3 antibody was then removed from the filter, and the filter was incubated again with anti Na$^+$/K$^+$ ATPase antibody as a control for loading equal amounts of protein. The filter was washed again to remove the anti Na$^+$/K$^+$ ATPase antibody and was further incubated with the anti-β3 antibody to confirm the presence of β3 protein which is present only in the wild-type fibroblasts protein extract.

3.1.11   Cavβ3 interaction with the IP3-receptor

So far the data indicate a localization of Cavβ3 protein within the cytoplasm, similar IP3R protein levels in both genotypes and an inhibiting effect of Cavβ3 on the IP3-dependent Ca^{2+} release. To investigate a direct interaction of Cavβ3 and the IP3-receptor we performed coimmunoprecipitation experiments. Cos-7 cells were co-transfected with the Cavβ3 cDNA and the cDNAs of mouse IP3R type 1, type 2 or type

3, respectively (These cDNAs have been cloned by Dr. Ulrich Wissenbach in our group). Using the Cavβ3 antibody, the β3 protein was immunoprecipitated; the precipitate was run by SDS-PAGE and analyzed by Western blot for the presence of β3 protein by using Cavβ3 antibody (Figure 3-12). Antibodies for the IP3Rs were used to check whether the IP3Rs are among the proteins associated with the precipitated Cavβ3 protein. Vice versa, using IP3Rs antibodies, the IP3R was immunoprecipitated, and the anti-Cavβ3 antibody was used to identify whether Cavβ3 protein is among the proteins associated with the precipitated IP3Rs. The data show that all three types of the IP3Rs (IP3R type 1, 2 and 3) can associate with the β3 protein and vice versa (Figure 3-12). These coimmunoprecipitation data ascertain our hypothesis that Cavβ3 protein directly interacts with the IP3R.
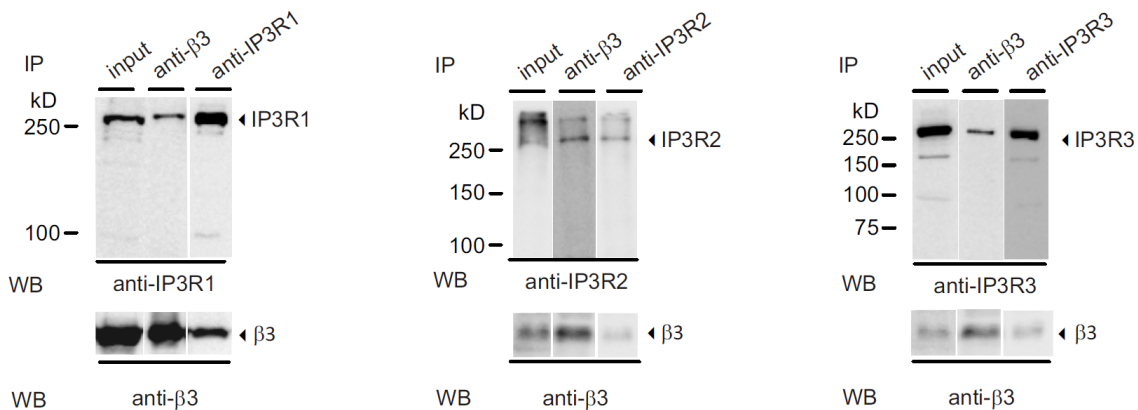
Figure 3-12. Cavβ3-IP3R interaction

Coimmunoprecipitation of Cavβ3 protein and IP3R type 1 (left blot), type 2 (middle blot) and type 3 (right blot) from lysates of Cos-7 cells co-expressing the cDNA of Cavβ3 and the cDNA of IP3R type 1 or 2 or 3, respectively. The first lane of each panel contains input from cell lysate to serve as a control. Using the anti-Cavβ3 antibody, the β3 protein was precipitated and among the proteins associated with the precipitated β3 proteins were the IP3Rs type 1, 2 and 3, respectively. Vice versa, using antibodies for IP3R type 1, 2 or 3, the IP3Rs proteins were precipitated and the Cavβ3 was among the proteins retained by the precipitated IP3Rs proteins.

3.1.12 Mapping the Cavβ3 domain responsible for the interaction with the IP3R

The Cavβ3 protein has two non-conserved domains, the NH_2- and the COOH-termini which are highly variable in length and amino acid composition compared to the β1, β2 and β4 proteins. It has also two conserved regions C1 and C2 of ~130 aa and ~150 aa in length respectively. The C1 domain shares homology with the Src homology domain 3 (SH3). The C2 domain has minor but detectable similarity to the guanylate kinase (GK) domain; nevertheless, it has no enzymatic activity. Both domains mediate specific protein-protein interactions; The GK domain contains the alpha binding pocket (ABP) which is responsible for the interaction with Cav1α1 and Cav2α1 proteins (see introduction). To map the region of β3 responsible for IP3R binding, we constructed Cavβ3 deletion mutants Cavβ3ΔSH3 (lacking the SH3 domain) and Cavβ3ΔGK (lacking the GK domain) (Figure 3-1). Because IP3R type 3 is the most prominent in MEFs, we concentrate on β3/IP3R3 interaction. The IP3R type 3 cDNA was co-expressed with the Cavβ3ΔSH3 cDNA or Cavβ3ΔGK cDNA in Cos-7 cells. Forty eight hours after transfection, cell lysates were prepared and coimmunoprecipitation was performed as described above in section 3.1.10 (Figure 3-13 A). The Cavβ3ΔGK protein was able to interact with the IP3R and was detected among the precipitated IP3R protein complex and vice versa. In contrast, deletion of the SH3 domain prevents Cavβ3-IP3R interaction and Cavβ3ΔSH3 was not detected among the precipitated IP3R protein complex and vice versa (Figure 3-13 A). To further examine whether deletion of Cavβ3-SH3 domain would also prevent the effect of Cavβ3 on IP3-dependent Ca^{2+} release, we expressed Cavβ3ΔSH3-IRES-GFP cDNA or the IRES-GFP cDNA as a control in Cos-7 cells. The expression of the Cavβ3ΔSH3 cDNA was controlled by Western blot (Figure 3-13 B) and by the presence of green fluorescence

in transfected cells. Twenty-four to forty eight hours after transfection, Cos-7 cells were loaded with Fura-2 Ca^{2+} dye and intracellular Ca^{2+} levels were measured as F340/380 ratio in transfected green fluorescent cells. Basic Ca^{2+} levels as well as ATP-induced Ca^{2+} release in Cavβ3ΔSH3 cDNA expressing Cos-7 cells and in control cells were not significantly different and Cavβ3ΔSH3 expression had no effect on the IP3-releasable calcium. Thus, deletion of the SH3 domain prevents the decrease of agonist-induced Ca^{2+} release which we have seen with the Cavβ3 full length protein (Figure 3-13 B and C, Figure 3-2 G and H). These data show that Cavβ3 interacts with the IP3R *via* its SH3 domain and that deletion of this SH3 domain prevents both the interaction with the IP3-receptor and its inhibitory effect on IP3-dependent Ca^{2+} release.
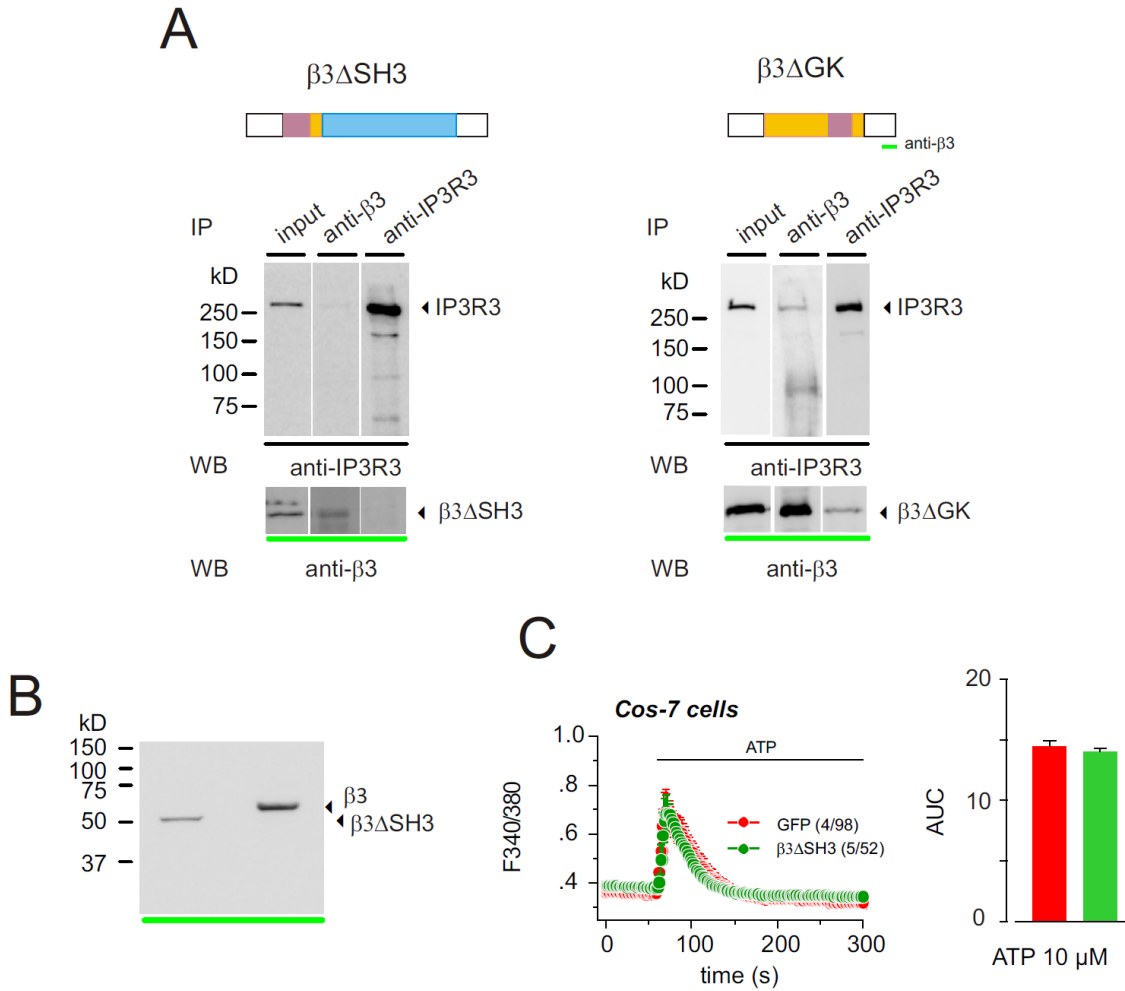
Figure 3-13. Cavβ3 protein modulates IP3-dependent Ca^{2+} release *via* its SH3 domain.

(A) Coimmunoprecipitation of IP3R type 3 and Cavβ3 mutants from lysates of Cos-7 cells co-expressing the cDNAs of Cavβ3ΔSH3 or Cavβ3ΔGK with the cDNA of IP3R3. The first lane of each panel contains input of cell lysate which serves as a control. Using the anti-Cavβ3 antibody, Cavβ3ΔSH3 protein was precipitated and IP3R3 protein was not detected among the precipitated proteins and vice versa (left panel). Using anti-Cavβ3 antibody, Cavβ3ΔGK protein was precipitated and among the proteins retained, the IP3R3 was associated and vice versa, using the anti-IP3R3 antibody, IP3R3 protein was precipitated and Cavβ3ΔGK was among the associated proteins (right panel). **(B)** Western blot analysis of protein extracts from Cos-7 cells Cavβ3 expressing the cDNAs of either Cavβ3 full length or Cavβ3ΔSH3 showing the Cavβ3 signal at ~55 kDa and the Cavβ3ΔSH3 at ~47 kDa. **(C)** Fura-2 ratiometric traces

before and after the application of ATP (10 µM) in Cos-7 cells expressing the Cavβ3ΔSH3-IRES-GFP cDNA or the cDNA of GFP as a control. Statistical analysis of the area under the curve of 52 cells expressing the Cavβ3ΔSH3 cDNA recorded in 3 experiments (green bars) and 98 control cells recorded in 4 experiments (red bars) ($\bar{x}$ ± S.E.M.) showing that deletion of the SH3 domain of Cavβ3 protein attenuates its suppressor effect on IP3-dependent Ca^{2+} release.

3.1.13   Mapping the IP3-receptor domain responsible for the interaction with the Cavβ3

In general SH3 domains bind to proline-rich structures of proteins. The IP3Rs cover more than 2600 amino acid residues; the mouse IP3R3 covers 2670 amino acid residues. The primary structure of all IP3Rs can be divided into N-terminal cytoplasmic region containing; the N-terminal coupling domain, the IP3-binding domain and the internal regulatory and coupling domain. The transmembrane domain is located near to the C-terminus, comprises six transmembrane helices with the N- and C-terminus projected into the cytosol and constitutes around 10 % of the whole amino acid sequence of the IP3R (Figure 3-14 A and B) (Mikoshiba, 2007). With the aim to identify where Cavβ3 protein interacts on the IP3R, we established a GST pull-down assay using purified recombinant Cavβ3-GST fusion protein and *in vitro* translated cDNA fragments derived from the mouse IP3R type3. These IP3R3 fragments cover the whole IP3R3 amino acid sequence and they have a length ranging from ~150 to ~1200 amino acid residues (Figure 3-14 B). To ensure successful *in vitro* transcription/translation and ^{35}S-Methionine labeling of the IP3R3 fragments, we first resolved samples from each fragment by SDS-PAGE, then the gels were exposed to X-ray films and phosphor-imager screens in order to visualize the ^{35}S-labeled protein. The corresponding autoradiograms (Figure 3-14 C) show ^{35}S-labeled IP3R3 fragments

F1 to F11 with only little signs of protein degradations. Cavβ3-GST fusion protein prebound to glutathione agarose beads were incubated with the ^{35}S-labeled IP3R3 fragments. Thereafter complexes were denatured using SDS-containing buffer and the proteins were resolved by SDS-PAGE and stained with coomassie blue. The stain shows equal loading of Cavβ3-GST protein per incubation and per lane (Figure 3-14 C lower bots). After drying, the gels were exposed to a phosphor imaging screen for 2 days (or X-ray films for one week) and the screen was read using the phosphor-imager. The resulting autoradiograms (Figure 3-14 D) show the binding of IP3R3 fragments F1, F4, F6, F7, F10 and F11 to the Cavβ3-GST protein but no binding of fragments F2, F3, F5, F8 and F9. We exposed even for a very long time to see if we detect any bands for F2, F3, F5, F8 and F9 but we did not see any signal. Furthermore, the fragments F1, F4, F6, F7, F10 and F11 were incubated with recombinant GST alone to exclude nonspecific binding. Autoradiograms (Figure 3-14 E) show that F4 and F6 were not retained by GST indicating that they constitute the specific binding site of IP3R3 for the Cavβ3 protein. In summary Cavβ3 binds directly to the IP3R3 *in vitro* (Figure 3-14). The Cavβ3 protein has two binding regions on the mouse IP3R3; the first one is located on the amino acids 346-917and the second is located on the amino acid residues 1387-2249.

A. Model of IP3-receptor
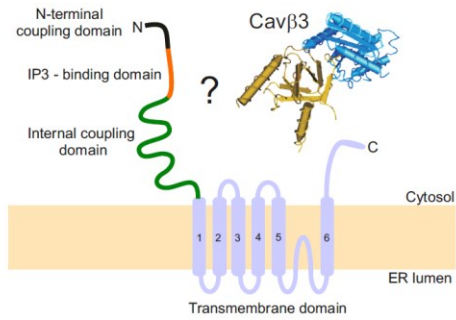
B. ³⁵S-labelled mIP3R3 fragments
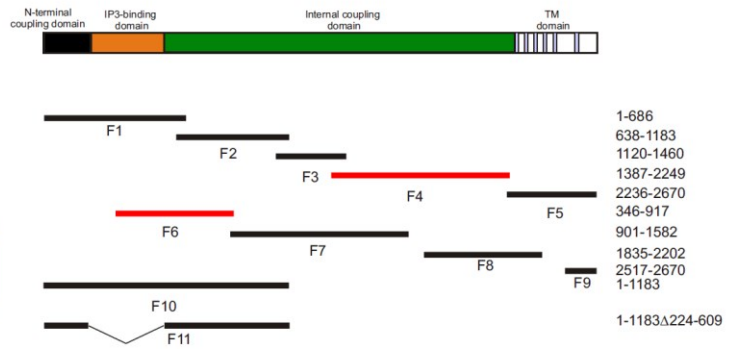
C. ³⁵S Autoradiogram of mIP3R3 fragments - *In vitro* translation
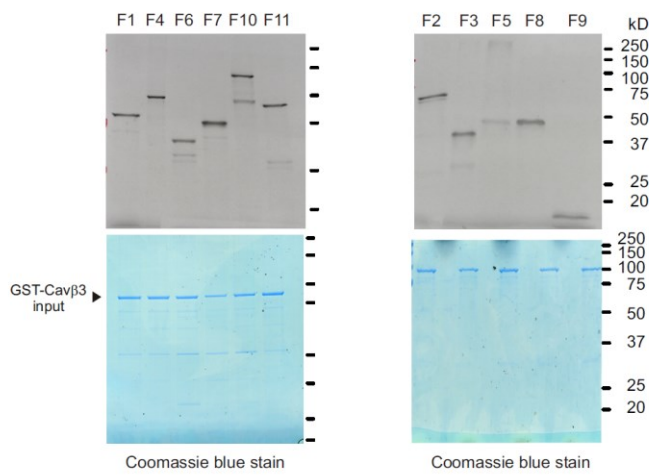
D. ³⁵S Autoradiogram - Retention by GST-Cavβ3
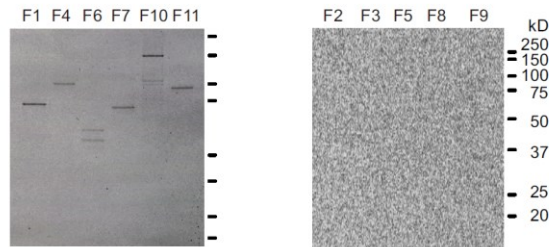
E. ³⁵S Autoradiogram - Retention by GST
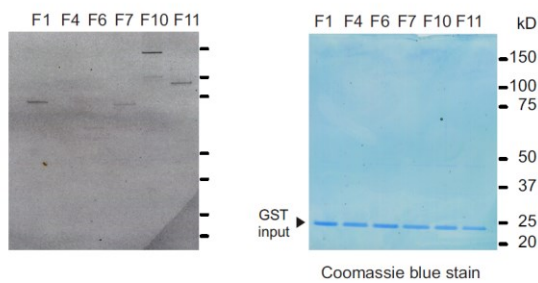
Figure 3-14 Mapping of Cavβ3 binding to the IP3R

(A) Scheme showing the IP3-receptor monomer structure with the molecular domains and the Cavβ3 crystal structure binding to the IP3R. **(B)** Library of IP3R3 fragments used for mapping the β3-binding region. **(C, upper blots)** Autoradiograms of *in vitro* translated IP3R3 fragments F1 to F11 (50 000 cpm for each fragment) labeled with ^{35}S-Methionine after SDS-PAGE separation showing efficient transcription/translation of the corresponding cDNA. **(C, lower blots)** Coomassie blue stained Cavβ3-GST fusion protein input. **(D)** Each *in vitro* translated fragment (300,000 cpm) was incubated with purified Cavβ3-GST fusion protein pre-bound to glutathione agarose beads at room temperature for 30 min. After five times washing, the IP3R3 fragments bound to Cavβ3-GST were resolved by SDS-PAGE. Autoradiograms show that F1, F4, F6, F7, F10 and F11 were retained by Cavβ3-GST but not the other fragments F2, F3, F5, F8 and F9 (even with much longer exposure time). **(E, left blot)** As a negative control, the positive IP3R3 fragments F1, F4, F6, F7, F10 and F11 were incubated with purified GST protein alone. Fragments F1, F7, F10 and F11 but not F4 and F6 were retained by GST alone. **(E, right blot)** Coomassie blue stained GST protein input. The mouse IP3R3 fragment F4 (amino acid residues 1387-2249) and fragment F6 (amino acid residues 346-917 contain the binding domain for Cavβ3 protein.

3.2 Physiological impact of Cavβ3 protein on fibroblasts in vivo

So far the data show that β3 is expressed in fibroblasts, decreases agonist-induced Ca^{2+} release from intracellular stores of these cells by apparently binding to two distinct regions of the cytosolic N-terminus of the IP3-receptor type 3. The question now is what could be the consequences of these Cavβ3 actions *in vivo*?

3.2.1 Mouse embryonic fibroblasts migration

Fibroblasts are migrating cells and are involved in various physiological and pathophysiological processes (Sixt, 2012). Intracellular Ca^{2+} levels has been shown to

regulate cell migration (Leiper et al., 2006; Zheng and Poo, 2007; Yamada et al., 2010; Xu and Chisholm, 2011; Lovisolo et al., 2012). To evaluate whether Cavβ3-dependent modulation of cytosolic Ca^{2+} translates into altered cell migration, we compared the motility of primary fibroblasts from wild-type and β3-deficient mice using two types of migration assays; the scratch migration assay (Figure 3-15) and the chemotactic Boyden chamber assay (Figure 3-16). The scratch assay was performed on a confluent cell monolayer of wild-type and β3-deficient MEFs. After performing the "scratch" using a 200 µl pipette tip, cells from both genotypes migrate into the scratch area and close the gap (Figure 3-15 A). Cell migration rate was measured as a percentage of the initial scratch area 6 hours after setting the scratch. β3-deficient MEFs migrated and closed the scratched area significantly faster than MEFs from wild-type mice (Figure 3-15 B and C). To exclude any effect of cell proliferation, scratch migration assay was performed in the presence of either 10 % or 1 % FCS. At 10 % FCS we can see both processes; the cell proliferation and migration, whereas at 1 % FCS we could minimize the cell proliferation and we can see mostly the migration. Scratch migration assay performed in the presence of 10 % (Figure 3-15 B) or 1 % FCS (Figure 3-15 C) showed similar migration pattern ruling out the possibility of cell proliferation contribution to the β3 observed phenotype. β3-deficient MEFs migrated significantly faster than wild-type MEFs under both conditions. One explanation for the faster migration of β3-deficient MEFs is that higher IP3-induced Ca^{2+} release in β3-deficient MEFs (Figure 3-5) might contribute and induce faster cell migration. To further examine the effect of β3 protein on cell migration, we performed a chemotactic migration assay (Figure 3-16) where the cells are plated on the upper compartment of the chamber with FCS-free medium and the cells were stimulated to migrate through the 8 µm pores of polycarbonate filter toward the 1 % FCS. In this assay, the β3-deficient MEFs traversed the filter

significantly less than wild-type MEFs after five hours of incubation (Figure 3-16 B). Apparently this difference in the migration behavior might be caused by differences in chemotactic behavior, either a particular increased sensitivity to the serum deprivation within the upper chamber or to 1% FCS in the lower chamber. Taken together deletion of Cavβ3 subunit alters cell migration and chemotactic behavior of fibroblasts.
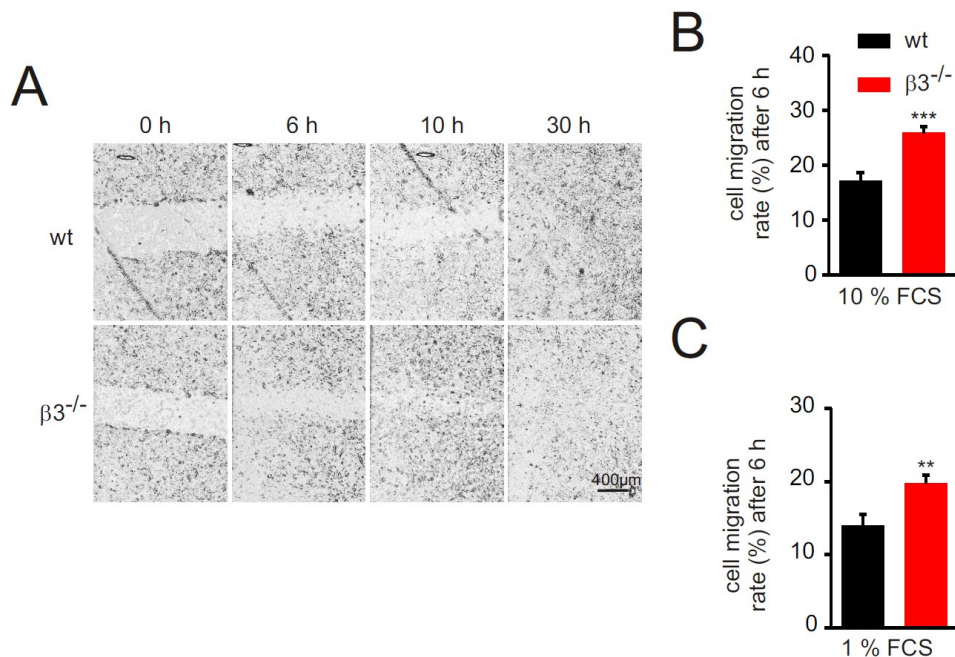
Figure 3-15. Scratch migration assay.

(A) Representative images of migration from wild-type and β3-deficient MEFs. Cell monolayer images in the presence of 10 % FCS taken immediately after setting a scratch (0 h) then 6, 10 and 30 hours later. The scratch area is completely closed in both genotypes after 30 hours **(B, C)** Summary of cell migration rate calculated relative to the initial scratch area after 6 hours in the presence of 10 % FCS (B) or 1 % FCS (C) showing increased migration rate of β3-deficient MEFs (red) compared to wild-type MEFs (black bar graph) in both conditions (1 % and 10 % FCS). Data shown as x̄ ± S.E.M. with the experiment done three times with three independent cell preparations (** P<0.005, *** P<0.001; Student t-test).
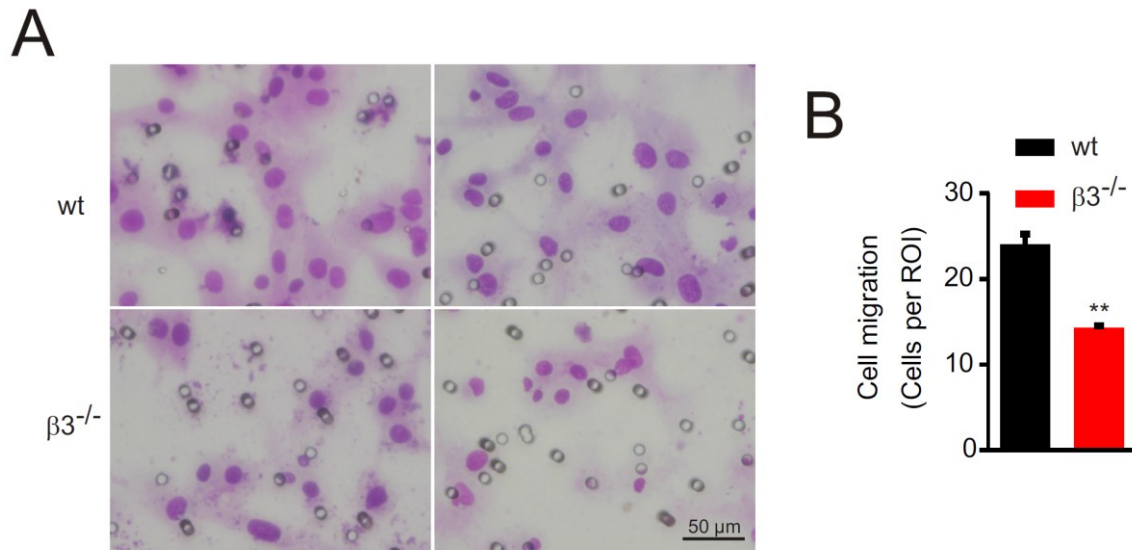
Figure 3-16. Chemotactic Boyden chamber assay

(A) Representative live microscopic images of MEFs from wild-type and β3-deficient mice which have traversed the 8 µm pores of polycarbonate filters to reach the lower compartment containing the chemo-attractant (1 % FCS). **(B)** Statistical analysis shown as x̄ ± S.E.M of the number of wild-type (black) and β3-deficient (red) MEFs which traversed the filter per region of interest (ROI) after 5 hours. The mean was calculated from at least three wells per experiment and cells in 20 ROIs/well were counted. This experiment was performed three times with three independent MEFs preparation (** $P < 0.005$; Student t-test).

3.2.2 Growth characteristic in MEFs lacking the Cavβ3 protein

The migration behavior of fibroblasts was not influenced by the amount of FCS present in the culture medium and β3-deficient cells showed faster migration in both condition either 1 % FCS or 10 % FCS. An argument against cell proliferation contribution to the enhanced β3-deficient fibroblasts migration in the scratch assay (Figure 3-15). In order ensure further that the cell motility behavior of β3-deficient MEFs was not due to a higher cell viability or proliferation, we studied the viability and proliferation of the fibroblasts from both genotypes for 8 days by flow cytometry as described above in

material and methods section 2.20. There was no significant difference in proliferation (Figure 3-17 A) and in cell viability (Figure 3-17 B) of embryonic fibroblasts. Wild-type and β3-deficient fibroblasts shared comparable cell proliferation as well as cell viability, ruling out that these cell properties have any influence on the migration behavior of β3-deficient MEFs.
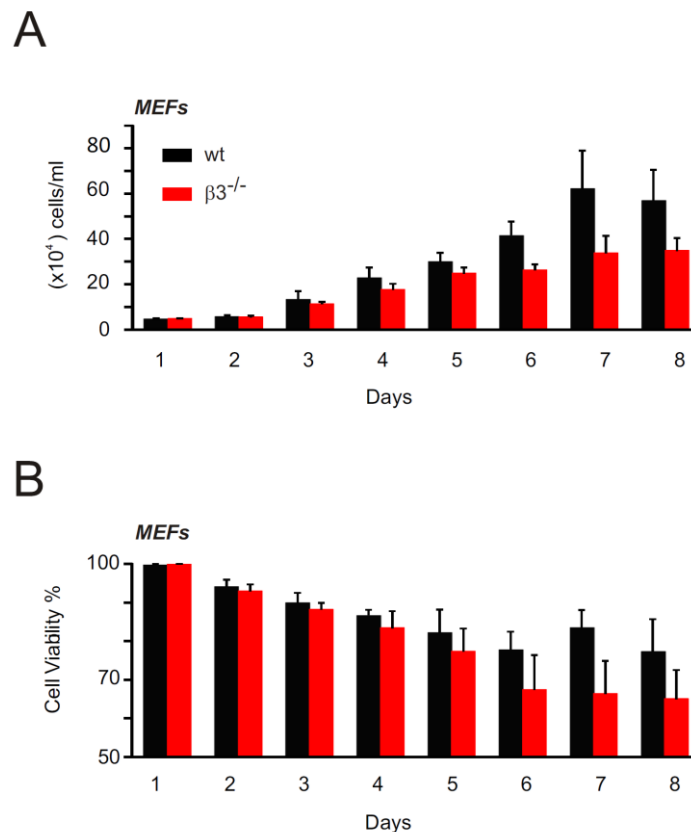
Figure 3-17. Growth characteristics of wild-type and β3-deficient fibroblasts

Cell proliferation **(A)** and cell viability **(B)** of wild-type and β3-deficient fibroblasts over eight days. Embryonic fibroblasts were plated at $5 \cdot 10^4$ cells per Ø 3.5 cm dishes (8 dishes for each genotype and for each set of experiment) and counted at the indicated time points as described in materials and methods section 2.20. Means ± S.E.M. of cell numbers and cell viability percentage at each time point were calculated from four independent experiments with two independent fibroblasts preparations.

3.2.3 G- to F-actin ratio and myosin IIA expression in MEFs

In many cases cell motility depends on polymerization and depolymerization of actin (Machesky and Insall, 1999). Therefore we started to study the ratio of monomeric actin versus polymerized actin filaments in wild-type and β3-deficient MEFs as a possible underlying mechanism of cell migration phenotype of β3-deficient MEFs. Phalloidin which stabilizes F-actin filaments and urea which leads to depolymerization of actin filaments were used to separate the actin filaments from the globular actin fraction. These proteins of globular G-actin and the F-actin filaments fraction were run on SDS-PAGE and blotted to a filter, which was incubated in the presence of an anti-actin antibody. Densitometric quantification of the immunostain intensity as well as the staining of actin filaments using Alexa Fluor 594-conjugated phalloidin did not reveal significant differences in the ration of monomeric versus polymerized actin filaments (G/F actin ratio) between wild-type and β3-deficient fibroblasts (Figure 3-18 A, C and D). It has been shown that myosin IIA expression acts negatively on cell migration in the *in vitro* scratch assay (Tanaka et al., 2010). Therefore we stained MEFs from wild-type and β3-deficient mice with anti-myosin IIA antibody to assess the expression of myosin IIA. According to the immunostaining data, myosin IIA was present in cells from both in both genotypes and with similar levels (Figure 3-18 A). Next, lysates from wild-type and β3-deficient MEFs were run on SDS-PAGE and blotted to a filter, which was incubated in the presence of anti-myosin IIA antibody (Figure 3-18 B). The immunoblotting data shows no significant difference in the myosin IIA expression in wild-type and β3-deficient MEFs.
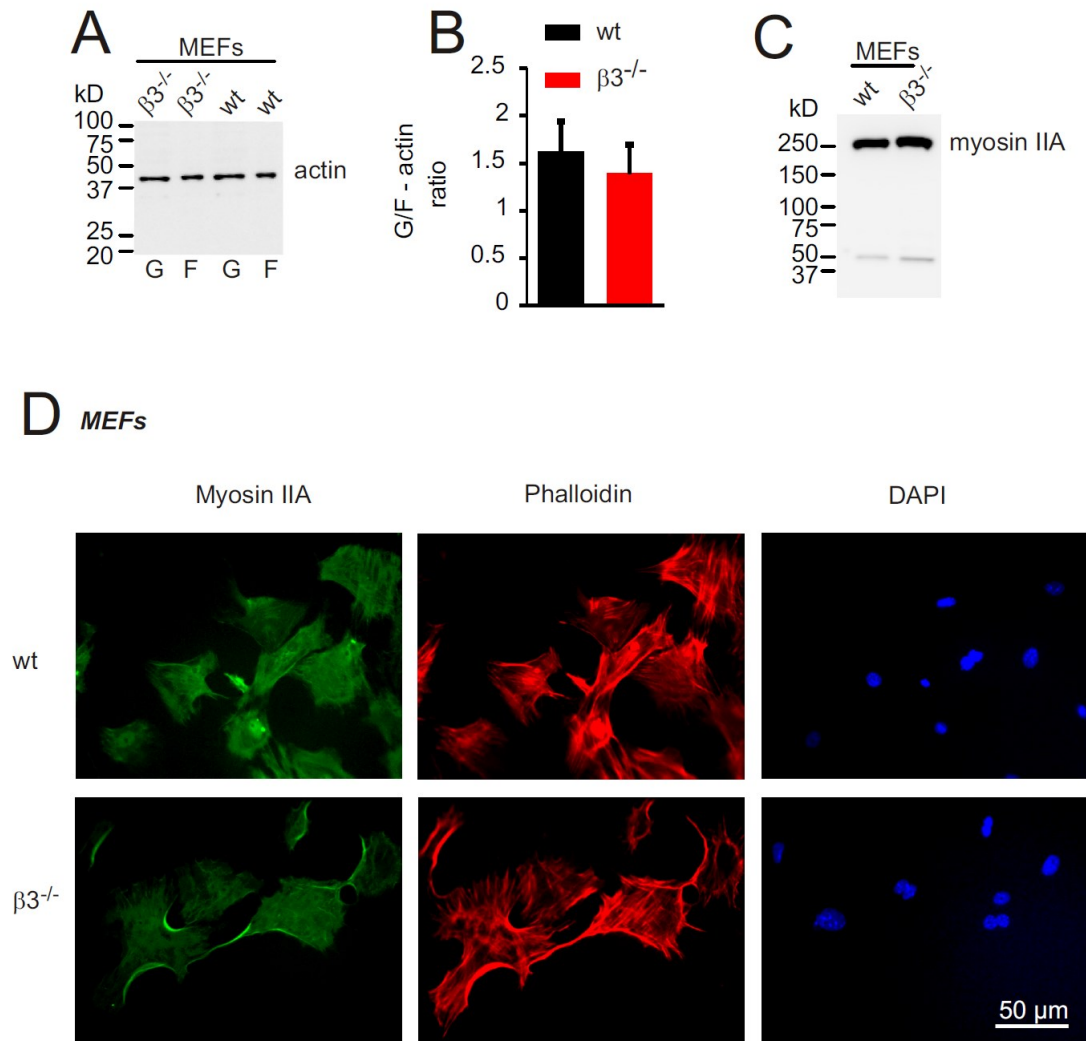
Figure 3-18. G-actin, F-actin and Myosin IIA expression in MEFs

(A) Western blot of G- and F-actin fractions from wild-type and β3-deficient MEFs lysate using anti-actin antibody. **(B)** Summary of densitometric quantification of immunostain in (A) [repeated at least twice] shown as $\bar{x} \pm$ S.E.M. **(C)** Western blot of myosin IIA in wild-type and β3-deficient MEFs lysate showing similar myosin IIA protein levels in both genotypes. **(C)** Myosin IIA and F-actin stained in wild-type and β3-deficient MEFs using anti-myosin IIA, Alexa Fluor 594-conjugated phalloidin (for actin filaments) and DAPI (for nuclear staining).

3.2.4 β3-deficient MEFs secrete more collagen than wild-type MEFs

Collagen has been shown as a suitable substrate for cell migration (Rocnik et al., 1998). To evaluate Cavβ3 protein impact on collagen secretion, we plated wild-type and β3-deficient MEFs at equal density and maintained cells in medium containing 10 % serum for twenty four hours. Then, medium was changed to medium containing only 1 % serum and incubated for another forty eight hours. Afterwards, the amount of soluble collagen secreted in the culture medium was measured using the Sircol dye which binds specifically to the $(Gly-x-y)_n$ helical structure of collagen types I to XIV as described in materials and methods in section 2.22. We found that β3-deficient MEFs secrete significantly more collagen compared to wild-type cells (Figure 3-19 A). Collagen secretion has been shown to be calcium dependent (Bonen and Schmid, 1991). This enhancement in collagen secretion might be explained by the increased IP3-releasable Ca^{2+} in β3-deficient MEFs (Figure 3-5) and may contribute to the faster migration of β3-deficient fibroblasts (Figure 3-15).

3.2.5 Accelerated skin wound closure in mice deficient for Cavβ3

Fibroblasts play a crucial role in the formation of wound repair and tissue remodeling (Gawronska-Kozak, 2011). Because we found faster migration of β3-deficient fibroblasts in the scratch assay, often used as an *in vitro* "wound healing" model, and because β3-deficient cells secrete more collagen we wondered whether wound healing *in vivo* is different in the presence and absence of β3 protein. For this purpose we used a skin fold chamber (Sorg et al., 2007) and generated a circular wound of 2 mm diameter on the shaved back of wild-type and Cavβ3-deficient mice (8 animals per genotype of 8-12 weeks old and 26-30 g weight) (Figure 2-7, Figure 3-19 C). The

wound was performed by removing the complete skin with epidermis and dermis. To compare skin wound healing between both genotypes, the wound area in the skin fold chamber was photographed directly after wounding (day 0) and then after 3, 6, 10 and 14 days post wounding (Figure 3-19 C). Thereafter the wound areas were quantitated on digital images and the wound area at a given day was expressed as a percentage of the initial wound area (Figure 3-19 D). The process of wound closure with complete epithelialization continued for 14 days in both genotypes, similar to previously published studies (Eming et al., 2007). However, we found that wound closure is accelerated in β3-deficient mice compared to wild-type controls Figure 3-19 C and D). On day 10, the wound in β3-deficient mice was almost completely closed compared to wild-type animals ($p < 0.05$) (Figure 3-19 D). Closer inspection of the wound area showed acceleration of wound closure in β3-deficient mice compared to wild-type controls which were statistically significant already on days 3 and day 6 ($p < 0.05$) (Figure 3-19 D). Taken together fibroblasts migrate faster and secrete more collagen and these properties may essentially determine the accelerated skin wound healing in β3-deficient mice. The migration assays and the collagen secretion were measured using embryonic fibroblasts, but these properties might well be translated to skin fibroblasts which also do express the β3 gene (Figure 3-19 B). We did not find differences in collagen deposition or in the number of neutrophils within the closed wound area 14 days post-wounding (Figure 3-20).
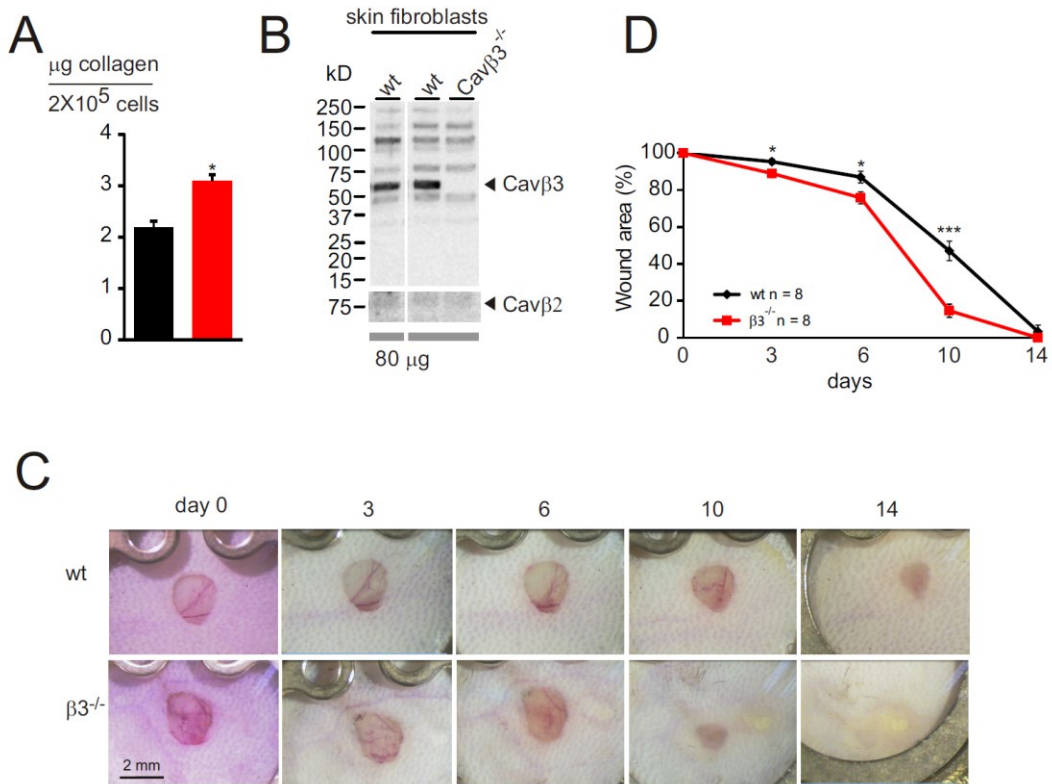
Figure 3-19. Accelerated wound closure in β3-deficient mice

(A) Collagen secretion from wild-type and β3-deficient fibroblasts was measured after culturing the cells for forty eight hours in media containing 1 % FCS. β3-deficient fibroblasts secrete significantly more collagen compared to wild-type cells. Results are expressed as the mean x̄ ± S.E.M. of three independent experiments (* P<0.05; Student t-test). **(B)** Western blot of wild-type and β3-deficient primary skin fibroblasts lysates using anti-Cavβ3 and anti-Cavβ2 specific antibodies and the same amount of protein (80 µg) was loaded per lane showing Cavβ3 expression in primary mouse skin fibroblasts from wild-type cells. The Cavβ3 protein is absent in β3-deficient skin fibroblasts. **(C)** Images display the skin fold chamber directly after wounding (day 0) and after 3, 6, 10 and 14 days post wounding. The continuous process of wound closure, with complete epithelialization is shown over 14 days in both genotypes. **(D)** At the time points indicated, the wound area was determined using a computer-assisted image analysis program (CapImage) and plotted as percentage of the wound area immediately after injury at day 0 (x̄ ± S.E.M. of n = 8 β3-deficient mice and the corresponding wild-type controls). Wound closure is significantly accelerated in β3-deficient mice and it is almost closed at day 10.
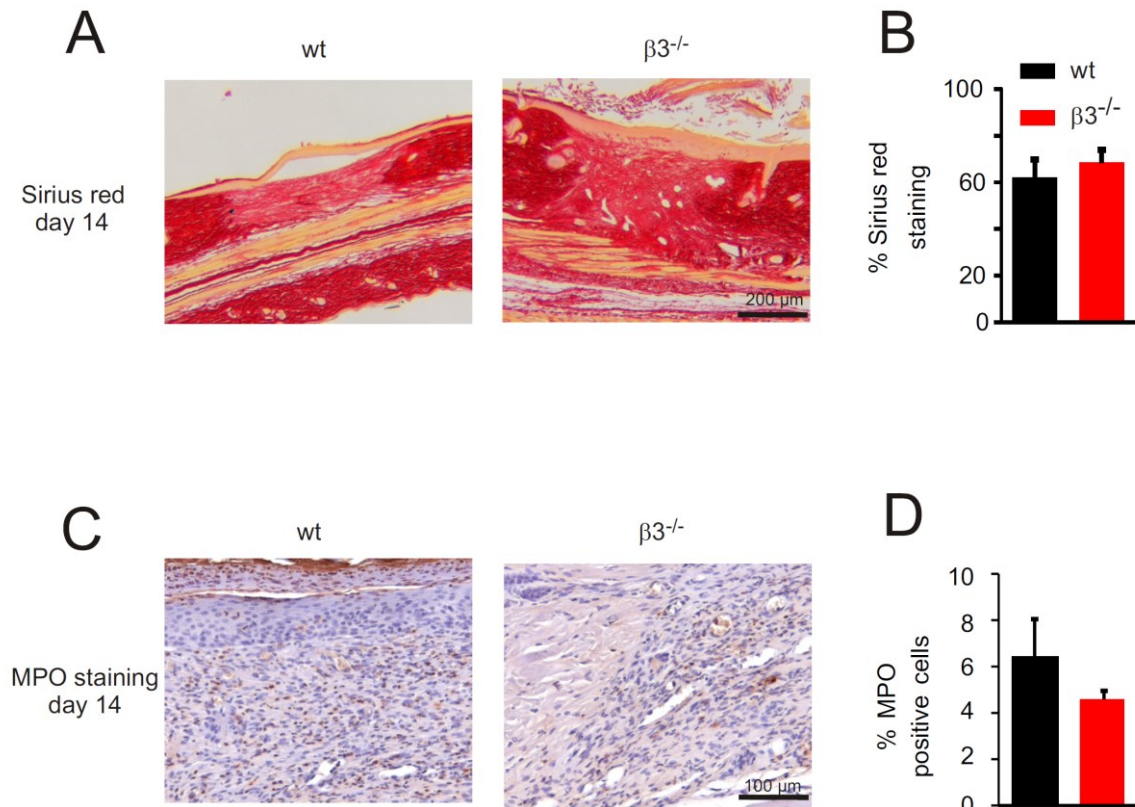
Figure 3-20. Histological analysis of skin area after wound closure.

Paraffin sections (5 μm) from wild-type and β3-deficient mouse skin wounded area 14 days post-wounding stained with Sirius red **(A)** for collagen fibers and with anti-myeloperoxidase (anti-MPO) **(C)** for neutrophils staining. **(B, D)** Summary shows the amount of Sirius red stained collagen (B, x̄ ± S.E.M.) and fraction of MPO positive cells (D, x̄ ± S.E.M.) in skin areas after wound closure from wild-type (black) and β3-deficient animals (red). No significant difference between both genotypes was detectable.

4 Discussion

Cavβs subcellular targeting. The Cavβ subunits are mostly localized all over the cell. (Ruth et al., 1989; Perez-Reyes et al., 1992). Exceptionally Cavβ2N3 and Cavβ2N5 are tethered to the plasma membrane via a palmitoylation at cysteine 3 and 4 in the N-terminus of Cavβ2N3 (Qin et al., 1998) or by electrostatic interaction of the N-terminus of Cavβ2N5 (Miranda-Laferte et al., 2014). Notably, Cavβ3 protein either expressed alone or in the presence of the Cavα1 pore forming subunit shows a cytoplasmic localization (Dolphin, 2003; Suh et al., 2012; Beguin et al., 2014). In agreement with these previous observations, we could show Cavβ3 localization within the cytoplasm by using different techniques. Confocal images of Cos-7 and HEK293 cells expressing cDNAs encoding a β3-GFP fusion protein show a cytoplasmic β3-GFP localization even when co-expressed with the cDNA of Cav1.2 (α1) subunit (Figure 3-2 A and C). Analyzing protein fractions obtained by subcellular fractionation of HEK293 expressing the Cavβ3 cDNA and MEFs we identified the Cavβ3 protein in the fractions mainly containing membranes, cytosol and soluble nuclear components (Figure 3-10). This experiment also shows that the expression of the Cavβ3 cDNA in HEK293 cells does not lead to any mislocalization of the β3 protein because it shows the same distribution as the endogenous β3 protein in MEFs (Figure 3-10). The predominant cytoplasmic localization of Cavβ3 was one of the reasons starting to look for novel functions of the Cavβ3 protein independently of its function as a subunit of the voltage-gated Ca2+ channels.

Non-excitable cells express the β subunits of voltage-gated calcium channels. A major Ca^{2+} entry pathway in excitable cells are voltage-gated Ca^{2+} channels mainly constituted of the pore forming α1 subunit and the auxiliary β subunit (Catterall, 2000). However, subunits of voltage-gated calcium channels have been shown to be expressed also in a number of non-excitable cells including immune cells (Badou et al., 2006; Bergh et al., 2006; Jha et al., 2009). In T-lymphocytes short transcript fragments of the four members of the Cav1 family (Cav1.1, Cav1.2, Cav1.3 and Cav1.4) were detectable by RT-PCR as well as the four auxiliary subunits β1, β2, β3 and β4 (Badou et al., 2006; Jha et al., 2009). Nevertheless, high potassium depolarization does not trigger any Ca^{2+} influx in these cells arguing against the presence of functional voltage-gated calcium channels (Jha et al., 2009). The L-type Ca^{2+} channel Cav1.2 has been shown to be the primary channel responsible for Ca^{2+} influx into actively proliferating osteoblasts which are non-excitable cells (Bergh et al., 2006). However, blockers of this Cav1.2 L-type channels are widely used to treat hypertension but no unwanted effects of these drugs on bone metabolism have been reported so far. Because hypertension is very frequent and its treatment requires continuous administration of these drugs during the whole life, such unwanted effects should have been noticed. Most probably this situation also argues against the presence of functional voltage-gated calcium channels in osteoblasts. We here show the presence of Cavβ3 and Cavβ2 proteins in fibroblasts (Figure 3-4 A) which are non-excitable cells (Fahrenbach et al., 2007). MEFs from β3-deficient mice only express the cacnb2 gene but not the genes for β1 or β4 proteins and we have not seen any compensatory increase of Cavβ2 protein in the absence of β3 protein (Figure 3-4 A). High potassium induced-depolarization activates voltage-gated calcium channels and elicits Ca^{2+} influx for example in wild-type cardiomyocytes but also in HEK293 cells

expressing the cDNA of L-type Ca^{2+} channel (Cav1.2 α1c) and Cavβ3. However high potassium induced depolarization did not trigger any Ca^{2+} entry in wild-type and β3-deficient MEFs indicating the absence of functional voltage-gated calcium channels in these cells. The expression of Cavβ2 and Cavβ3 subunits and the lack of any functional voltage-gated Ca^{2+} channels in MEFs made these cells a very suitable model to study novel functions of the Cavβ3 protein which are not related to Cav1.2 and voltage-gated calcium entry, respectively.

Cavβ3 desensitizes IP3-receptor to low IP3 concentrations. Based on the predominant localization of Cavβ3 within the cytoplasm (Figure 3-2 A and C, Figure 3-10), its expression in cells lacking functional voltage-gated calcium channels (Figure 3-4) and on previous studies by our group (Berggren et al., 2004; Muller et al., 2010) we started to investigate Ca^{2+} channel-independent roles of Cavβ3 by recording agonist-induced Ca^{2+} release from internal stores in different cell systems. We used the carbachol and ATP agonists for the Gq-coupled muscarinic receptor and P2Y receptors endogenously expressed in HEK293 cells (muscarinic receptors) and Cos-7 cells (P2Y receptors). In the absence of extracellular Ca^{2+}, both agonists increase cytosolic calcium by releasing it from intracellular stores. Overexpressing the Cavβ3 cDNA in HEK293 and Cos-7 cells reduced this agonist-induced Ca^{2+} release (Figure 3-2 E, F, G and H). The degree of reduction was more pronounced in Cos-7 cells as compared to HEK293 cells. HEK293 cells endogenously express the β3 gene and very low amounts of β3 protein were detectable in Western blot (Figure 3-2 B). Apparently, these low amounts of endogenous β3 already impair Ca^{2+} release. Additional β3 protein, as obtained by cDNA expression, has only low a small effect in HEK293 cells compared to Cos-7 cells which do not endogenously express the β3 gene. In MEFs

Ca^{2+} release was observed in the presence of bradykinin and LPA acting on endogenously expressed bradykinin and LPA receptors. Deletion of Cavβ3 in MEFs (isolated from β3-deficient mice) led to increased agonist-induced Ca^{2+} release in comparison to wild-type MEFs (Figure 3-5). During the course of this project we have been trying different Gq-coupled receptor activator (vasopressin, ATP, LPA, bradykinin, serotonin, thrombin and histamine) to induce calcium release in primary mouse embryonic fibroblasts. The most consistent results were obtained by bradykinin and LPA and a high number of MEFs (~ 50% of total plated cells) did respond. Bradykinin, LPA, ATP and carbachol are all known to respectively activate Gq-coupled receptors which in turn activate PLC-β hydrolyzing the PIP2 into DAG and IP3. IP3 by itself binds to IP3R and opens the IP3R channel leading to Ca^{2+} release. In the presence of the PLC inhibitor U73122 (Bleasdale et al., 1989) the Ca^{2+} release induced by bradykinin or ATP in MEFs and Cos-7 cells, respectively, was completely abolished (Figure 3-7). At least 4 hypotheses might explain this novel finding of Cavβ3-dependent reduction of agonist-induced Ca^{2+} release: (1) either β3 influences the filling state of the ER-Ca^{2+} stores, (2) β3 expression downregulates the IP3-receptor expression, (3) β3 impairs the IP3R function or (4) β3 modulates the Gq-coupled receptor signaling pathway. Because Cavβ3-deficient and wild-type fibroblasts have shown similar thapsigargin-induced Ca^{2+} release (Figure 3-6 B and C) the hypothesis of different filling state of the ER-Ca^{2+} store is ruled out. No diferences in the expression of IP3R3 were observed between wild-type and Cavβ3-deficient fibroblasts ruling out the second hypothesis of downregulation of IP3R by expression of the Cavβ3 subunit. The key experiment supporting and confirming either the third or the fourth hypothesis is to activate IP3R directly by IP3 and induce Ca^{2+} release without activating any upstream Gq-coupled receptor pathway. If under this condition we could still see the

β3 effect, the third hypothesis might be right, if not then the fourth hypothesis. An experimental way to directly stimulate Ca^{2+} release *via* IP3-receptors comprises the application of "caged-IP3". This approach allows the defined liberation of IP3 by "uncaging" it through UV-light flashes. Accordingly, and in collaboration with Dr. Xin Hui from the group of Peter Lipp, Cos-7 cells expressing the Cavβ3 cDNA or control non-transfected cells and wild-type and β3-deficient MEFs were loaded with caged-IP3 and consecutively UV light flashes of increasing energy were applied leading to the uncaging of increasing amounts of IP3. The increasing amount of IP3 leads to a graded increasing activation of the IP3R with increasing amounts of Ca^{2+} released into the cytosol. The cytosolic Ca^{2+} amplitude can be plotted to the energy of each UV flash, which in turn is a measure for the IP3 concentration. Cavβ3-deficient cells show higher sensitivity to IP3 and as a result the amount of Ca^{2+} release is larger compared to Cavβ3 containing cells (Figure 3-3 and Figure 3-8). This experiment strongly supports our third hypothesis that β3 interacts with the IP3R channel and thereby inhibits IP3-dependent Ca^{2+} release. Deletion of β3 leads to enhanced IP3R sensitivity to IP3 and thereby increased IP3-releasable Ca^{2+}.

The cytoplasmic β3 localization is required for the inhibition of IP3-dependent Ca^{2+} release. We thought that the cytoplasmic localization of Cavβ3 is required for the IP3-dependent calcium release modulation. To confirm this hypothesis, we targeted the β3 subunit to the plasma membrane by fusing the N-terminal 11 amino acid residues of Lyn upstream of the N-terminus of the β3 protein. The 11 amino acid sequences comprise the amino acids Gly-Cys-Ile-Lys-Ser where the glycine (Gly) becomes myristoylated and the cysteine (Cys) becomes

palmitoylated. By myristoylation a 14 carbon saturated fatty acid (myristic acid) is covalently attached by an amide bond to the α-amino group of a glycine residue. By palmitoylation a 16 carbon saturated fatty acid (palmitic acid) is covalently attached by a thioester bond to the α-amino group of a cysteine residue. By these lipid modifications, the β3 protein becomes tethered to the plasma membrane. To visualize the tethered β3 by confocal imaging, I fused the cDNA of YFP or RFP to the 3' end of the Lyn-β3 cDNA construct (Figure 3-1). When expressed in Cos-7 cells these constructs showed membrane localization in confocal images either in the presence or absence of Cav1.2 channel (Figure 3-9 A). The membrane targeted β3 protein lost its propriety to inhibit the IP3-releasable Ca^{2+} in two different sets of experiments; in agonist induced Ca^{2+} release experiment and in Ca^{2+} release obtained by uncaging IP3 (Figure 3-9). In summary, this membrane targeted β3 different to the non-targeted version is not able to interfere with the IP3-dependent Ca^{2+} release, supporting our hypothesis that cytoplasmic localization of the Cavβ3 is required for this effect.

SH3 domain of Cavβ3 mediates its interaction with the IP3R.

Cavβ proteins have been shown to interact with several proteins other than Cav1 and Cav2 channels. The Cavβ3 protein has been shown to interact with the following proteins: the β-anchoring and regulatory protein (BARP) (Beguin et al., 2014), Kir/Gem (Beguin et al., 2001), Pax6 (Zhang et al., 2010), RIM I (Kiyonaka et al., 2007) and Synaptotagmin I (Vendel et al., 2006). Based on our finding of predominant localization of Cavβ3 protein within the cytoplasm and its interference with the IP3-induced calcium release from internal stores in different assays, we started to investigate the interaction of β3 protein with the IP3R channel. By coimmunoprecipitation we could show for the first time that when we immunoprecipitated β3 protein, from cell lysates expressing

both the β3 and IP3R cDNAs, using anti-β3 antibody, the IP3Rs type 1, 2 and 3, respectively were associated with the Cavβ3 protein and vice versa (Figure 3-12). These results support the hypothesis that the β3 binds to the IP3R and acts as a brake on the IP3R channel leading to less Ca^{2+} release in response to either Gq-coupled receptor stimulation or to uncaging of IP3. It has been long recognized that Cavβ proteins consist of a conserved core region flanked by non-conserved N- and C-termini. Frequent splicing of the primary transcripts gives rise to a variety of N-termini for each of the four Cavβ genes. In the core region, a Src homology (SH) 3 domain, a Hook domain and a guanylate kinase (GK) domain can be distinguished. The GK domain is catalytically inactive. At its C-terminus it contains the α1-binding pocket (ABP) which binds with high affinity to a conserved 18-residues sequence (the α1-interaction domain, or AID) (Almagor et al., 2012). The Src homology (SH) 3 domain is a common protein interaction modul known to interact with PxxP-containing motifs. In order to identify the Cavβ3-domain responsible for this Cavβ3-IP3R interaction we generated Cavβ3 mutants lacking either the four initial β-strands of SH3 domain (Cavβ3ΔSH3) or the GK domain (Cavβ3ΔGK) (Figure 3-1). Each of these mutants was expressed with the IP3R3 cDNA in Cos-7 cells and performed a coimmunoprecipitation experiment. Deletion of the SH3 domain, but not the GK domain, abolishes Cavβ3-IP3R interaction in coimmunoprecipitation experiment (Figure 3-13 A). In contrast to wild-type Cavβ3, the Cavβ3ΔSH3 mutant lost its effectiveness to reduce agonist-induced Ca^{2+} release in Cos-7 cells (Figure 3-13 B and C). Coimmunoprecipitation and calcium imaging data using the Cavβ3 mutants strongly indicates that Cavβ3 protein interacts with the IP3-receptor via its SH3 domain and thereby modulates the IP3-releasable Ca^{2+}. Based on Ca^{2+} imaging data using agonist-induced Ca^{2+} release or caged-IP3 and the biochemical data we surmise two binding sites for the Cavβ3 on the

IP3R. Either Cavβ3 binds to the IP3-binding pocket and competes with the IP3 leading to a competitive inhibition of the IP3-releasable Ca^{2+}, or Cavβ3 binds to another domain away from the IP3-binding pocket and inducing conformational changes which leads to a decrease in the sensitivity of IP3R to IP3.

Amino acids 346-917 and 1387-2249 of the IP3R3 are defined as a β3-subunit binding domains. Several proteins have been described to interact with the IP3R and to modulate its function. Homer, Calmodulin and RACK1 have been found to interact with the N-terminal coupling domain. IRBIT (IP3R binding protein released with the inositol 1,4,5-trisphosphate) was shown to bind to the IP3-binding core. RACK1, FKBP12, Bcl-2 and CaM have been reported to bind to the internal coupling domain, whereas Cyt C and 4.1N proteins were shown to bind to the C-terminal tail (Mikoshiba, 2007). We could show that the Cavβ3 protein interacts with the IP3R3. With the aim to identify the binding region of Cavβ3 protein on the IP3R we performed a GST pull down assay, where the Cavβ3 protein was fused to GST and 11 cDNA fragments covering the complete mouse IP3R3 amino acid sequence were cloned. The Cavβ3-GST fusion protein was immobilized the glutathione agarose beads and incubated with the ^{35}S-methionine labeled IP3R3 fragments. The mouse IP3R3 fragments F4 covering amino acid residues from 1387 to 2249 and the F6 covering the amino acid residues from 346 to 917 were retained by the Cavβ3-GST fusion protein but not with the GST alone indicating a specific interaction for these two fragments. In coimmunoprecipitation experiments, we used the whole cell lysates (Figure 3-12), and we could not differentiate whether the β3 protein bound directly to the IP3R or indirectly via other unknown proteins present in the cell lysate. The *in vitro* pull down assay

(Figure 3-14) confirms a direct binding of the β3 protein to the IP3R because only the two proteins are incubated together in this *in vitro* assay. Similar to RACK1 protein previously shown to interact with two distinct site on the IP3R (aa 90-110 and aa 538-729) (Patterson et al., 2004), we could show that the β3 protein binds to the internal coupling domain of the mouse IP3R3 in two distinct site. The first binding site is located at amino acid residues 346 to 917 and the second binding site is located at the amino acid residues 1387 to 2249. Because the IP3R is a tetramer, it might be that β3 protein binds to the first binding site on one monomer and another β3 protein binds to the second binding site of another monomer.

The IP3R fragments F1, F7, F10 and F11 were retained by the Cavβ3-GST fusion protein as well as by the GST alone. These results make it difficult to ascertain whether these fragments (F1, F7, F10 and F11) are really binding to the β3 protein or not. Nevertheless the F1, F7, F10 and F11 fragments overlap with the fragments F4 and F6 (which specifically bind to the IP3R) suggesting that the binding which we see to the Cavβ3-GST fusion protein might be specific. Agonist induced Ca^{2+} release, uncaging of IP3 and biochemical analysis data suggest that Cavβ3 protein interacts and decreases the sensitivity of the IP3R to IP3 molecules. It has been shown that residues in the region of 1-223 and 651-1130 are critical for functional coupling between IP3 binding and the channel opening (Mikoshiba, 2007). It has also been proposed that binding of IP3 to the IP3-binding core induces conformational changes transmitted *via* the N-terminal coupling domain and internal coupling domain to the C-terminal tail triggering channel opening (Mikoshiba, 2007). Based on our data and on previous studies, we propose in this study that the Cavβ3 binds to the internal coupling domain at two distinct sites and might either decrease the affinity of IP3-binding core to the IP3 molecules or decreases the flexibility of the IP3R channel opening.

Cavβ3 modulates intracellular Ca²⁺ and cell motility. We could show

that the Cavβ3 protein interferes on the IP3-releasable Ca²⁺ in mouse embryonic

fibroblasts, and thereby identify a novel role of β3 in cells which lack functional voltage-

gated calcium channels. Fibroblasts are connective tissue cells, are migrating cells and

produce different types of collagen and extracellular matrix proteins (Souders et al.,

2009). Calcium signaling on the other hand plays an important role in cell motility

(Pietruck et al., 1997; Leiper et al., 2006; Yamada et al., 2010; Xu and Chisholm, 2011).

Our data show that fibroblasts lacking the Cavβ3 migrate faster and close the scratch

in shorter time compared to wild-type cells (Figure 3-15). Apparently, cells lacking the

β3 protein elicit more Ca²⁺ release upon scratch and thus migrate faster. In a

chemotactic migration system where the cells are attracted to migrate towards FCS,

β3-deficient fibroblasts show less migration than wild-type cells (Figure 3-16). This

differential behavior in scratch versus chemotactic migration assay has been observed

by Getty et al., using a Batten disease gene CLN3-deficient MEFs (Getty et al., 2011).

This differential migration behavior of CLN3-deficient MEFs was reported to be

apparently due to different cell morphology or cell size or due to a particular sensitivity

to serum deprivation within the upper chamber of the chemotactic assay. One reason

that might explain why less β3-deficient fibroblasts are passing the filter pores toward

FCS could be a bigger cell size or a different morphology of β3-deficient fibroblasts.

Alternatively, β3-deficient fibroblasts are less attracted by FCS within the lower

chamber. The closure of the gap in the scratch migration assay is known as

combination of both cell motility and cell proliferation. Viability of the cells plays an

important role in cell motility as well. To control that the migration behavior of β3-

deficient fibroblasts observed in the scratch migration assay is due to faster cell motility

and not to higher cell proliferation or better cell viability we performed two sets of experiments. The first we performed the migration assay in the presence of 10 % FCS where we can see both cell migration and proliferation and in the presence of 1 % FCS where the cell proliferation is very minimal (Figure 3-15). The second we studied the cell proliferation and viability of wild-type and β3-deficient MEFs for 8 days (Figure 3-17). Our data show comparable proliferation and viability between both genotypes supporting our conclusion that β3-deficient fibroblasts migrate faster than wild-type controls in the scratch assay.

Actin polymerization and collagen secretion. Polymerization and depolymerization of actin are important determinants of cell motility (Storch et al., 2012). We have studied actin polymerization in wild-type and β3-deficient fibroblasts by Western blot and fluorescent staining by phalloidin. The underlying idea was that the increased agonist-induced Ca^{2+} release in β3-deficient fibroblasts could have an impact on the monomeric globular and the actin filaments balance and thereby influence cell motility, but G/F actin ratio and stress fibers of filamentous actin are not significantly changed in both genotypes (Figure 3-18). Apparently, the increased scratch migration phenotype in β3-deficient fibroblasts might be due to another parameter. Extracellular matrix plays an important role in the control of cell behavior. Fibroblasts contribute to the secretion of extracellular matrix and secrete specially one of the major extracellular matrix component collagen (Enoch, 2005; Andrew Hsu, 2010). Collagen has been shown to play an important role *in vivo* and *in vitro* on cell differentiation and on the control of cell proliferation and migration (Schor, 1980). Interestingly, collagen secretion was significantly increased in β3-deficient fibroblasts compared to wild-type cells (Figure 3-19). It has been previously shown that bradykinin

receptor stimulation in mesangial cells results in increased collagen secretion (Girolami et al., 1995). Enhancement of agonist-induced Ca^{2+} release in β3-deficient cells might explain the increased collagen secretion in these cells. This increased collagen secretion observed in β3-deficient fibroblasts might also explain this faster migration as collagen maybe used as trail for cells to facilitate and direct their migration.

Cavβ3 impact on skin wound healing. During skin wound repair, fibroblasts are proliferating and are attracted to migrate towards the wound area either from the edge of the wound or from the bone marrow. Fibroblasts within the wound produce various components of the extracellular matrix, mainly in the form of collagen (Enoch, 2005; Gurtner et al., 2008). Accordingly, we started to study dermal wound repair in β3-deficient mice compared to wild-type mice. We have used a previously described model of skin wound healing using a skin fold chamber described by (Sorg et al., 2007). The first advantage of this skin fold chamber model is to minimize skin contraction which significantly influences skin wound healing in mice. The second advantage of this model is that the wound is covered by a glass coverslip reducing the possibility of infections which might delay the healing process. The third advantage is that one can follow under the microscope the wound healing process over time. Our data show that the skin wound healing is accelerated in β3-deficient mice; The wounds closed significantly earlier (10 days) compared to wounds of wild-type controls (Figure 3-19) which show a normal skin wound healing and epithelialization over 14 days similar as previously described (Eming et al., 2007; Sorg et al., 2007). During the inflammatory phase (3-6 days post wounding) we could detect a minor but significant acceleration of wound repair in β3-deficient mice. During the remodeling phase where fibroblasts play a crucial role by migrating into the wound and secreting collagen, the acceleration

of wound repair in β3-deficient mice become more predominant (Figure 3-19 C and D). This time dependent difference seen in skin wound repair in β3-deficient mice argue for a combination of accelerated fibroblasts migration as well as an enhancement in collagen secretion. Nevertheless, the influence of T-lymphocytes and keratinocytes cannot be excluded at this stage of our study especially since β3-deficient CD8^{+} T-lymphocytes show a survival defect which might reduce the immune response phase and thus might affect skin wound repair. Fibroblasts specific β3 gene deletion can be the option of choice to clarify whether the skin fibroblasts, are the key determinant of accelerated skin wound healing or whether it is influenced by additional cell types. Although collagen secretion in β3-deficient fibroblasts is enhanced, we could not see any significant increase in collagen deposition in skin wound tissue 14 days post wounding. Either the technique used (Sirius red staining) is not sensitive enough to detect the differences in collagen secretion within the wounded tissue from wild-type and β3-deficient animals , or the increase in collagen deposition occurs earlier during the wound healing process and then goes back to normal level after complete wound healing in both genotypes.

5 Conclusion and perspectives

Here we discovered a previously unrecognized function of Cavβ3 protein which is independent of its function as a subunit of voltage-gated calcium channels (Figure 5-1). Loss of Cavβ3 resulted in enhancement of IP3-releasable Ca^{2+} in primary mouse embryonic fibroblast and vice versa the expression of the Cavβ3 cDNA in Cos-7 and HEK293 cells decreased the IP3-dependent Ca^{2+} release. We demonstrate that Cavβ3 protein desensitizes cells for low concentrations of IP3 by a direct interaction of Cavβ3 and IP3Rs *via* the SH3 domain of the Cavβ3 protein. Deletion of the Cavβ3-SH3 domain or targeting the β3 protein to the plasma membrane (Lyn-β3) abolishes completely its Ca^{2+} suppressor effect. Interestingly, by glutathione S-transferase-pull-down experiment two novel binding sites for Cavβ3 protein were mapped to amino acid residues 346-917 and amino acid residues 1387-2249 of the mouse IP3R3. The direct interaction of Cavβ3 with the IP3Rs and the modulation of its sensitivity to IP3 may constitute the molecular explanation of the increased Ca^{2+} oscillation frequency in β3-deficient pancreatic islets and the more efficient glucose clearance in cacnb3-deficient mice. The most profound observation of our study was the accelerated skin wound healing in mice lacking the Cavβ3 protein. This newly discovered phenotype of Cavβ3-deficient mice might be due to the increased IP3-releasable Ca^{2+} triggering skin fibroblasts to migrate into the wound area in a faster manner and to secrete more collagen helping in repairing the wound more efficiently. Useful knowledge has been gained using Cavβ3-deficient mice, and it would be desirable to study the skin wound healing in mice which lack cacnb3 gene expression only in skin fibroblasts. To better understand how Cavβ3 desensitizes the IP3-receptor to low concentrations of IP3, a high resolution structure of Cavβ3 in complex with the IP3R may constitute an option.

It has been proposed that small molecule inhibitors of Cavβ3 subunit might represent future therapies against diabetes (Berggren and Flockerzi, 2003) and hypertension (Kharade et al., 2013). Our novel finding might also be a hope for patients suffering from delayed skin wound healing for a new therapy. We suggest that the downregulation of Cavβ3 by siRNA or the inhibition of the Cavβ3 protein locally may represent novel therapeutic approaches to accelerate skin wound healing. These perspectives are long-term goals and need further studies and is also without doubt technically challenging but seems promising.
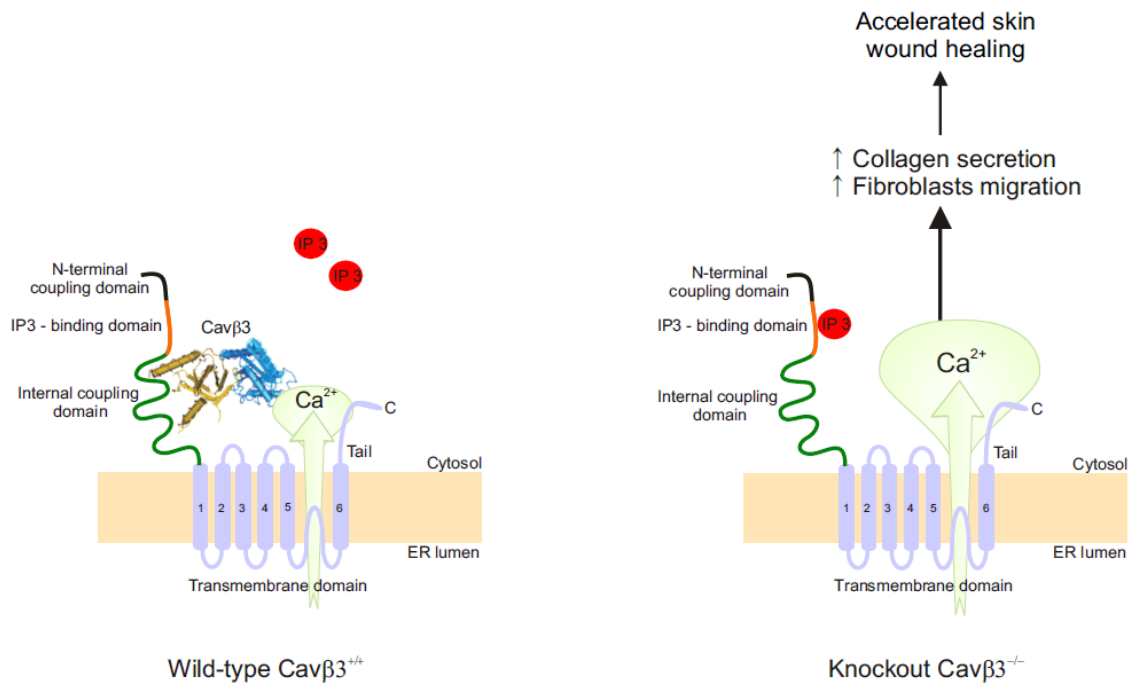
Figure 5-1 Schematic illustration of the novel Cav-independent function of the Cavβ3 protein.

In wild-type (Cavβ3$^{+/+}$), the β3 protein binds to the internal coupling domain of the IP3-receptor and decreases the IP3R sensitivity to IP3 and thereby decreases the IP3-releasable calcium. In the absence of β3 protein (Cavβ3$^{-/-}$), the IP3R channel is more sensitive to IP3 leading to increased IP3-releasable calcium. This effect leads to enhanced collagen secretion and faster migration of fibroblasts and thereby results in accelerated skin wound healing.

6 References

Almagor, L., Chomsky-Hecht, O., Ben-Mocha, A., Hendin-Barak, D., Dascal, N., and Hirsch, J.A. (2012). "The role of a voltage-dependent Ca^{2+} channel intracellular linker: a structure-function analysis". J Neurosci **32**, 7602-7613.

Alvarez, J., Hamplova, J., Hohaus, A., Morano, I., Haase, H., and Vassort, G. (2004). "Calcium current in rat cardiomyocytes is modulated by the carboxyl-terminal ahnak domain". J Biol Chem **279**, 12456-12461.

Andrew Hsu, M., and Thomas A. Mustoe, MD, FACS (2010). "The Principles Of Wound Healing". 2010 - elsevieradvantagecom.

Astori, S., Wimmer, R.D., Prosser, H.M., Corti, C., Corsi, M., Liaudet, N., Volterra, A., Franken, P., Adelman, J.P., and Luthi, A. (2011). "The Ca(V)3.3 calcium channel is the major sleep spindle pacemaker in thalamus". Proc Natl Acad Sci U S A **108**, 13823-13828.

Badou, A., Jha, M.K., Matza, D., Mehal, W.Z., Freichel, M., Flockerzi, V., and Flavell, R.A. (2006). "Critical role for the beta regulatory subunits of Cav channels in T lymphocyte function". Proc Natl Acad Sci U S A **103**, 15529-15534.

Ball, S.L., McEnery, M.W., Yunker, A.M., Shin, H.S., and Gregg, R.G. (2011). "Distribution of voltage gated calcium channel beta subunits in the mouse retina". Brain Res **1412**, 1-8.

Ball, S.L., Powers, P.A., Shin, H.S., Morgans, C.W., Peachey, N.S., and Gregg, R.G. (2002). "Role of the beta(2) subunit of voltage-dependent calcium channels in the retinal outer plexiform layer". Invest Ophthalmol Vis Sci **43**, 1595-1603.

Bech-Hansen, N.T., Naylor, M.J., Maybaum, T.A., Pearce, W.G., Koop, B., Fishman, G.A., Mets, M., Musarella, M.A., and Boycott, K.M. (1998). "Loss-of-function mutations in a calcium-channel alpha1-subunit gene in Xp11.23 cause incomplete X-linked congenital stationary night blindness". Nat Genet **19**, 264-267.

Beguin, P., Nagashima, K., Gonoi, T., Shibasaki, T., Takahashi, K., Kashima, Y., Ozaki, N., Geering, K., Iwanaga, T., and Seino, S. (2001). "Regulation of Ca^{2+} channel expression at the cell surface by the small G-protein kir/Gem". Nature **411**, 701-706.

Beguin, P., Nagashima, K., Mahalakshmi, R.N., Vigot, R., Matsunaga, A., Miki, T., Ng, M.Y., Ng, Y.J., Lim, C.H., Tay, H.S.*, et al.* (2014). "BARP suppresses voltage-gated calcium channel activity and Ca^{2+}-evoked exocytosis". J Cell Biol **205**, 233-249.

Berggren, P.O., and Flockerzi, V. (2003). "inhibition of the β3 subunit of L-type Ca^{2+} channels". World intellectual property organization **WO2003078630 A1**.

Berggren, P.O., Yang, S.N., Murakami, M., Efanov, A.M., Uhles, S., Kohler, M., Moede, T., Fernstrom, A., Appelskog, I.B., Aspinwall, C.A.*, et al.* (2004). "Removal of Ca^{2+} channel beta3 subunit enhances Ca^{2+} oscillation frequency and insulin exocytosis". Cell **119**, 273-284.

REFERENCES

Bergh, J.J., Shao, Y., Puente, E., Duncan, R.L., and Farach-Carson, M.C. (2006). "Osteoblast Ca^{2+} permeability and voltage-sensitive Ca^{2+} channel expression is temporally regulated by 1,25-dihydroxyvitamin D(3)". Am J Physiol Cell Physiol **290**, C822-831.

Bernardo, J.F., Magyar, C.E., Sneddon, W.B., and Friedman, P.A. (2009). "Impaired renal calcium absorption in mice lacking calcium channel beta 3 subunits". Can J Physiol Pharmacol **87**, 522-530.

Bird, G.S., Rossier, M.F., Hughes, A.R., Shears, S.B., Armstrong, D.L., and Putney, J.W., Jr. (1991). "Activation of Ca^{2+} entry into acinar cells by a non-phosphorylatable inositol trisphosphate". Nature **352**, 162-165.

Bleasdale, J.E., Bundy, G.L., Bunting, S., Fitzpatrick, F.A., Huff, R.M., Sun, F.F., and Pike, J.E. (1989). "Inhibition of phospholipase C dependent processes by U-73, 122". Adv Prostaglandin Thromboxane Leukot Res **19**, 590-593.

Bogdanov, Y., Brice, N.L., Canti, C., Page, K.M., Li, M., Volsen, S.G., and Dolphin, A.C. (2000). "Acidic motif responsible for plasma membrane association of the voltage-dependent calcium channel beta1b subunit". Eur J Neurosci **12**, 894-902.

Bonen, D.K., and Schmid, T.M. (1991). "Elevated extracellular calcium concentrations induce type X collagen synthesis in chondrocyte cultures". J Cell Biol **115**, 1171-1178.

Boulay, G., Brown, D.M., Qin, N., Jiang, M., Dietrich, A., Zhu, M.X., Chen, Z., Birnbaumer, M., Mikoshiba, K., and Birnbaumer, L. (1999). "Modulation of Ca^{2+} entry by polypeptides of the inositol 1,4, 5-trisphosphate receptor (IP3R) that bind transient receptor potential (TRP): evidence for roles of TRP and IP3R in store depletion-activated Ca^{2+} entry". Proc Natl Acad Sci U S A **96**, 14955-14960.

Bouron, A., Potreau, D., Besse, C., and Raymond, G. (1990). "An efficient isolation procedure of Ca-tolerant ventricular myocytes from ferret heart for applications in electrophysiological studies". Biol Cell **70**, 121-127.

Boyden, S. (1962). "The chemotactic effect of mixtures of antibody and antigen on polymorphonuclear leucocytes". J Exp Med **115**, 453-466.

Buraei, Z., and Yang, J. (2010). "The ss subunit of voltage-gated Ca^{2+} channels". Physiol Rev **90**, 1461-1506.

Burgess, D.L., Biddlecome, G.H., McDonough, S.I., Diaz, M.E., Zilinski, C.A., Bean, B.P., Campbell, K.P., and Noebels, J.L. (1999). "beta subunit reshuffling modifies N- and P/Q-type Ca^{2+} channel subunit compositions in lethargic mouse brain". Mol Cell Neurosci **13**, 293-311.

Burgess, D.L., Jones, J.M., Meisler, M.H., and Noebels, J.L. (1997). "Mutation of the Ca^{2+} channel beta subunit gene Cchb4 is associated with ataxia and seizures in the lethargic (lh) mouse". Cell **88**, 385-392.

Canti, C., Bogdanov, Y., and Dolphin, A.C. (2000). "Interaction between G proteins and accessory subunits in the regulation of 1B calcium channels in Xenopus oocytes". J Physiol **527 Pt 3**, 419-432.

REFERENCES

Catterall, W.A. (2000). "Structure and regulation of voltage-gated Ca^{2+} channels". Annu Rev Cell Dev Biol **16**, 521-555.

Catterall, W.A., Perez-Reyes, E., Snutch, T.P., and Striessnig, J. (2005). "International Union of Pharmacology. XLVIII. Nomenclature and structure-function relationships of voltage-gated calcium channels". Pharmacol Rev **57**, 411-425.

Chang, B., Heckenlively, J.R., Bayley, P.R., Brecha, N.C., Davisson, M.T., Hawes, N.L., Hirano, A.A., Hurd, R.E., Ikeda, A., Johnson, B.A., *et al.* (2006). "The nob2 mouse, a null mutation in Cacna1f: anatomical and functional abnormalities in the outer retina and their consequences on ganglion cell visual responses". Vis Neurosci **23**, 11-24.

Chaudhari, N. (1992). "A single nucleotide deletion in the skeletal muscle-specific calcium channel transcript of muscular dysgenesis (mdg) mice". J Biol Chem **267**, 25636-25639.

Chen, Y.H., Li, M.H., Zhang, Y., He, L.L., Yamada, Y., Fitzmaurice, A., Shen, Y., Zhang, H., Tong, L., and Yang, J. (2004). "Structural basis of the alpha1-beta subunit interaction of voltage-gated Ca^{2+} channels". Nature **429**, 675-680.

Cheng, W., Altafaj, X., Ronjat, M., and Coronado, R. (2005). "Interaction between the dihydropyridine receptor Ca^{2+} channel beta-subunit and ryanodine receptor type 1 strengthens excitation-contraction coupling". Proc Natl Acad Sci U S A **102**, 19225-19230.

Colecraft, H.M., Alseikhan, B., Takahashi, S.X., Chaudhuri, D., Mittman, S., Yegnasubramanian, V., Alvania, R.S., Johns, D.C., Marban, E., and Yue, D.T. (2002). "Novel functional properties of Ca^{2+} channel beta subunits revealed by their expression in adult rat heart cells". J Physiol **541**, 435-452.

Curtis, B.M., and Catterall, W.A. (1984). "Purification of the calcium antagonist receptor of the voltage-sensitive calcium channel from skeletal muscle transverse tubules". Biochemistry **23**, 2113-2118.

Dalton, S., Takahashi, S.X., Miriyala, J., and Colecraft, H.M. (2005). "A single CaVbeta can reconstitute both trafficking and macroscopic conductance of voltage-dependent calcium channels". J Physiol **567**, 757-769.

De Waard, M., Pragnell, M., and Campbell, K.P. (1994). "Ca^{2+} channel regulation by a conserved beta subunit domain". Neuron **13**, 495-503.

Dolphin, A.C. (2003). "Beta subunits of voltage-gated calcium channels". J Bioenerg Biomembr **35**, 599-620.

Dolphin, A.C. (2012). "Calcium channel auxiliary alpha2delta and beta subunits: trafficking and one step beyond". Nat Rev Neurosci **13**, 542-555.

Dolphin, A.C. (2013). "The alpha2delta subunits of voltage-gated calcium channels". Biochim Biophys Acta **1828**, 1541-1549.

Eming, S.A., Werner, S., Bugnon, P., Wickenhauser, C., Siewe, L., Utermohlen, O., Davidson, J.M., Krieg, T., and Roers, A. (2007). "Accelerated wound closure in mice deficient for interleukin-10". Am J Pathol **170**, 188-202.

Enoch, S. (2005). "Basic science of wound healing". Basic science **26:2**.

Etemad, S., Obermair, G.J., Bindreither, D., Benedetti, A., Stanika, R., Di Biase, V., Burtscher, V., Koschak, A., Kofler, R., Geley, S.*, et al.* (2014). "Differential neuronal targeting of a new and two known calcium channel beta4 subunit splice variants correlates with their regulation of gene expression". J Neurosci **34**, 1446-1461.

Fahrenbach, J.P., Mejia-Alvarez, R., and Banach, K. (2007). "The relevance of non-excitable cells for cardiac pacemaker function". J Physiol **585**, 565-578.

Fan, M., Zhang, W.K., Buraei, Z., and Yang, J. (2012). "Molecular determinants of Gem protein inhibition of P/Q-type Ca^{2+} channels". J Biol Chem **287**, 22749-22758.

Felgner, P.L., Gadek, T.R., Holm, M., Roman, R., Chan, H.W., Wenz, M., Northrop, J.P., Ringold, G.M., and Danielsen, M. (1987). "Lipofection: a highly efficient, lipid-mediated DNA-transfection procedure". Proc Natl Acad Sci U S A **84**, 7413-7417.

Flaherty, K.M., McKay, D.B., Kabsch, W., and Holmes, K.C. (1991). "Similarity of the three-dimensional structures of actin and the ATPase fragment of a 70-kDa heat shock cognate protein". Proc Natl Acad Sci U S A **88**, 5041-5045.

Flockerzi, V., Oeken, H.J., Hofmann, F., Pelzer, D., Cavalie, A., and Trautwein, W. (1986). "Purified dihydropyridine-binding site from skeletal muscle t-tubules is a functional calcium channel". Nature **323**, 66-68.

Freise, D., Held, B., Wissenbach, U., Pfeifer, A., Trost, C., Himmerkus, N., Schweig, U., Freichel, M., Biel, M., Hofmann, F.*, et al.* (2000). "Absence of the gamma subunit of the skeletal muscle dihydropyridine receptor increases L-type Ca^{2+} currents and alters channel inactivation properties". J Biol Chem **275**, 14476-14481.

Freise, D., Himmerkus, N., Schroth, G., Trost, C., Weissgerber, P., Freichel, M., and Flockerzi, V. (1999). "Mutations of calcium channel beta subunit genes in mice". Biol Chem **380**, 897-902.

Gawronska-Kozak, B. (2011). "Scarless skin wound healing in FOXN1 deficient (nude) mice is associated with distinctive matrix metalloproteinase expression". Matrix Biol **30**, 290-300.

Gee, N.S., Brown, J.P., Dissanayake, V.U., Offord, J., Thurlow, R., and Woodruff, G.N. (1996). "The novel anticonvulsant drug, gabapentin (Neurontin), binds to the alpha2delta subunit of a calcium channel". J Biol Chem **271**, 5768-5776.

Getty, A.L., Benedict, J.W., and Pearce, D.A. (2011). "A novel interaction of CLN3 with nonmuscle myosin-IIB and defects in cell motility of Cln3(-/-) cells". Exp Cell Res **317**, 51-69.

Girolami, J.P., Ouardani, M., Bascands, J.L., Pecher, C., Bompart, G., and Leung-Tack, J. (1995). "Comparison of B1 and B2 receptor activation on intracellular calcium,

cell proliferation, and extracellular collagen secretion in mesangial cells from normal and diabetic rats". <u>Can J Physiol Pharmacol</u> **73**, 848-853.

Gonzalez-Gutierrez, G., Miranda-Laferte, E., Neely, A., and Hidalgo, P. (2007). "The Src homology 3 domain of the beta-subunit of voltage-gated calcium channels promotes endocytosis via dynamin interaction". <u>J Biol Chem</u> **282**, 2156-2162.

Gregg, R.G., Messing, A., Strube, C., Beurg, M., Moss, R., Behan, M., Sukhareva, M., Haynes, S., Powell, J.A., Coronado, R.*, et al.* (1996). "Absence of the beta subunit (cchb1) of the skeletal muscle dihydropyridine receptor alters expression of the alpha 1 subunit and eliminates excitation-contraction coupling". <u>Proc Natl Acad Sci U S A</u> **93**, 13961-13966.

Gurtner, G.C., Werner, S., Barrandon, Y., and Longaker, M.T. (2008). "Wound repair and regeneration". <u>Nature</u> **453**, 314-321.

Haase, H. (2007). "Ahnak, a new player in beta-adrenergic regulation of the cardiac L-type Ca^{2+} channel". <u>Cardiovasc Res</u> **73**, 19-25.

Haase, H., Podzuweit, T., Lutsch, G., Hohaus, A., Kostka, S., Lindschau, C., Kott, M., Kraft, R., and Morano, I. (1999). "Signaling from beta-adrenoceptor to L-type calcium channel: identification of a novel cardiac protein kinase A target possessing similarities to AHNAK". <u>Faseb J</u> **13**, 2161-2172.

Held, B., Tsvilovskyy, V., Meissner, M., Kaestner, L., Ludwig, A., Mossmang, S., Lipp, P., Freichel, M., and Flockerzi, V. (2007). "Ca^{2+} channel currents and contraction in Cavbeta3-deficient ileum smooth muscle from mouse". <u>Cell Calcium</u> **42**, 477-487.

Hibino, H., Pironkova, R., Onwumere, O., Rousset, M., Charnet, P., Hudspeth, A.J., and Lesage, F. (2003). "Direct interaction with a nuclear protein and regulation of gene silencing by a variant of the Ca^{2+}-channel beta 4 subunit". <u>Proc Natl Acad Sci U S A</u> **100**, 307-312.

Hofmann, F., Flockerzi, V., Kahl, S., and Wegener, J.W. (2014). "L-type CaV1.2 calcium channels: from in vitro findings to in vivo function". <u>Physiol Rev</u> **94**, 303-326.

Hullin, R., Khan, I.F., Wirtz, S., Mohacsi, P., Varadi, G., Schwartz, A., and Herzig, S. (2003). "Cardiac L-type calcium channel beta-subunits expressed in human heart have differential effects on single channel characteristics". <u>J Biol Chem</u> **278**, 21623-21630.

Hullin, R., Singer-Lahat, D., Freichel, M., Biel, M., Dascal, N., Hofmann, F., and Flockerzi, V. (1992). "Calcium channel beta subunit heterogeneity: functional expression of cloned cDNA from heart, aorta and brain". <u>Embo J</u> **11**, 885-890.

Jeon, D., Song, I., Guido, W., Kim, K., Kim, E., Oh, U., and Shin, H.S. (2008). "Ablation of Ca^{2+} channel beta3 subunit leads to enhanced N-methyl-D-aspartate receptor-dependent long term potentiation and improved long term memory". <u>J Biol Chem</u> **283**, 12093-12101.

Jha, M.K., Badou, A., Meissner, M., McRory, J.E., Freichel, M., Flockerzi, V., and Flavell, R.A. (2009). "Defective survival of naive CD8+ T lymphocytes in the absence

of the beta3 regulatory subunit of voltage-gated calcium channels". Nat Immunol **10**, 1275-1282.

Jing, X., Li, D.Q., Olofsson, C.S., Salehi, A., Surve, V.V., Caballero, J., Ivarsson, R., Lundquist, I., Pereverzev, A., Schneider, T.*, et al.* (2005). "Cav2.3 calcium channels control second-phase insulin release". J Clin Invest **115**, 146-154.

Jones, L.P., Wei, S.K., and Yue, D.T. (1998). "Mechanism of auxiliary subunit modulation of neuronal alpha1E calcium channels". J Gen Physiol **112**, 125-143.

Josephson, I.R., and Varadi, G. (1996). "The beta subunit increases Ca2+ currents and gating charge movements of human cardiac L-type Ca2+ channels". Biophys J **70**, 1285-1293.

Katiyar, R., Weissgerber, P., Roth, E., Dorr, J., Sothilingam, V., Garcia Garrido, M., Beck, S.C., Seeliger, M., Beck, A., Schmitz, F.*, et al.* (2015). "Influence of the beta2-subunit of L-type voltage-gated Cav channels on the structural and functional development of photoreceptor ribbon synapses". Invest Ophthalmol Vis Sci.

Kharade, S.V., Sonkusare, S.K., Srivastava, A.K., Thakali, K.M., Fletcher, T.W., Rhee, S.W., and Rusch, N.J. (2013). "The beta3 subunit contributes to vascular calcium channel upregulation and hypertension in angiotensin II-infused C57BL/6 mice". Hypertension **61**, 137-142.

Kiyonaka, S., Wakamori, M., Miki, T., Uriu, Y., Nonaka, M., Bito, H., Beedle, A.M., Mori, E., Hara, Y., De Waard, M.*, et al.* (2007). "RIM1 confers sustained activity and neurotransmitter vesicle anchoring to presynaptic Ca^{2+} channels". Nat Neurosci **10**, 691-701.

Kuhn, S., Knirsch, M., Ruttiger, L., Kasperek, S., Winter, H., Freichel, M., Flockerzi, V., Knipper, M., and Engel, J. (2009). "Ba^{2+} currents in inner and outer hair cells of mice lacking the voltage-dependent Ca^{2+} channel subunits beta3 or beta4". Channels (Austin) **3**, 366-376.

Kurien, B.T., and Scofield, R.H. (2006). "Western blotting". Methods **38**, 283-293.

Laschke, M.W., Vollmar, B., and Menger, M.D. (2011). "The dorsal skinfold chamber: window into the dynamic interaction of biomaterials with their surrounding host tissue". Eur Cell Mater **22**, 147-164; discussion 164-147.

Leiper, L.J., Walczysko, P., Kucerova, R., Ou, J., Shanley, L.J., Lawson, D., Forrester, J.V., McCaig, C.D., Zhao, M., and Collinson, J.M. (2006). "The roles of calcium signaling and ERK1/2 phosphorylation in a Pax6+/- mouse model of epithelial wound-healing delay". BMC Biol **4**, 27.

Link, S., Meissner, M., Held, B., Beck, A., Weissgerber, P., Freichel, M., and Flockerzi, V. (2009). "Diversity and developmental expression of L-type calcium channel beta2 proteins and their influence on calcium current in murine heart". J Biol Chem **284**, 30129-30137.

REFERENCES

Lovisolo, D., Ariano, P., and Distasi, C. (2012). "Calcium signaling in neuronal motility: pharmacological tools for investigating specific pathways". Curr Med Chem **19**, 5793-5801.

Ludwig, A., Flockerzi, V., and Hofmann, F. (1997). "Regional expression and cellular localization of the alpha1 and beta subunit of high voltage-activated calcium channels in rat brain". J Neurosci **17**, 1339-1349.

Machesky, L.M., and Insall, R.H. (1999). "Signaling to actin dynamics". J Cell Biol **146**, 267-272.

Marquart, A., and Flockerzi, V. (1997). "alpha1-beta interaction in voltage-gated cardiac L-type calcium channels". FEBS Lett **407**, 137-140.

Matza, D., Badou, A., Kobayashi, K.S., Goldsmith-Pestana, K., Masuda, Y., Komuro, A., McMahon-Pratt, D., Marchesi, V.T., and Flavell, R.A. (2008). "A scaffold protein, AHNAK1, is required for calcium signaling during T cell activation". Immunity **28**, 64-74.

Meissner, M., Weissgerber, P., Londono, J.E., Prenen, J., Link, S., Ruppenthal, S., Molkentin, J.D., Lipp, P., Nilius, B., Freichel, M.*, et al.* (2011). "Moderate calcium channel dysfunction in adult mice with inducible cardiomyocyte-specific excision of the cacnb2 gene". J Biol Chem **286**, 15875-15882.

Mikoshiba, K. (2007). "IP3 receptor/Ca^{2+} channel: from discovery to new signaling concepts". J Neurochem **102**, 1426-1446.

Miranda-Laferte, E., Ewers, D., Guzman, R.E., Jordan, N., Schmidt, S., and Hidalgo, P. (2014). "The N-terminal domain tethers the voltage-gated calcium channel beta2e-subunit to the plasma membrane via electrostatic and hydrophobic interactions". J Biol Chem **289**, 10387-10398.

Mitcheson, J.S., Hancox, J.C., and Levi, A.J. (1998). "Cultured adult cardiac myocytes: future applications, culture methods, morphological and electrophysiological properties". Cardiovasc Res **39**, 280-300.

Moon, I.S., Lee, H., Park, S.D., and Seog, D.H. (2010). "Immunonucleochemistry: a new method for in situ detection of antigens in the nucleus of cells in culture". Cytotechnology **62**, 83-93.

Mori, Y., Friedrich, T., Kim, M.S., Mikami, A., Nakai, J., Ruth, P., Bosse, E., Hofmann, F., Flockerzi, V., Furuichi, T.*, et al.* (1991). "Primary structure and functional expression from complementary DNA of a brain calcium channel". Nature **350**, 398-402.

Muller, C.S., Haupt, A., Bildl, W., Schindler, J., Knaus, H.G., Meissner, M., Rammner, B., Striessnig, J., Flockerzi, V., Fakler, B.*, et al.* (2010). "Quantitative proteomics of the Cav2 channel nano-environments in the mammalian brain". Proc Natl Acad Sci U S A **107**, 14950-14957.

Murakami, M., Fleischmann, B., De Felipe, C., Freichel, M., Trost, C., Ludwig, A., Wissenbach, U., Schwegler, H., Hofmann, F., Hescheler, J.*, et al.* (2002). "Pain

perception in mice lacking the beta3 subunit of voltage-activated calcium channels". J Biol Chem **277**, 40342-40351.

Murakami, M., Nakagawasai, O., Yanai, K., Nunoki, K., Tan-No, K., Tadano, T., and Iijima, T. (2007). "Modified behavioral characteristics following ablation of the voltage-dependent calcium channel beta3 subunit". Brain Res **1160**, 102-112.

Murakami, M., Yamamura, H., Murakami, A., Okamura, T., Nunoki, K., Mitui-Saito, M., Muraki, K., Hano, T., Imaizumi, Y., Flockerzi, T*., et al.* (2000). "Conserved smooth muscle contractility and blood pressure increase in response to high-salt diet in mice lacking the beta3 subunit of the voltage-dependent calcium channel". J Cardiovasc Pharmacol **36 Suppl 2**, S69-73.

Namkung, Y., Smith, S.M., Lee, S.B., Skrypnyk, N.V., Kim, H.L., Chin, H., Scheller, R.H., Tsien, R.W., and Shin, H.S. (1998). "Targeted disruption of the Ca^{2+} channel beta3 subunit reduces N- and L-type Ca^{2+} channel activity and alters the voltage-dependent activation of P/Q-type Ca^{2+} channels in neurons". Proc Natl Acad Sci U S A **95**, 12010-12015.

Nicoll, R.A., Tomita, S., and Bredt, D.S. (2006). "Auxiliary subunits assist AMPA-type glutamate receptors". Science **311**, 1253-1256.

Ohta, T., Ohba, T., Suzuki, T., Watanabe, H., Sasano, H., and Murakami, M. (2010). "Decreased calcium channel currents and facilitated epinephrine release in the Ca^{2+} channel beta3 subunit-null mice". Biochem Biophys Res Commun **394**, 464-469.

Opatowsky, Y., Chen, C.C., Campbell, K.P., and Hirsch, J.A. (2004). "Structural analysis of the voltage-dependent calcium channel beta subunit functional core and its complex with the alpha 1 interaction domain". Neuron **42**, 387-399.

Paredes, R.M., Etzler, J.C., Watts, L.T., Zheng, W., and Lechleiter, J.D. (2008). "Chemical calcium indicators". Methods **46**, 143-151.

Patterson, R.L., van Rossum, D.B., Barrow, R.K., and Snyder, S.H. (2004). "RACK1 binds to inositol 1,4,5-trisphosphate receptors and mediates Ca^{2+} release". Proc Natl Acad Sci U S A **101**, 2328-2332.

Perez-Reyes, E., Castellano, A., Kim, H.S., Bertrand, P., Baggstrom, E., Lacerda, A.E., Wei, X.Y., and Birnbaumer, L. (1992). "Cloning and expression of a cardiac/brain beta subunit of the L-type calcium channel". J Biol Chem **267**, 1792-1797.

Perez-Reyes, E., Kim, H.S., Lacerda, A.E., Horne, W., Wei, X.Y., Rampe, D., Campbell, K.P., Brown, A.M., and Birnbaumer, L. (1989). "Induction of calcium currents by the expression of the alpha 1-subunit of the dihydropyridine receptor from skeletal muscle". Nature **340**, 233-236.

Pietruck, F., Busch, S., Virchow, S., Brockmeyer, N., and Siffert, W. (1997). "Signalling properties of lysophosphatidic acid in primary human skin fibroblasts: role of pertussis toxin-sensitive GTP-binding proteins". Naunyn Schmiedebergs Arch Pharmacol **355**, 1-7.

Platzer, J., Engel, J., Schrott-Fischer, A., Stephan, K., Bova, S., Chen, H., Zheng, H., and Striessnig, J. (2000). "Congenital deafness and sinoatrial node dysfunction in mice lacking class D L-type Ca^{2+} channels". Cell **102**, 89-97.

Poenie, M., and Tsien, R. (1986). "Fura-2: a powerful new tool for measuring and imaging [Ca2+]i in single cells". Prog Clin Biol Res **210**, 53-56.

Powers, P.A., Liu, S., Hogan, K., and Gregg, R.G. (1992). "Skeletal muscle and brain isoforms of a beta-subunit of human voltage-dependent calcium channels are encoded by a single gene". J Biol Chem **267**, 22967-22972.

Pragnell, M., De Waard, M., Mori, Y., Tanabe, T., Snutch, T.P., and Campbell, K.P. (1994). "Calcium channel beta-subunit binds to a conserved motif in the I-II cytoplasmic linker of the alpha 1-subunit". Nature **368**, 67-70.

Qin, N., Platano, D., Olcese, R., Costantin, J.L., Stefani, E., and Birnbaumer, L. (1998). "Unique regulatory properties of the type 2a Ca^{2+} channel beta subunit caused by palmitoylation". Proc Natl Acad Sci U S A **95**, 4690-4695.

Rocnik, E.F., Chan, B.M., and Pickering, J.G. (1998). "Evidence for a role of collagen synthesis in arterial smooth muscle cell migration". J Clin Invest **101**, 1889-1898.

Ruth, P., Rohrkasten, A., Biel, M., Bosse, E., Regulla, S., Meyer, H.E., Flockerzi, V., and Hofmann, F. (1989). "Primary structure of the beta subunit of the DHP-sensitive calcium channel from skeletal muscle". Science **245**, 1115-1118.

Schor, S.L. (1980). "Cell proliferation and migration on collagen substrata in vitro". J Cell Sci **41**, 159-175.

Seisenberger, C., Specht, V., Welling, A., Platzer, J., Pfeifer, A., Kuhbandner, S., Striessnig, J., Klugbauer, N., Feil, R., and Hofmann, F. (2000). "Functional embryonic cardiomyocytes after disruption of the L-type alpha1C (Cav1.2) calcium channel gene in the mouse". J Biol Chem **275**, 39193-39199.

Shao, Y., Czymmek, K.J., Jones, P.A., Fomin, V.P., Akanbi, K., Duncan, R.L., and Farach-Carson, M.C. (2009). "Dynamic interactions between L-type voltage-sensitive calcium channel Cav1.2 subunits and ahnak in osteoblastic cells". Am J Physiol Cell Physiol **296**, C1067-1078.

Shtivelman, E., Cohen, F.E., and Bishop, J.M. (1992). "A human gene (AHNAK) encoding an unusually large protein with a 1.2-microns polyionic rod structure". Proc Natl Acad Sci U S A **89**, 5472-5476.

Simms, B.A., and Zamponi, G.W. (2014). "Neuronal voltage-gated calcium channels: structure, function, and dysfunction". Neuron **82**, 24-45.

Singer, D., Biel, M., Lotan, I., Flockerzi, V., Hofmann, F., and Dascal, N. (1991). "The roles of the subunits in the function of the calcium channel". Science **253**, 1553-1557.

Singh, U., Sun, T., Looman, C., Heuchel, R., Elliott, R., Freichel, M., Meissner, M., Flockerzi, V., and Fundele, R. (2007). "Expression and function of the gene encoding

the voltage-dependent calcium channel beta3-subunit in the mouse placenta". Placenta **28**, 412-420.

Sixt, M. (2012). "Cell migration: fibroblasts find a new way to get ahead". J Cell Biol **197**, 347-349.

Smith, P.K., Krohn, R.I., Hermanson, G.T., Mallia, A.K., Gartner, F.H., Provenzano, M.D., Fujimoto, E.K., Goeke, N.M., Olson, B.J., and Klenk, D.C. (1985). "Measurement of protein using bicinchoninic acid". Anal Biochem **150**, 76-85.

Sorg, H., Krueger, C., and Vollmar, B. (2007). "Intravital insights in skin wound healing using the mouse dorsal skin fold chamber". J Anat **211**, 810-818.

Souders, C.A., Bowers, S.L., and Baudino, T.A. (2009). "Cardiac fibroblast: the renaissance cell". Circ Res **105**, 1164-1176.

Storch, U., Forst, A.L., Philipp, M., Gudermann, T., and Mederos y Schnitzler, M. (2012). "Transient receptor potential channel 1 (TRPC1) reduces calcium permeability in heteromeric channel complexes". J Biol Chem **287**, 3530-3540.

Subramanyam, P., Obermair, G.J., Baumgartner, S., Gebhart, M., Striessnig, J., Kaufmann, W.A., Geley, S., and Flucher, B.E. (2009). "Activity and calcium regulate nuclear targeting of the calcium channel beta4b subunit in nerve and muscle cells". Channels (Austin) **3**, 343-355.

Suh, B.C., Kim, D.I., Falkenburger, B.H., and Hille, B. (2012). "Membrane-localized beta-subunits alter the PIP2 regulation of high-voltage activated Ca^{2+} channels". Proc Natl Acad Sci U S A **109**, 3161-3166.

Tadmouri, A., Kiyonaka, S., Barbado, M., Rousset, M., Fablet, K., Sawamura, S., Bahembera, E., Pernet-Gallay, K., Arnoult, C., Miki, T.*, et al.* (2012). "Cacnb4 directly couples electrical activity to gene expression, a process defective in juvenile epilepsy". Embo J **31**, 3730-3744.

Takahashi, M., Seagar, M.J., Jones, J.F., Reber, B.F., and Catterall, W.A. (1987). "Subunit structure of dihydropyridine-sensitive calcium channels from skeletal muscle". Proc Natl Acad Sci U S A **84**, 5478-5482.

Tanabe, T., Takeshima, H., Mikami, A., Flockerzi, V., Takahashi, H., Kangawa, K., Kojima, M., Matsuo, H., Hirose, T., and Numa, S. (1987). "Primary structure of the receptor for calcium channel blockers from skeletal muscle". Nature **328**, 313-318.

Tanaka, C., Ito, S., Nishio, N., Kodera, Y., Sakurai, H., Suzuki, H., Nakao, A., and Isobe, K. (2010). "GADD34 suppresses wound healing by upregulating expression of myosin IIA". Transgenic Res **19**, 637-645.

Tareilus, E., Roux, M., Qin, N., Olcese, R., Zhou, J., Stefani, E., and Birnbaumer, L. (1997). "A Xenopus oocyte beta subunit: evidence for a role in the assembly/expression of voltage-gated calcium channels that is separate from its role as a regulatory subunit". Proc Natl Acad Sci U S A **94**, 1703-1708.

REFERENCES

Tu, H., Nelson, O., Bezprozvanny, A., Wang, Z., Lee, S.F., Hao, Y.H., Serneels, L., De Strooper, B., Yu, G., and Bezprozvanny, I. (2006). "Presenilins form ER Ca^{2+} leak channels, a function disrupted by familial Alzheimer's disease-linked mutations". Cell **126**, 981-993.

Van Petegem, F., Clark, K.A., Chatelain, F.C., and Minor, D.L., Jr. (2004). "Structure of a complex between a voltage-gated calcium channel beta-subunit and an alpha-subunit domain". Nature **429**, 671-675.

Vendel, A.C., Terry, M.D., Striegel, A.R., Iverson, N.M., Leuranguer, V., Rithner, C.D., Lyons, B.A., Pickard, G.E., Tobet, S.A., and Horne, W.A. (2006). "Alternative splicing of the voltage-gated Ca^{2+} channel beta4 subunit creates a uniquely folded N-terminal protein binding domain with cell-specific expression in the cerebellar cortex". J Neurosci **26**, 2635-2644.

Walker, D., and De Waard, M. (1998). "Subunit interaction sites in voltage-dependent Ca^{2+} channels: role in channel function". Trends Neurosci **21**, 148-154.

Weissgerber, P., Held, B., Bloch, W., Kaestner, L., Chien, K.R., Fleischmann, B.K., Lipp, P., Flockerzi, V., and Freichel, M. (2006). "Reduced cardiac L-type Ca^{2+} current in Ca(V)beta2$^{-/-}$ embryos impairs cardiac development and contraction with secondary defects in vascular maturation". Circ Res **99**, 749-757.

Weng, L., Enomoto, A., Miyoshi, H., Takahashi, K., Asai, N., Morone, N., Jiang, P., An, J., Kato, T., Kuroda, K., *et al.* (2014). "Regulation of cargo-selective endocytosis by dynamin 2 GTPase-activating protein girdin". Embo J **33**, 2098-2112.

Wettschureck, N., and Offermanns, S. (2005). "Mammalian G proteins and their cell type specific functions". Physiol Rev **85**, 1159-1204.

Wong, V.W., Sorkin, M., Glotzbach, J.P., Longaker, M.T., and Gurtner, G.C. (2011). "Surgical approaches to create murine models of human wound healing". J Biomed Biotechnol **2011**, 969618.

Xu, S., and Chisholm, A.D. (2011). "A Galphaq-Ca^{2+} signaling pathway promotes actin-mediated epidermal wound closure in C. elegans". Curr Biol **21**, 1960-1967.

Xu, X., Lee, Y.J., Holm, J.B., Terry, M.D., Oswald, R.E., and Horne, W.A. (2011). "The Ca^{2+} channel beta4c subunit interacts with heterochromatin protein 1 via a PXVXL binding motif". J Biol Chem **286**, 9677-9687.

Yamada, T., Ueda, T., Ugawa, S., Ishida, Y., Imayasu, M., Koyama, S., and Shimada, S. (2010). "Functional expression of transient receptor potential vanilloid 3 (TRPV3) in corneal epithelial cells: involvement in thermosensation and wound healing". Exp Eye Res **90**, 121-129.

Yu, K., Xiao, Q., Cui, G., Lee, A., and Hartzell, H.C. (2008). "The best disease-linked Cl^- channel hBest1 regulates Cav1 (L-type) Ca^{2+} channels via src-homology-binding domains". J Neurosci **28**, 5660-5670.

Zhang, Y., Yamada, Y., Fan, M., Bangaru, S.D., Lin, B., and Yang, J. (2010). "The beta subunit of voltage-gated Ca^{2+} channels interacts with and regulates the activity of a novel isoform of Pax6". J Biol Chem **285**, 2527-2536.

Zheng, J.Q., and Poo, M.M. (2007). "Calcium signaling in neuronal motility". Annu Rev Cell Dev Biol **23**, 375-404.

Curriculum vitae

PERSONAL DATA

Name: Anouar Belkacemi

Date/Place of birth: 7th of February 1985 in Souk Naamane/Algeria

Nationality: Algerian

Marital Status: Married

EDUCATION

University Degree	**"PhD Thesis"** (supervised by Prof. Veit Flockerzi)
University	Saarland University Medical Center, Homburg/Germany.
Major	Pharmacology and Toxicology
Graduation Year	2015

University Degree	**"Master Thesis"** (supervised by Prof. Veit Flockerzi)
University	Saarland University Medical Center, Homburg/Germany.
Major	Pharmacology and Toxicology
Graduation Year	01.08.2010 – 15.05.2011

University Degree	**"Diplome de Pharmacien"**
University	Hadj Lakhdar University, Batna/ Algeria.
Major	Pharmacy
Graduation Year	Summer of 2008.

Secondary School Degree

University   King Saud Secondary School of Al-Baha- Saudi Arabia.

Major   Sciences Branch

Graduation Year   Summer of 2003.

STIPENDS AND HONORS:

October 2010 to March 2012: Member of the Research Training Group GRK 845, Saarland University/ TU Kaiserslautern.

Jun 2012 to date: Scholarship of the International Research Training Group "IRTG1830", Saarland University/TU Kaiserslautern/Alberta University–Canada

Jun 2013 to date: Elected colleagians spokesperson of the International Research Training Group "IRTG1830".

April 2014: Poster prize - the 80th Annual Meeting of the German Society of Pharmacology and Toxicology, Hannover, Germany.

April 2014: Poster prize - The 57th Annual Meeting of the Canadian Society for Molecular Biosciences, Banff, Canada.

LANGUAGE PROFICIENCY

Arabic   Mother Language

English   Written and spoken fluently

French   Written and spoken fluently

German   Basic (B1)

Publications

Abstracts

S. Link, **A. Belkacemi**, K. Frohnweiler, A. Beck, V. Flockerzi, (2011) Proteins interacting with the Ca^{2+} channel CaVβ3 subunit, Naunyn-Schmiedeberg´s Arch Pharmacol 383, 77th Annual Meeting Deutsche Gesellschaft für Experimentelle und Klinische Pharmakologie und Toxikologie in Frankfurt am Main.

A. Belkacemi, M. W. Laschke, C. Scheuer, A. Beck, V. Flockerzi, (2012) Enhanced fibroblast motility in the absence of the β3 regulatory subunit of voltage-activated calcium channels, *Naunyn-Schmiedeberg´s Arch Pharmacol* 385, 78th Annual Meeting Deutsche Gesellschaft für Experimentelle und Klinische Pharmakologie und Toxikologie in Dresden.

A. Belkacemi, M. W. Laschke, C. Scheuer, A. Beck, M. D. Menger, V. Flockerzi, (2012) Altered fibroblast motility and wound healing in mice deficient in the β3 subunit of voltage-activated calcium channels, The European Calcium Channel Conference in Alpbach, Tyrol, Austria.

A. Belkacemi, J. Dörr, P. Weißgerber, A. Beck, V. Flockerzi, (2014) Deletion of the Ca^{2+} channel β3 subunit affects agonist induced Ca^{2+} release in fibroblasts, Naunyn-Schmiedeberg´s Arch Pharmacol 387, 80th Annual Meeting Deutsche Gesellschaft für Experimentelle und Klinische Pharmakologie und Toxikologie in Hannover.

A. Belkacemi, V. Flockerzi, (2014) New functions of the calcium channel β3 subunit, The 57th Annual Meeting of the Canadian Society for Molecular Biosciences, Banff, Canada.

A. Belkacemi, V. Flockerzi, (2014) Novel function of Ca^{2+} channel β3 subunit in fibroblasts, Conference on Receptors, G proteins and integration of Ca^{2+} signaling in the cardiovascular system, Berlin-Buch.

Journal articles

M. Fischer , S. Horn, **A. Belkacemi**, K. Kojer, C Petrungaro, M. Habich, M. Ali, V. Küttner, M. Bien, F. Kauff, J. Dengjel, JM. Herrmann, J. Riemer. (2013) Protein import and oxidative folding in the mitochondrial intermembrane space of intact mammalian cells, Mol Biol Cell. 2013 Jul; 24(14):2160-70

F. Hofmann, **A. Belkacemi** and V. Flockerzi, (2015). Emerging alternative functions for the auxiliary subunits of the voltage-gated calcium channel. Current Molecular Pharmacology in press.